SYNTHESIS AND CHARACTERIZATION OF POLYANILINE FOR HYDRAZINE DETECTION

KAVIRAJAA PANDIAN A/L SAMBASEVAM

THESIS SUBMITTED IN FULFILMENT OF THE REQUIREMENTS FOR THE DEGREE OF DOCTOR OF PHILOSOPHY

FACULTY OF SCIENCE
UNIVERSITY OF MALAYA
KUALA LUMPUR

2015

UNIVERSITI MALAYA

ORIGINAL WORK DECLARATION

Name of Candidate: **KAVIRAJAA PANDIAN A/L SAMBASEVAM**
(I.C/Passport No:

Registration/Matric No: **SHC 110019**

Name of Degree: **DOCTOR OF PHILOSOPHY (EXCEPT MATHEMATICS AND SCIENCE PHILOSOPHY)**

Title of Project Paper/Research Report/Dissertation/Thesis ("this Work"):

SYNTHESIS AND CHARACTERIZATION OF POLYANILINE FOR HYDRAZINE DETECTION

Field of Study: **ADVANCE MATERIALS**

I do solemnly and sincerely declare that:

(1) I am the sole author/writer of this Work;
(2) This Work is original;
(3) Any use of any work in which copyright exists was done by way of fair dealing and for permitted purposes and any excerpt or extract from, or reference to or reproduction of any copyright work has been disclosed expressly and sufficiently and the title of the Work and its authorship have been acknowledged in this Work;
(4) I do not have any actual knowledge nor do I ought reasonably to know that the making of this work constitutes an infringement of any copyright work;
(5) I hereby assign all and every rights in the copyright to this Work to the University of Malaya ("UM"), who henceforth shall be owner of the copyright in this Work and that any reproduction or use in any form or by any means whatsoever is prohibited without the written consent of UM having been first had and obtained;
(6) I am fully aware that if in the course of making this Work I have infringed any copyright whether intentionally or otherwise, I may be subject to legal action or any other action as may be determined by UM.

Candidate's Signature Date

Subscribed and solemnly declared before,

Witness's Signature Date

Name:

Designation

ABSTRACT

Among the conducting polymers, polyaniline (PAni) is studied most extensively due to the ease of synthesis, high conductivity and low production cost. Hydrazine from fuels, pesticide and corrosion inhibitor industries are a toxic compound which can cause neurotoxicity and carcinogenicity. In this study, a series of PAni were synthesized and applied as a chemical sensor for hydrazine detection. The sensor responses of PAni were monitored by ultraviolet-visible (UV-Vis) analysis in hydrazine detection. Besides, the sensor response was supported by conductivity study and Fourier transform infrared (FTIR) analysis to identify the chemical interaction between the PAni and the hydrazine. Doped-PAni were synthesized through chemical oxidative polymerization by using different sodium dioctyl sulfosuccinate salt dopant ratio (monomer:dopant = 5:3,5:5,5:7) under various polymerization temperatures (-10 ˚C to 25 ˚C). Similar procedure was repeated by addition of TiO_2 nanoparticles (10 – 40%) through in-situ polymerization to produce PAni/TiO_2 nanocomposites. FTIR, UV-Vis and x-ray diffractometry (XRD) analysis confirmed the chemical structure of all PAni. Conductivity, morphology and elemental analysis of doped-PAni were studied by resistivity meter, field emission scanning electron microscope (FESEM) and energy dispersive x-ray (EDX) analysis, respectively. For chemical sensor study, all PAni showed significant decrease at polaron peak (~780 nm) in UV-Vis spectra upon immersion in hydrazine. Doped-PAni synthesized with highest dopant ratio (5:7) at subzero polymerization temperature (-5 ˚C) provided more reactive sites to interact with hydrazine, thus giving rapid response time (7 s) with highest sensitivity compare to those with lower dopant ratio and other temperatures. Besides, PAni/TiO_2 nanocomposites (5:7, -5 ˚C) with addition of 20% TiO_2 offered good synergetic effect between PAni and TiO_2 in order to detect hydrazine more effectively. The conductivity response for PAni (5:7, -5 ˚C, 20% TiO_2) in hydrazine detection showed significant decrease in conductivity due to the reduction by hydrazine to convert conducting PAni (emeraldine salt-ES) to insulating PAni (leucoemeraldine-LE). Besides that, FTIR analysis of PAni showed decrease in the intensity ratio of quinoid/benzenoid (I_Q/I_B) from ~1 to 0.80 (increment in benzenoid units) upon immersion of PAni in hydrazine. FTIR analysis showed good agreement with conductivity data because LE consists of more benzenoid unit compared to ES. PAni (5:7, -5 ˚C, 20% TiO_2) exhibited good reusability up to 10 cycles and excellent selectivity in the presence of interfering species such as 2-propanol, sodium hydroxide, formic acid and ammonia in hydrazine detection. The method validation of PAni (5:7, -5 ˚C, 20% TiO_2) by UV-Vis measurement showed a linear calibration curve for hydrazine (0.05 – 5.00 ppm) with good correlation coefficient of 0.9928 and limit of detection (LOD) of 0.05 ppm (lower than OSHA standard:1 ppm). PAni (5:7, -5 ˚C, 20% TiO_2) showed excellent recovery (93 – 105 %) and good relative standard deviation (R.S.D.) (0.3 – 4.2 %) for spiked real samples in laboratory tap water and river water (0.5 – 1.0 ppm) during hydrazine detection. In conclusion, PAni (5:7, -5 ˚C, 20% TiO_2) that exhibited rapid response, highest sensitivity, satisfactory recovery (real sample), good reusability and selectivity is highly recommended as chemical sensor for hydrazine detection.

ABSTRAK

Antara polimer konduktif, polianilina (PAni) diekspolarasi paling luas kerana kemudahan sintesis, kekonduksian yang tinggi dan kos pengeluaran yang rendah. Hidrazin daripada industri bahan api dan antikakisan adalah sebatian toksik yang akan menyebabkan keracunan saraf dan kekarsinogenan. Dalam kajian ini, suatu siri PAni disintesis dan digunakan sebagai sensor kimia untuk mengesan hidrazin. Respon sensor PAni dipantau oleh analisis ultraungu-nampak (UV-Vis) untuk mengesan hidrazin. Selain itu, respon sensor bagi PAni disokong oleh kajian kekonduksian dan analisis *Fourier transform* inframerah (FTIR) untuk mengenal pasti interaksi kimia yang berlaku di antara PAni dan hidrazin. PAni-terdop disintesis melalui pempolimeran oksidatif kimia dengan menggunakan garam natrium dioktil sulfosuksinat dengan nisbah dopan yang berbeza (monomer:dopan = 5:3,5:5,5:7) suhu pempolimeran yang berbeza (-10 hingga 25 ˚C). Prosedur yang sama diulang dengan penambahan partikel nano TiO_2 (10 - 40%) melalui pempolimeran *in-situ* untuk menghasilkan nanokomposit PAni/TiO_2. Analisis FTIR, UV-Vis dan Sinar-X (XRD) mengesahkan struktur kimia bagi kesemua PAni. Kekonduksian, morfologi dan analisis unsur bagi PAni-terdop dikaji oleh meter kerintangan, FESEM dan tenaga sinar-X serakan (EDX) analisis, masing-masing. Untuk kajian sensor kimia, kesemua PAni menunjukkan penurunan yang signifikasi pada puncak polaron (~780 nm) di spektrum UV-Vis apabila direndam dalam hidrazin. PAni disintesis dengan nisbah dopan tertinggi (5: 7) pada suhu *subzero* yang rendah (-5 ˚C) menyediakan tapak reaktif yang banyak untuk interaksi dengan hidrazin, dan bertindak balas cepat (7 s) dengan kepekaan tertinggi berbanding dengan PAni yang mempunyai nisbah dopan yang lebih rendah dan suhu yang lain. Di samping itu, nanokomposit PAni/TiO_2 (5: 7, -5 ˚C) yang ditambahkan dengan 20% TiO_2 dapat menawarkan kesan sinergi yang baik bagi PAni dan TiO_2 untuk mengesan hidrazin dengan lebih berkesan. Selain itu, analisis FTIR bagi PAni menunjukkan penurunan dalam nisbah keamatan quinoid/benzenoid (I_Q/I_B) dari ~ 1 – 0.80 (penambahan dalam unit benzenoid) apabila PAni direndam di dalam hidrazin. Analisis FTIR menunjukkan kesesuaian dengan data kekonduksian kerana LE mengandungi lebih banyak unit benzenoid berbanding dengan ES. PAni (5: 7, -5 ˚C, 20% TiO_2) mempamerkan kitar semula sebanyak 10 kitaran dan selektiviti yang baik dengan kehadiran spesies penggangu seperti 2-propanol, natrium hidroksida, asid formik dan ammonia dalam pengesanan hidrazin. Pengesahan kaedah bagi PAni (5: 7, -5 ˚C, 20% TiO_2) dilakukan dengan pengukuran UV-Vis dan menunjukkan kalibrasi *linear* (0.05 – 5.00 ppm) untuk hidrazin dengan pekali korelasi yang baik sebanyak 0.9928 dan had pengesanan (LOD) sebanyak 0.05 ppm (rendah daripada standard OSHA:1 ppm). PAni (5: 7, -5 ˚C, 20% TiO_2) menunjukkan pemulihan yang sangat baik (93-105%) dan RSD yang baik (0.3 - 4.2 %) bagi sampel dari air paip makmal dan air sungai (0.5 - 1.0 ppm) semasa pengesanan hidrazin. Kesimpulannya, PAni (5: 7, -5 ˚C, 20% TiO_2) yang bertindak balas dengan respon yang pemulihan yang memuaskan (sampel sebenar), kitar semula dan selektiviti yang baik sangat dianjurkan sebagai sensor kimia bagi pengesanan hidrazin.

ACKNOWLEDGEMENT

I would like to express my special appreciation and thanks to my supervisors Dr. Phang Sook Wai and Dr. Sharifah Mohamad, you have been a tremendous mentor for me. I would like to thank you for encouraging my research and for allowing me to grow as a research scientist. Your advice on both research as well as on my career have been priceless. I would also like to thank my lab members, Koh Yen Nee, Chiam Yeong Siang, and Nirosa for serving as my lab members even at hardship. I also want to thank you for letting my defense be an enjoyable moment, and for your brilliant comments and suggestions, thanks to you. I would especially like to thank Department of Chemistry staffs who have been there to support me when I needed the assistance on department facilities. Not forgetting Faculty of Science for all the conference funds to attend local conferences. Besides that, I would like to extend my acknowledgement to Kementerian Pendidikan Tinggi for MyBrain15 (MyPHD) scholarships which supported me throughout my Ph.D. period.

A special thanks to my family. Words cannot express how grateful I am to my mother, father and my sister for all of the sacrifices that you've made on my behalf. Your prayer for me was what sustained me thus far. I would also like to thank all of my friends Muggundha Raoov, Hemawathy Surikumaran, Tilagam Marimuthu who supported me in writing, and incented me to strive towards my goal. At the end I would like to express my appreciation to the GOD for giving me the patience in complete this 3 wonderful years of doctorate studies.

TABLE OF CONTENTS

TITLE		PAGE
TITLE PAGE		i
ORIGINAL WORK DECLARATION		ii
ABSTRACT		iii
ABSTRAK		iv
ACKNOWLEDGEMENT		v
TABLE OF CONTENTS		vi
LIST OF FIGURES		xii
LIST OF TABLES		xviii
LIST OF SYMBOLS AND ABBREVIATIONS		xx
LIST OF APPENDICES		xxii
CHAPTER 1 INTRODUCTION		1
1.1	**Background of study**	1
1.2	**Objectives of the research**	3
1.3	**Scope of the study**	3
1.4	**Outline of the thesis**	4
CHAPTER 2 LITERATURE REVIEW		6
2.1	**Polymers**	6
2.2	**Background of conducting polymers**	7
2.3	**Polyaniline (PAni)**	11
	2.3.1 Introduction of PAni	11
	2.3.2 Application of PAni	12
2.4	**Sensors**	16
	2.4.1 Biosensor	17
	2.4.2 Chemical sensors	17

2.4.3 Application of PAni in chemical sensor 21

2.5 Hydrazine 21

2.5.1 Introduction to hydrazine 21

2.5.1 Application of PAni in hydrazine detection 23

CHAPTER 3 METHODOLOGY 27

3.1 Chemicals 27

3.2 Apparatus 28

3.3 Synthesis of PAni 29

3.3.1 Synthesis of PAni/AOT (different dopant ratio) 29

3.3.2 Synthesis of PAni/AOT (different polymerization temperatures) 33

3.3.3 Synthesis of PAni/TiO_2 nanocomposites (different TiO_2 ratio) 33

3.3.4 Synthesis of PAni/TiO_2 nanocomposites (different polymerization temperatures) 34

3.4 Characterizations of PAni 35

3.4.1 Fourier transform infrared (FTIR) spectrometer 35

3.4.2 Ultraviolet-visible (UV-Vis) spectrometer 36

3.4.3 X-ray Diffractometer (XRD) 36

3.4.4 Field emission scanning electron microscope (FESEM) 36

3.4.5 Energy dispersive x-ray spectrometer (EDX) 37

3.4.6 Resistivity meter 37

3.5 Responses of PAni in hydrazine detection 38

3.5.1 UV-Vis responses 38

3.5.2 Conductivity responses 39

3.5.3 FTIR structural analysis 40

3.6 Sensor performances of PAni/Ti20, -5 ˚C in hydrazine detection 40

3.6.1 Effect of film thickness 41

3.6.2 Reusability study 41

3.6.3 Selectivity study 42

3.6.4 Long term stability 42

3.7 Method validation 43

3.8 Real sample analysis 44

CHAPTER 4 RESULTS AND DISCUSSION 45

4.1 PAni/AOT (different dopant ratio) in hydrazine detection 45

4.1.1 Characterizations of PAni/AOT (different dopant ratio) 45

4.1.1 (a) FTIR analysis 46

4.1.1 (b) UV-Vis analysis 48

4.1.1 (c) XRD analysis 49

4.1.1 (d) FESEM analysis 50

4.1.1 (e) EDX analysis 51

4.1.1 (f) Conductivity analysis 52

4.1.2 Responses of PAni/AOT (different dopant ratio) sensors in hydrazine detection 53

4.1.2 (a) UV-Vis responses 54

4.1.2 (b) Conductivity responses 56

4.1.2 (c) FTIR structural analysis 58

4.2 PAni/AOT (different polymerization temperature) in hydrazine detection 61

4.2.1 Characterizations of PAni/AOT (different polymerization temperature) 61

4.2.1 (a) FTIR analysis 61

4.2.1 (b) UV-Vis analysis 63

4.2.1 (c) XRD analysis 64

4.2.1 (d) FESEM analysis 65

4.2.1 (e) EDX analysis 66

4.2.1 (f) Conductivity analysis 68

4.2.2 Responses of PAni/AOT (different polymerization temperatures) sensors in hydrazine detection 69

4.2.2 (a) UV-Vis responses 69

4.2.2 (b) Conductivity responses 71

4.2.2 (c) FTIR structural analysis 73

4.3 PAni/TiO_2 nanocomposites with different TiO_2 ratio in hydrazine detection 76

4.3.1 Characterizations of PAni/TiO_2 nanocomposites (different TiO_2 ratio) 77

4.3.1 (a) FTIR analysis 77

4.3.1 (b) UV-Vis analysis 79

4.3.1 (c) XRD analysis 81

4.3.1 (d) FESEM analysis 82

4.3.1 (e) EDX analysis 83

4.3.1 (f) Conductivity analysis 84

4.3.2 Responses of pristine PAni and PAni/TiO_2 nanocomposite (different TiO_2 ratio) sensors in hydrazine detection 85

4.3.2 (a) UV-Vis responses 85

4.3.2 (b) Conductivity responses 87

4.3.2 (c) FTIR structural analysis 89

4.4 PAni/Ti20 nanocomposites with different polymerization temperatures in hydrazine detection 92

4.4.1 Characterizations of PAni/Ti20 nanocomposites (different polymerization temperatures) 92

4.4.1 (a) FTIR analysis 93

4.4.1 (b) UV-Vis analysis 94

4.4.1 (c) XRD analysis 95

4.4.1 (d) FESEM analysis 96

4.4.1 (e) EDX analysis 98

4.4.1 (f) Conductivity analysis 99

4.4.2 Responses of PAni/Ti20 nanocomposite (different polymerization temperature) sensors in hydrazine detection 100

4.4.2 (a) UV-Vis responses 101

4.4.2 (b) Conductivity responses 103

4.4.2 (c) FTIR structural analysis 105

4.5 Sensor performance of PAni/Ti20, -5 ˚C in hydrazine detection 108

4.5.1 Effect of film thickness 108

4.5.2 Reusability study 109

4.5.3 Selectivity of PAni/Ti20, -5 ˚C nanocomposite in hydrazine detection 111

4.5.4 Long term stability of PAni/Ti20, -5 ˚C nanocomposites in hydrazine detection 114

4.6 Method validation 115

4.7 Real samples analysis 117

4.8 Summary of PAni sensors in hydrazine detection 119

CHAPTER 5 CONCLUSION 123

5.1 Conclusion 123

5.2 Suggestions for future works 125

REFERENCES 126

APPENDICES 147

LIST OF FIGURES

Figure	Title	Page
2.1	Various oxidation states of PAni	12
2.2	Basic fabrication of OLED by using PAni composite	14
2.3	Chemical structure of hydrazine	21
3.1	Glasswares and apparatus used for polymer synthesis	28
3.2	Circulating cooling bath set up used for polymerization at subzero temperature	28
3.3	Aspirator pump set up used for washing purpose after polymerization	29
3.4	Chemical structure of sodium dioctyl sulfosuccinate (AOT)	30
3.5	Polymerization set up for PAni synthesis	30
3.6	Dispersion of PAni precipitate into toluene solution using separating funnel	32
3.7	Ultrasonication set up for dispersion of TiO_2 nanoparticles in Ani/AOT reaction mixture	34
3.8	Simple PAni sensor setup for hydrazine detection	39
4.1	FTIR spectra of PAni **1**, PAni **2** and PAni **3**	47
4.2	UV-Vis spectra of PAni **1**, PAni **2** and PAni **3**	48
4.3	X-ray diffractograms of PAni **1**, PAni **2** and PAni **3**	50
4.4	FESEM images of (a) PAni **1**, (b) PAni **2** and (c) PAni **3** at magnification of 20,000 × and (d) PAni **3** at magnification of 2,500 ×	51
4.5	EDX spectra of PAni **1**, PAni **2** and PAni **3** synthesized at 0 ˚C	52

4.6	Normalized UV-Vis absorbance of PAni **1**, PAni **2** and PAni **3** for hydrazine detection (1 ppm) between 0 – 5 min. (Inset: The absorbance peak of PAni **3** at ~780 nm in hydrazine detection)	55
4.7	Interaction of ES with hydrazine to form LE	55
4.8	Normalized UV-Vis absorbance of PAni **1**, PAni **2** and PAni **3** in different concentration of hydrazine detection (1 – 100 ppm)	56
4.9	Normalized conductivity of PAni **1**, PAni **2** and PAni **3** for hydrazine detection (1 ppm)	57
4.10	Normalized conductivity of PAni **1**, PAni **2** and PAni **3** in the detection of hydrazine (1 – 100 ppm) at 0.12 min (immediate response)	58
4.11	FTIR spectra of PAni **3** (a) before and (b) after immersion in 1 ppm of hydrazine (Inset: Intensity of I_{1612} and I_{1520})	59
4.12	Schematic diagram of PAni/AOT that synthesized with different dopant ratio	60
4.13	FTIR spectra of PAni, -10 ˚C, PAni, -5 ˚C, PAni, 0 ˚C and PAni, 25 ˚C	62
4.14	UV-Vis spectra of PAni, -10 ˚C, PAni, -5 ˚C, PAni, 0 ˚C, and PAni, 25 ˚C	64
4.15	XRD patterns of PAni, -10 ˚C, PAni, -5 ˚C, PAni, 0 ˚C and PAni, 25 ˚	65
4.16	FESEM images of PAni, -10 ˚C, PAni, -5 ˚C, PAni, 0 ˚C and PAni, 25 ˚C with magnification of 20,000 ×	66

4.17	EDX spectra of PAni, -10 ˚C, PAni, -5 ˚C, PAni, 0 ˚C and PAni, 25 ˚C	67
4.18	Normalized UV-Vis absorbance of PAni, -10 ˚C, PAni, -5 ˚C, PAni, 0 ˚C and PAni, 25 ˚C in hydrazine detection (1 ppm). (Inset: The absorbance peak of PAni, -5 ˚C at ~780 nm in hydrazine detection)	70
4.19	Normalized UV-Vis absorbance of PAni, -10 ˚C, PAni, -5 ˚C, PAni, 0 ˚C and PAni, 25 ˚C against different concentration of hydrazine (1 – 100 ppm)	71
4.20	Normalized conductivity of PAni, -10 ˚C, PAni, -5 ˚C, PAni, 0 ˚C and PAni, 25 ˚C in hydrazine detection (1 ppm) between 0 – 5 min	72
4.21	Normalized conductivity of PAni, -10 ˚C, PAni, -5 ˚C, PAni, 0 ˚C and PAni, 25 ˚C in hydrazine detection (1 – 100 ppm)	73
4.22	FTIR spectra of PAni, -5 ˚C (a) before and (b) after immersion in hydrazine (1 ppm)	74
4.23	Schematic diagram of PAni/AOT that synthesized at various polymerization temperatures	76
4.24	FTIR spectra of pristine PAni and PAni/TiO_2 nanocomposites with different TiO_2 ratio	78
4.25	UV-Vis absorption spectra of pristine PAni and PAni/TiO_2 nanocomposites with different TiO_2 ratios	80
4.26	X-ray diffractograms of pristine PAni and PAni/TiO_2 nanocomposites with different TiO_2 ratios	81
4.27	FESEM images of pristine PAni, PAni/Ti10, PAni/Ti20 and PAni/Ti40 at magnification of 20,000 ×	82

4.28	EDX spectra of pristine PAni and PAni/TiO_2 nanocomposites with different ratio of TiO_2	83
4.29	Normalized UV-Vis absorbance of pristine PAni, PAni/Ti10, PAni/Ti20 and PAni/Ti40 for hydrazine detection (1 ppm) between 0 – 5 min. (Inset: The absorbance peak of PAni/Ti20 at ~795 nm in hydrazine detection)	86
4.30	Normalized UV-Vis absorbance of pristine PAni, PAni/Ti10, PAni/Ti20 and PAni/Ti40 in different concentration of hydrazine detection (1 – 100 ppm)	87
4.31	Normalized conductivity pristine of PAni, PAni/Ti10, PAni/Ti20 and PAni/Ti40 in hydrazine detection (1 ppm) with respect to time	88
4.32	Normalized conductivity of pristine PAni, PAni/Ti10, PAni/Ti20 and PAni/Ti40 in hydrazine detection (1 – 100 ppm).	89
4.33	FTIR response of PAni/Ti20 (a) before and (b) after immersion in hydrazine (1 ppm)	90
4.34	Schematic digram of PAni/TiO_2 nanocomposites with different TiO_2 ratios in PAni matrices	91
4.35	FTIR spectra of PAni/Ti20, -5 ˚C, PAni/Ti20, 0 ˚C and PAni/Ti20, 25 ˚C	93
4.36	UV-Vis spectra of PAni/Ti20, -5 ˚C, PAni/Ti20, 0 ˚C and PAni/Ti20, 25 ˚C	95
4.37	X-ray diffractograms of PAni/Ti20, -5 ˚C, PAni/Ti20, 0 ˚C and PAni/Ti20, 25 ˚C with different polymerization temperatures	96

4.38	FESEM images of (a) PAni/Ti20, -5 ˚C, (b) PAni/Ti20, 0 ˚C and (c) PAni/Ti20, 25 ˚C at mangnifications of 20,000 × and (d) PAni/Ti20, -5 ˚C at magnifications of 5,000 ×	98
4.39	EDX spectra of PAni/Ti20 nanocomposites with different polymerization temperatures	99
4.40	Normalized UV-Vis absorbance of PAni/Ti20, -5 ˚C, PAni/Ti20, 0 ˚C and PAni/Ti20, 25 ˚C for hydrazine detection (1 ppm) between 0 – 5 min. (Inset: The absorbance peak of PAni/Ti20 at ~795 nm in hydrazine detection)	101
4.41	Normalized UV-Vis absorbance of PAni/Ti20, -5 ˚C, PAni/Ti20, 0 ˚C and PAni/Ti20, 25 ˚C in different concentration of hydrazine detection (1 – 100 ppm)	103
4.42	Normalized conductivity of PAni/Ti20, -5 ˚C, PAni/Ti20, 0 ˚C and PAni/Ti20, 25 ˚C in hydrazine detection (1 ppm)	104
4.43	Normalized conductivity of PAni/Ti20, -5 ˚C, PAni/Ti20, 0 ˚C and PAni/Ti20, 25 ˚C Ti40 in different concentrations of hydrazine (1 – 100 ppm)	105
4.44	FTIR of PAni/Ti20, -5 ˚C (a) before and (b) after immersion in hydrazine (1 ppm)	106
4.45	Schematic diagram of PAni/Ti20 synthsized at different polymerization temperatures	107
4.46	UV-Vis response of PAni/Ti20, -5 ˚C with different film thickness in hydrazine detection (1 ppm) at 0.12 min	109
4.47	Reusability of PAni/Ti20, -5 ˚C during hydrazine detection (Dedoped by hydrazine and redoped by HCl)	111

4.48	Reversible mechanism of ES state (before immersion in hydrazine) and LE state (after immersion in hydrazine) of PAni/Ti20, -5 ˚C upon dedoping (hydrazine) and redoping (HCl) processes	111
4.49	UV-Vis spectra of (a) PAni/Ti20, -5 ˚C before immersion and after immersion in (b) hydrazine (c) formic acid, (d) 2-propanol, (e) sodium hydroxide, (f) ammonia and (g) combination of hydrazine and other interfering species for selectivity study.	113
4.50	Long term stability of PAni/Ti20, -5 ˚C up to 60 days	114
4.51	Calibration curve of PAni/Ti20, -5 ˚C in hydrazine detection with concentration range of 0.05 – 5.00 ppm	116
4.52	The water used for real sample analysis was collected from Sungai Batu, Selayang	117

LIST OF TABLES

Table	Title	Page
2.1	Different types of conducting polymers and their application	10
2.2	Unique properties of PAni and its applications	16
2.3	Various types of chemical sensors	20
2.4	PAni sensors in hydrazine detection and their performances	26
3.1	Chemical compositions of PAni synthesized at different dopant ratio	32
4.1	Distinctive peaks of PAni synthesized with different dopant ratio	47
4.2	The assignments of UV-Vis absorbance peaks for PAni synthesized with different dopant ratio	49
4.3	Conductivities of PAni/AOT synthesized with different dopant ratio	53
4.4	Distinctive peaks of PAni synthesized at different polymerization temperatures	62
4.5	The assignments of UV-Vis absorption peaks for PAni synthesized at different polymerization temperature	64
4.6	Conductivities of PAni/AOT synthesized with different polymerization temperatures	69
4.7	Distinctive peaks of pristine PAni and PAni/TiO_2 nanocomposites synthesized with different TiO_2 ratio	79
4.8	The assignments of UV-Vis absorption for pristine PAni and PAni/TiO_2 nanocomposites synthesized with different TiO_2 ratio	80

4.9	Conductivities of pristine PAni and PAni/TiO_2 nanocomposites	85
4.10	Functional groups present in PAni/Ti20 that synthesized at different polymerization temperatures	94
4.11	The assignments of UV-Vis absorption peaks for PAni/TiO_2 nanocomposites synthesized with different polymerization temperatures	95
4.12	Conductivities of PAni/Ti20 synthesized at various polymerization temperatures	100
4.13	Analytical performance of PAni sensors (different synthesis parameters) in hydrazine detection that obtained from calibration curves	116
4.14	Spiked, found, recovery and RSD values of PAni/Ti20, -5 ˚C in tap water during hydrazine detection	118
4.15	Spiked, found, recovery and RSD values of PAni/Ti20, -5 ˚C in river water during hydrazine detection	118
4.16	Effect of conductivity on PAni (different dopant ratio) in sensor performance during hydrazine detection	119
4.17	Effect of conductivity on PAni (different polymerization temperatures) in sensor performance during hydrazine detection	120
4.18	Effect of conductivity on PAni/TiO_2 nanocomposites (different TiO_2 ratio) in sensor performance during hydrazine detection	121
4.19	Effect of conductivity on PAni/Ti20 nanocomposites (different polymerization temperature) in sensor performance during hydrazine detection	122

LIST OF SYMBOLS AND ABBREVIATIONS

Ani	Aniline
AOT	Sodium dioctyl sulfosuccinate
APS	Ammonium persulfate
CP	conducting polymer
d.p.	decimal places
EDX	Energy dispersive x-ray
ES	emeraldine salt
FA	Formic acid
FESEM	Field emission scanning electron microscope
FTIR	Fourier transform infrared
FTO	fluorine doped tin oxide
LE	leucoemeraldine
LiCl	Lithium Chloride
LOD	limit of detection
LOQ	limit of quantification
PAni	Polyaniline
rpm	rotation per minute
RSD	relative standard deviation
SEM	Scanning electron microscope
TEM	Transmission electron microscope
UV-Vis	Ultraviolet-visible
XRD	X-ray Diffractometer
PAni **1**	polyaniline with Aniline/AOT ratio of 5/3 synthesized at 0 ˚C
PAni **2**	polyaniline with Aniline/AOT ratio of 5/5 synthesized at 0 ˚C

PAni **3** polyaniline with Aniline/AOT ratio of 5/7 synthesized at 0 ˚C

PAni, -10 ˚C polyaniline with Aniline/AOT ratio of 5/7 synthesized at -10 ˚C

PAni, -5 ˚C polyaniline with Aniline/AOT ratio of 5/7 synthesized at -5 ˚C

PAni, 25 ˚C polyaniline with Aniline/AOT ratio of 5/7 synthesized at 25 ˚C

PAni/Ti10 polyaniline with Aniline/AOT ratio of 5/7 synthesized 0 ˚C in the presence of 10 % titanium dioxide nanoparticles

PAni/Ti20 polyaniline with Aniline/AOT ratio of 5/7 synthesized 0 ˚C in the presence of 20 % titanium dioxide nanoparticles

PAni/Ti40 polyaniline with Aniline/AOT ratio of 5/7 synthesized 0 ˚C in the presence of 40 % titanium dioxide nanoparticles

PAni/Ti20, -5 ˚C polyaniline with Aniline/AOT ratio of 5/7 synthesized -5 ˚C in the presence of 20 % titanium dioxide nanoparticles

PAni/Ti20, 0 ˚C polyaniline with Aniline/AOT ratio of 5/7 synthesized 0 ˚C in the presence of 20 % titanium dioxide nanoparticles

PAni/Ti20, 25 ˚C polyaniline with Aniline/AOT ratio of 5/7 synthesized 25 ˚C in the presence of 20 % titanium dioxide nanoparticles

LIST OF APPENDICES

Appendix	Title	Page
A	FTIR Analysis	144
B	Conductivity Measurement	146
C	Calibration Curves of PAni	147
D	List of Publications	149
E	List of Proceedings	151
F	Awards	152

CHAPTER 1 INTRODUCTION

1.1 Background of study

Hydrazine is a significant industrial chemical which possess vast application in many fields. Owing to its base and strong reducing properties, hydrazine is mainly used in agricultural chemical (pesticides and insecticides), textiles dyes, corrosion protection in water treatment blowers, jet and rocket fuels (Hosseini and Momeni, 2010; Sovey et al., 1993; Umasankar et al., 2011; Yang et al., 2011). However, hydrazine imposes substantial toxic effects to humans which include damage to the liver, kidney and blood abnormalities (Safavi and Tohidi, 2012).

Due to the toxicological effect of hydrazine, development of sensitive, selective, user-friendly and most importantly inexpensive sensor need to be explored for the detection and quantitative determination of hydrazine in real samples. Up to date, several methods have evolved for rapid and sensitive detection of hydrazine such as chromatography, electrochemistry, chemiluminescence and spectroscopic methods (Ivanov et al., 2010; Jayasri and Narayanan, 2007; Liu et al., 1974; Mori et al., 2004; Seifart et al., 1995; Wang et al., 2010). Besides that, detection of hydrazine has been extensively studied by using various materials, such as different metal oxides, electrodes and semiconductors (Chakraborty and Raj, 2010; Li et al., 2011; Lin et al., 2013; Lyutov and Tsakova, 2011).

Unfortunately, these methods and materials possessed several drawbacks such as expensive instrumentation, time consuming, cumbersome operational techniques and

expensive electrode modifications. Therefore, improvement in developing a sensitive, selective, user-friendly and inexpensive hydrazine sensor to overcome the drawbacks of the traditional sensors still open a space to be explored.

The effective and sensitive sensor technology has paid much attention on electrically conducting polymers (CP) since the past decade (Ruschau et al., 1989). CPs are owned by a class of organic material which can be synthesized by chemical or electrochemical methods with different synthesis parameters, such as different types of monomer, synthesis temperature and types of dopants. All CPs possess redox behavior with distinguishable chemical memory, hence they have been considered as an effective material for chemical and biological sensors (Koul et al., 2001).

Among the CPs, polyaniline (PAni) has received widespread attraction due to its ease of synthesis (MacDiarmid, 1997; Wang et al., 2013), high conductivity, low cost and good environmental stability (Macdiarmid et al., 1985; Wang et al., 2009). However, the great potential of PAni is masked by its disadvantages such as insolubility, infusibility and hence, poor processability (Saïdi et al., 2014). Attempts have been made to improve its solubility, of which the most widely used strategy is to dope PAni with suitable surfactants, such as sodium dodecyl sulfate (SDS), dodecylbenzenesulphonic acid (DBSA) (Cao et al., 1992), camphor sulphonic acid (CSA) (Cao and Smith, 1993) and etc. PAni is much preferred over conventional metals as sensing material due to several factors, such as it can be operated at lower applied voltages and temperatures, unique acid-base chemistry and it interacts more favorably with both organic and inorganic compounds (Gabor, 2006).

1.2 Objectives of the research

The overall objective of this thesis is developing a sensitive, selective, user-friendly and most importantly inexpensive PAni sensor for hydrazine detection. The specific aims of the work include:

1. To prepare polyaniline (PAni) with and without TiO_2 in the presence of dopants and construct sensor for the detection and determination of hydrazine.
2. To characterize all PAni with different synthesis parameters by using Fourier transform infrared (FTIR) and ultraviolet-visible (UV-Vis) spectrometers, x-ray diffractometer (XRD), field emission scanning electron microscope (FESEM) coupled with energy dispersive x-ray (EDX) and resistivity meter (four point probe).
3. To calibrate the sensor and study the sensitivity and its application in sample analysis.

1.3 Scope of the study

Taking consideration on the toxicological effect of hydrazine, this study has been focused on the synthesis of PAni via chemical oxidative polymerization. This polymerization technique was chosen due to several advantages such as can be synthesized in bulk, inexpensive starting materials and simple preparation methods compare to conventional electropolymerization of PAni. All PAni syntheses were carried out in the presence of sodium dioctyl sulfosuccinate (AOT) dopant. AOT dopant was chosen in this study due to the presence of sulphonyl group in AOT that will enhance the solubility of PAni in toluene.

The first study was focused on the performance of PAni/AOT with different synthesis parameter such as different dopant ratio (Ani/AOT mole ratio of 5/3, 5/5 and 5/7) and different polymerization temperatures (-10 ˚C, -5 ˚C, 0 ˚C and 25 ˚C). The second sudy was focused on PAni/TiO_2 nanocomposites with different TiO_2 ratios (10%, 20% and 40%) and different polymerization temperatures (-5 ˚C, 0 ˚C and 25 ˚C).

All PAni were optimized with respect to time to find out the shortest response time of PAni in hydrazine detection (1 – 100 ppm). The responses of PAni in hydrazine detection were studied by using UV-Vis spectrometer as main study. The conductivity studies and FTIR structural analysis were carried out to understand the chemical interactions that occur between PAni and hydrazine during hydrazine detection.

Among all PAni synthesized in this study, the best performing PAni in hydrazine detection was chosen to study the sensor properties such as effect of film thickness, reusability, selectivity, long term stability and method validations followed by real sample analysis.

1.4 Outline of the thesis

Brief introduction on the effect of hydrazine and the advantages of PAni as chemical sensor has been discussed in Chapter 1. The objectives of this thesis also have been outlined in this section.

In Chapter 2, there is a critical literature review on polymers, conducting polymers and sensors. Sensors that have been previously developed for hydrazine detection are compared and this Chapter 2 was completed by the up to date application of PAni in hydrazine detection.

In Chapter 3, the experimental design of PAni chemical sensor has been discussed. It began with the materials used in this study and followed by the synthesis of PAni with different synthesis parameters. This chapter also discusses on the brief introduction of instruments and characterizations that carried out on the PAni obtained in this study.

Chapter 4 consists of both results and discussion on the characterizations and in-depth discussion about the interactions that occurred between PAni and hydrazine during hydrazine detection. The interactions were discussed based on UV-Vis response as main study and supported by conductivity responses and FTIR structural analyses. The formations of PAni/AOT and PAni/TiO_2 nanocomposites together with their structural analyses have been given in schematic diagrams. Lastly, the sensor performances, method validations and real samples analyses of the best PAni in hydrazine detection were discussed in detail.

In Chapter 5, an overview and conclusion of the research findings were discussed. Suggestions for future works were discussed. This Chapter 5 followed by the references that used throughout this thesis.

Several appendices were given at the last section of this thesis. The appendices include the raw spectra obtained from FTIR, conductivity response, list of publications, proceedings and awards based on this thesis.

CHAPTER 2 LITERATURE REVIEW

2.1 Polymers

A naturally occurring or synthetic compound consisting of large molecules made up of a linked series of repeated simple monomers (Amlathe and Gupta, 1988; Yamada et al., 2003). Polymer science was first born in industrial laboratories due to the need to make and understand various plastics, rubber, adhesives, coatings and fibers. Only much later, polymer science emerges into the academic field (Golabi and Zare, 1999). Versatility of polymer science made it to be more interdisciplinary than most sciences, combining chemistry (Choudhary and Hansen, 1998), chemical engineering (Liu et al., 1974; Safavi, 2002), materials (Ibrahim et al., 2012; Umar et al., 2011) and other fields as well.

Polymer materials are playing an important role in niche application ever since the discovery of Bakelite resins few decades ago (Ravichandran and Baldwin, 1983). However, the scientists of that period realized that they did not understand many of the relationship between the chemical structures and physical properties of the resulted polymer based materials. The research that ensued, forms the basis for polymer science (Kamyabi et al., 2008; Maleki, Safavi et al., 2008; Zheng and Song, 2009).

Recently, development in polymer science has attracted greater attention of the research community due to the enormous advantages offered by polymers such as unique and imperative properties for advanced applications (Ruschau et al., 1989). These materials are being explored rapidly as the potential substitute to metal or ceramic based materials in a lot of applications such as automotive, aerospace, marine,

sporting goods and electronic industries (Koul et al., 2001). Among various polymer materials, conducting polymer (CP) related fields are growing intensively under increasing scrutiny due to their versatile properties (MacDiarmid, 1997; Wang et al., 2013).

2.2 Background of conducting polymers

Polymers have emerged as one of the most important materials in the twentieth century. The twenty-first century was undoubtedly seen the use of polymers move from primarily passive materials such as coatings and containers to active materials with useful optical, electronic, energy storage and mechanical properties. Indeed, this development has already begun with the discovery and study of CPs.

The importance and potential impact of this new class of material was recognized by the world scientific community when Hideki Shirakawa, Alan J. Heeger and Alan G. MacDiarmid were awarded the Nobel Prize in Chemistry in 2000 for their research in this field (Chaudhari and Kelkar, 1997; Wu, Lin et al., 2005). CPs can be divided into ionic or electronic types of CPs. Both ionic and electronic conducting polymers possess a variety of properties related to their electrochemical behaviors and potentials. Although these materials were known as new materials in terms of their properties, the first work describing the synthesis of a CP was published in the nineteenth century (Letheby, 1862).

It has been known for more than 40 years that the electronic conductivity of CPs are higher than that of other polymeric materials (Hatano et al., 1961; Menefee and Pao, 1962; Rose and Statham, 1950). Although they are not metallic, the possibility of

producing polymers with conductivities approaching those of metals was not recognized.

A key discovery that changed the outlook for producing highly CPs were the finding in 1973 that the inorganic polymer polysulfur nitride (SN)x was highly conducting (Walatka et al., 1973). The room-temperature conductivity of (SN)x was in the order of 10^3 S/cm, approaching the conductivity of copper, $\sim 10^5$ S/cm. Below a critical temperature of about 0.3 K, (SN)x becomes a superconductor (Greene et al., 1975). These discoveries were of particular importance because they proved the possibility of generating highly CPs, and stimulated the enormous amount of focus and activity necessary for the discovery of other polymeric conductors. In 1976 and 1977, the conductivity of (SN)x was enhanced by an order of magnitude following exposure to bromine or other oxidizing agents (Gill et al., 1977), suggesting that it was possible to increase the number of charge carriers via doping.

In 1958, polyacetylene was first synthesized by Natta et al. as a black powder and found to be a semiconductor with conductivity range of 10^{-11} to 10^{-3} S/cm, depending upon how the polymer was processed and manipulated (Karabulut, 2009). This polymer remained a scientific curiosity until the coworker of Prof. Dr. Hideki Shirakawa was accidentally synthesized the silvery polyacetylene thin film in 1967. It was found that the amount of Ziegler–Natta catalyst ($Ti(O\text{-}n\text{-}But)_4\text{-}Et_3Al$), used was three orders of magnitude higher than required. This film possessed a higher conductivity than the previous carbon black (graphite) powders. Shirakawa and coworkers had prepared crystalline polyacetylene films in the presence of Ziegler-Natta catalyst in between 1971 and 1975, however, the nature of conductivity was not pursued (Ito et al., 1974, 1975; Shirakawa and Ikeda, 1971).

Development of CPs were only reached after the discovery of metallic conductivity in crystalline polyacetylene films with the addition of dopants such as halogens during collaborative research involving Shirakawa, MacDiarmid and Heeger in 1977 (Chiang et al., 1977; Shirakawa et al., 1977). Doping is an essential process that would increase the conductivity of CPs due to the presence of charge carriers. There are two types of doping mechanism namely the p-type and n-type. In general, p-type of doping will be done by negatively charged dopant and it will form carbocations (holes) at polymer backbone. Meanwhile, n-type of doping is due to the positively charged dopant and it will form carboanions. The delocalization of these carbocations or carboanions are the key reason for a CP to possess metallic behavior (Ateh et al., 2006).

Following this work and theory, there has been an explosion of activity around the synthesis, characterization and application of conducting polymers in a wide range of fields from electronics to medicine. Table 2.1 shows the summary of about 25 types of conducting polymers and their related applications.

Table 2.1 Different types of conducting polymers and their application

Conducting Polymer	Application	Reference
Polypyrrole (PPy)	pH sensor	(Yue et al., 1996)
Polyaniline (PAni)	Hydrazine sensor	(Sambasevam et al., 2015)
Poly (3,4-ethylenedioxythiophene) (PEDOT)	Solar cell	(Song et al., 2014)
Polythiophene (PTh)	NO_2 sensor	(Navale et al., 2014)
Polythiophene-vinylene (PTh-V)	Solar cell	(Zou et al., 2009)
Poly(2,5-thienylenevinylene) (PTV)	Solar cell	(Kim et al., 2014)
Poly (3-alkylthiophene) (PAT)	Solar cell	(Campo et al., 2013)
Poly (p-phenylene) (PPP)	Composites	(Bian et al., 2014)
Poly-p-phenylene-sulphide (PPS)	Fuel cells	(Jurga et al., 2004)
Poly (p-phenylenevinylene) (PPV)	Membranes	(Sakaguchi et al., 2013)
Poly (phenyl-terephthalamide) (PPTA)	Fibers	(Qu et al., 2012)
Polyacetylene (PAc)	Batteries	(Bahceci and Esat, 2013)
Poly (isothianaphthene) (PITN)	Photovoltaic cell	(Sánchez et al., 2011)
Poly (α-naphthylamine) (PNA)	Extraction	(Bagheri et al.2013)
Polyazulene (PAZ)	Capacitor	(Grodzka et al., 2010)
Polyfuran (PFu)	Electrochromism	(Zhen et al., 2014)
Polyisoprene (PIP)	Stabilizer for natural rubber	(Piya-areetha et al., 2014)
Polybutadiene (PBD)	Memory devices	(Xie et al., 2014)
Poly (3-octylthiophene-3-methylthiophene) (POTMT)	Diodes	(Vardhanan et al., 1999)

2.3 Polyaniline (PAni)

2.3.1 Introduction of PAni

Among all CP, research interest has been growing around using PAni in various applications or in another word, PAni dominate the field of CPs due to its versatile properties (Ren and Zhang, 2010). It is because, PAni possess several advantages such as thermal stability up to 250 ˚C, ease of synthesis by chemical or electrochemical oxidative polymerization in the presence of various organic or aqueous media (Cochet et al., 2001). In addition, extraordinary properties of PAni such as low cost of starting materials, good environmental stability, tunable electrical conductivity and broader commercial and technological opportunities (Peng et al., 2003) such as solar cells (Wang et al., 2013), corrosion devices (Zheng and Song, 2009), organic light emitting diodes (Moulton et al., 2004), electromagnetic interference devices (Kim et al., 2001; MacDiarmid and Epstein, 1994) and bio/chemical sensors (Xia and Wang, 2001). These properties have given a large prospect in the further improvement of such a PAni to be used as a promising material in the electronic devices.

Polyaniline is a conjugated type of conducting polymer. PAni can be synthesized either using simple chemical oxidative polymerization or electrochemical method. PAni has evoked the major debate of scientific community since the discovery of this material to become a conductor or an insulator under certain conditions (Epstein et al., 1987). PAni has been synthesized and utilized decades ago before it was realized that the material could behave as a semiconductor. The research on PAni was initiated by Runge in 1834 and substantially continued by Letheby in 1862 (Letheby, 1862).

Figure 2.1 shows the chemical structure of PAni in various oxidation states. Among all the states, emeraldine salt (ES) is the only conducting state of PAni.

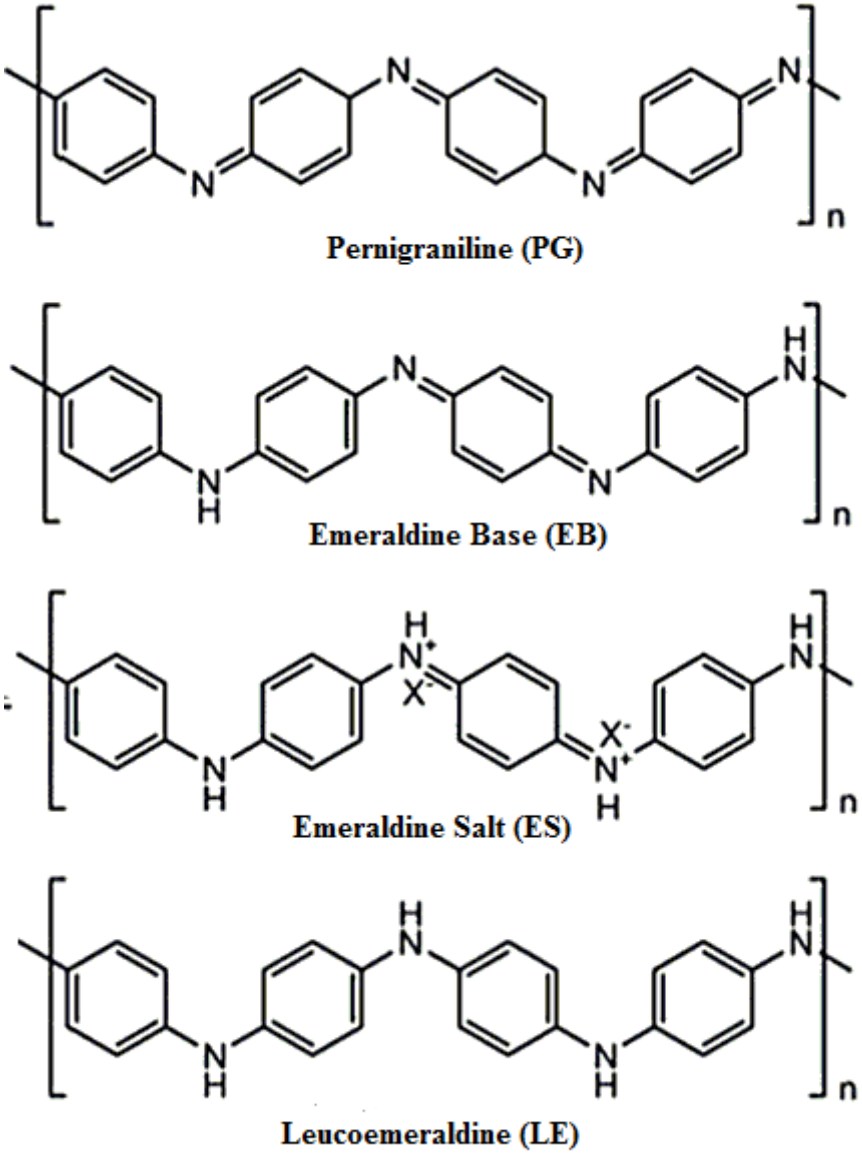

Figure 2.1 Various oxidation states of PAni.

2.3.2 Application of PAni

PAni is one of the CPs that have been extensively studied due to its unique properties such as electrically conductive in nature (Roth and Graupner, 1993), high

viscosity under electric field (Lee et al., 2005) and possessed different colours in acid-base conditions (Bai et al., 2007). In addition, PAni possessed reversible protonation-deprotonation (Syed and Dinesan, 1990) or reversible oxidation-reduction properties (Smela et al., 2005). Again, PAni can exist in different oxidation states depending on charging and discharging of ions into and from the polymer matrix (Bidan and Ehui, 1989).

Since PAni being electrically conductive in nature, it can be used for antistatic textile, conductive paints, ink, and electrostatic discharge materials (Hosoda et al., 2007; Roth and Graupner, 1993). Smart textiles such as sport garments and smart shirts can respond to the changes in environments and can be used to monitor the physiological status of patients. Bowman and Mattes (2005) have prepared high molecular weight PAni via wet spinning technique to yield highly conducting textile PAni fiber. Hino and co-workers synthesized PAni using different dopant and dispersed in epoxy resin with different ratio to prepare conductive adhesives (Hino et al., 2006). Yoshioka and Jabbour (2006) have introduced PAni suspension into an inkjet catridge which was fast and inexpensive microstructures that used in microelectronics.

In general, photo-induced absorption spectroscopy is used for erasable optical information storage capability of a material. The response of PAni to an electromagnetic field in optical regime made it suitable for application in erasable optical information and in non-linear optics (McCall et al., 1991). Different forms of PAni such as emerladine base (EB), leucoemeraldine (LE) and pernigraniline (PG) exhibit relatively weak or strong infrared vibrations and absorption peaks near to 1.4 – 1.5 eV. PAni exhibits a very long-lived photo-induced change due to the rotation of benzene which enables it as a media for erasable optical information storage. Besides

that, large three-ordered nonlinear optical (NLO) properties of PAni also enable it for the fabrication of photonic devices where it can be enhanced through structural changes or creating inter-penetrating polymer network (Petrov et al., 1995).

Besides that, another interesting properties of PAni is the ability of emitting colours upon various excitation states that was potentially applied in organic light emitting diodes (OLED) (Chen et al., 1996; Gaponik et al., 1999). A basic fabrication of OLED has been shown in Figure 2.2, based on the modification done by Gaponik and co-workers. EB form of PAni can be used as an emitting layer, indium-doped tin oxide (ITO) as the hole injector and magenesium/aluminium thin film as electron injector which emits nearly white light covering the range of visible light (380 – 750 nm) (Chen et al., 1996). The emitted colour was tunable from green to red, depending on the size of nanocrystals used in PAni. The use of nanocrystals in PAni films as the light emitting layer resulted in a considerable enhancement of the quantum efficiency in comparison with the polymer-free device with closely packed nanocrystals alone (Gaponik et al., 1999).

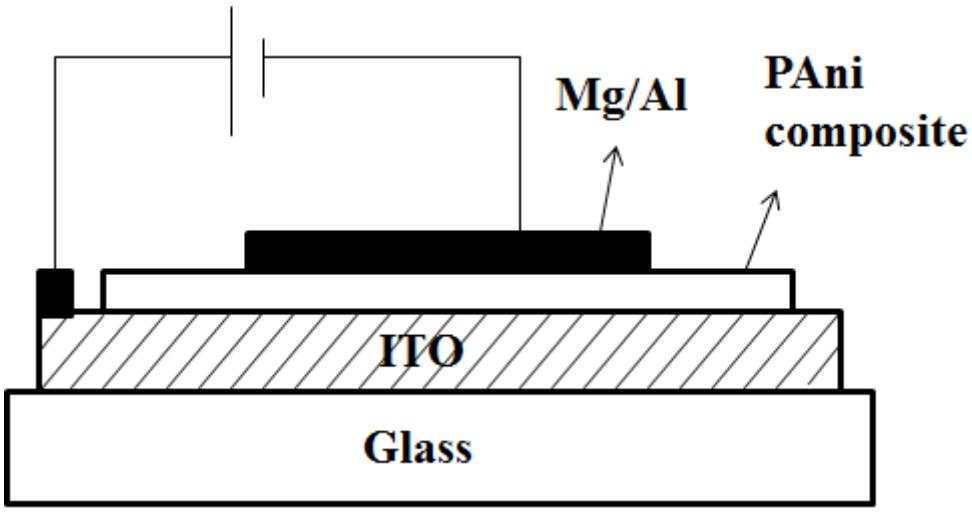

Figure 2.2 Basic fabrication of OLED by using PAni composite.

Moreover, substituted PAni are more sensitive to ozone gas when compared to some of the doped PAni (Ando et al., 2005). PAni/fluorinated ethylene propylene was prepared for chlorine gas detection (Jain et al., 2005). Poly(vinylidenefluoride) (PVF_2) coated PAni found to be sensitive for volatile organic compounds (Kim et al., 2005), meanwhile, composites of PAni with poly(vinylacetate) (PVAc) , polystyrene (PS) and polyvinyl-chloride (PVC) found to be sensitive to toxic gases (Hosseini and Entezami, 2001). PAni were also used to detect liquefied petroleum gas (Joshi et al., 2007), hydrogen peroxide (Zou et al., 2007), humidity (Nohria et al., 2006) and pH changes (Talaie et al., 2000). Electro-polymerized PAni/PVA composite was used to detect the growth of bacteria (Ren et al., 2007). The level of vitamin C was detected from the absorption change of PAni at 700 nm in UV-Vis measurement (Andreu et al., 2005). Besides that, colour changes in PAni due to the protonation-deprotonation upon exposure in different pH values can be used as an acid/base indicator (Syed and Dinesan, 1990).

Apart from the application of PAni discussed in this section, PAni also widely used for corrosion protection of steel, copper and iron (Lu et al., 1995), energy storage (Lu et al., 2007; Meng et al., 2009) and memory devices (Tseng et al., 2005). Some investigations are being carried out in electrochemical sensor system (Dhaoui et al., 2008), as catalyst (Kang et al., 1995), antioxidants (Kilmartin et al., 2005) and etc. The unique properties of PAni and its applications are summarized in Table 2.2.

Table 2.2 Unique properties of PAni and its applications

Unique properties	Application	References
Electrically conductive in nature	Conductive adhesive, ink, paint	(Hino et al., 2006)
	Antistatic textile	(Bowman and Mattes, 2005)
High capacitance value	Energy storage devices	(Meng et al., 2009)
	Capacitor	(Lu et al., 2007)
Response to electromagnetic field in optical regime	Erasable optical information storage	(McCall et al., 1991)
Colour emission under various excitation states	Organic light emitting diodes (OLED)	(Chen et al., 1996)
Interconversion from highly conductive to almost insulating	Digital memory device	(Tseng et al., 2005)
Electrical conductivity or colour changes	NH_3, CO_2, CO sensors	(Koul et al., 2001; Mirmohseni and Oladegaragoze, 2004)
Exposure to acidic, basic, neutral vapours or liquids	Volatile organic compound, toxic gas sensors	(Hosseini and Entezami, 2001; Ihdene et al., 2014)

2.4 Sensors

During past two decades, global research and development (R&D) in the field of sensor has increased exponentially in terms of financial investment, published literatures and number of active researchers. There are various types of sensors such as sensors in production control, biosensors (DNA, touch, pressure, glucose sensors), and chemical sensors (drug, amines, herbicides, stimulants, hydrazine) (Adhikari and Majumdar, 2004).

2.4.1 Biosensor

Biosensors comprise of bioreceptor (biological component) and a transducer to detect the analyte of interest. In general, biosensors will transform the biological changes into an electrical signal that can be interpreted by a transducer. Biosensors are widely used in medical diagnostics and environmental pollution control. Most of the common pollutants include heavy metals, nitrates, herbicides, pesticides, polyaromatic hydrocarbons, trichloroethylene and etc. Besides, the estimation of organic compounds in food manufacturing industries also is a paramount interest to monitor the food quality. Thus, the use of enzyme sensors can help in direct measurement of organic compounds (Adhikari and Majumdar, 2004; Turyan and Mandler, 1997). However, the use of enzymes in sensor will shorten the shelf-life and limits the practical application of the sensors.

2.4.2 Chemical sensors

Chemical sensor is an analytical material/device that would provide information about the changes that occur in the surroundings. In general, chemical sensor will give a measurable signal which is correlated with the concentration of an analyte. Table 2.3 shows the various types of chemical sensors.

The traditional chemical sensors that operate with solid-state devices give response based on its electrical changes that occur within its chemical environment. The electrical properties of this sensor are influenced by the presence of gas phase or liquid phase compounds. Silicon with a thin conductance channel at the surface is used in field

effect transistor (FET) sensors. The device uses the principle of changes in voltage during the detection of an analyte. FETs that work on silicon based chemical sensors have been developed in the past few decades but their progress were stuck due to the technological and fundamental problems of reproducibility, stability, sensitivity and selectivity (Brunink et al., 1991; Lloyd et al., 1983; Madru et al., 1987).

The working principles of semiconductor sensors are based on the conductance change upon interaction with the target analytes. Possible interactions include the conversion of semiconductor to another compound. Another possible interaction might be the extraction of electrons by oxygen that will decrease the conductivity of semiconductor. If the semiconductor exposed to organic vapor, it might regain the conductivity by oxidizing with the negatively charged oxygen (Advani et al., 1981; Mokwa et al., 1985; Nitta and Haradome, 1979; Tadeusz, 2012). The reversible changes in conductance of a semiconductor provided an interesting property that can be developed into a novel sensor materials and devices. A semiconducting metal oxide sensor such as Tin oxide (SnO2) was commercially produced for gas absorption and normally used in the detection of reducing gases in the air (Watson, 1984).

In solid electrolyte sensors, ionic mobility plays a crucial role in determining the conductivity rather than electron mobility, where the conductivity is dominated by one type of ion from the electrolyte. Therefore, solid electrolytes play an important role in commercial gas and ion sensors. By fixing the concentration at one side, the concentration of unknown species can be found by measuring potential across the membranes. Yttria (Y_2O_3) stabilized zirconia (ZrO_2) was used as solid electrolyte in the determination of oxygen in exhaust gases of automobiles, boilers and steel melts (Schindler et al., 1989). Besides that, lanthanum fluoride (LaF3) was also used for

oxygen detection at room temperature which gave about 90% of response in 2 min by indicating the drop in partial pressure of oxygen (Yamazoe et al., 1987).

Traditional chemical sensors dominated by ion complexes and electro-polymerized CPs that possessed drawbacks such as expensive, complicated and time consuming preparation methods. Therefore, exploration of new sensing stems which is inexpensive, easy preparation and selective is crucial.

Table 2.3 Various types of chemical sensors

Chemical sensors	Materials	Analyte	Reference
Semiconductor based solid-state sensors	Si	H^+, O_2, CO_2, H_2S	(Brunink et al., 1991; Lloyd et al., 1983; Madru et al., 1987)
Semiconducting metal oxide sensors	SnO_2, ZnO, TiO_2, NiO	H_2, CO, O_2, H_2S, N_2H_4, NH_3	(Advani et al., 1981; Mokwa et al., 1985; Nitta and Haradome, 1979; Tadeusz Hepel, 2012; Yamazoe et al., 1983)
Solid electrolyte sensors	Y_2O_3 stabilized ZrO_2	O_2 from exhaust, automobiles, boilers	(Schindler et al., 1989)
	LaF_3	O_2, CO_2, SO_2, NO	(Dubbe et al., 1995; Ikeda, 1995; Imanaka et al., 1993; Yamazoe et al., 1987; Yan and Liu, 1994)
	$SrCl_2$-KCl-AgCl	Chlorine	(Pelloux et al., 1980)
	$(AlPcF)_n$	NO_2	(Berthet et al., 1987)
	Antimonic acid, PVA/H_3PO_4	H_2	(Howe and Shilton, 1979; Miura et al., 1984)
Membranes	Ion exchange membranes	Cations and anions	(Bloch et al., 1967; LeBlanc and Grubb, 1976; Wang and Tuzhi, 1986)
	Charged carrier membrane	Anions	(Schulthess et al., 1985; Stepánek et al., 1986)
Organic semiconductors	Polyphenyl acetylacetone, phthalocyanine, polyamide	CO, CO_2, CH_4, H_2O, NO_2, chlorinated hydrocarbons	(Bott and Jones, 1986; Hermans, 1984; Müller and Lange, 1986)

2.4.3 Application of PAni in chemical sensor

Among all CPs, PAni based chemical sensors have attracted the interest of world-wide research community due to the unique properties of PAni to show changes in terms of electrical conductivity and colour towards acidic, basic and some neutral vapours or liquids that makes it to have significant application in sensor, detector and indicator applications (Bai et al., 2007; Kim et al., 2005; Ren et al., 2007; Talaie et al., 2000). Bai and co-workers have prepared ammonia sensor based on polypyrrole/sulfonated-polyaniline (PPY/SPAni) composite film that possessed high sensitivity and low limit of detection (Bai et al., 2007). Polyaniline/poly(vinyl alcohol) (PAni/PVA) composite electrode for carbon dioxide sensing was characterized by using impedance spectroscopy (Irimia-Vladu and Fergus, 2006).

2.5 Hydrazine

2.5.1 Introduction to hydrazine

Hydrazine is a colourless liquid with fishy and pungent odour. Several properties of hydrazine include caustic, fuming and hygroscopic at normal temperature and pressure. Figure 2.3 shows the chemical structure of hydrazine.

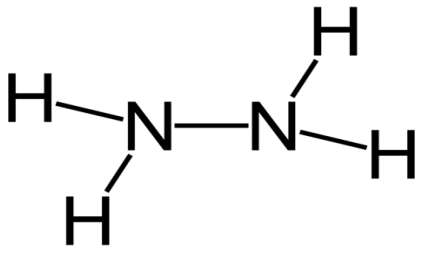

Figure 2.3 Chemical structure of hydrazine.

Hydrazine is a simple inorganic compound that possesses numerous potential applications in industries due to the nature of strong reducing agent and weak base (pKa ~8.10). Hydrazine has found its potential application in 'direct hydrazine hydrate fuel cell' (DHFC) since 1960s (Sakamoto et al., 2014). Several well established companies from Japan such as Governmental Industrial Research Institute of Osaka (GIRIO), Panasonic and Daihatsu Motor Co. Ltd. have invented and tested alkaline type DHFC in 1972 (Yamada et al., 2003). Recent developments in DHFC have indicated feasible and promising future in fuel cell vehicles (Asazawa et al., 2009).

However, hydrazine is a toxic compound that imposes substantial toxic effects for humans which include damage to the liver, kidney, irreversible deterioration of central nervous system (CNS) and blood abnormalities (Safavi and Tohidi, 2012). Due to the toxicological effect of hydrazine, development of sensitive, selective, user-friendly and most importantly inexpensive sensor need to be explored for the detection and quantitative determination of hydrazine in environmental samples. Up to date, several techniques, methods and materials have been proposed in hydrazine detection such as analytical techniques (Mori et al., 2004; Seifart et al., 1995), electrochemical methods (Ivanov et al., 2010; Jayasri and Narayanan, 2007; Wang et al., 2010), inorganic nanoparticles (Chakraborty and Raj, 2010; Li et al., 2011) and electrochemically synthesized CPs (Lin et al., 2013; Lyutov and Tsakova, 2011). Unfortunately, these techniques possessed drawbacks such as expensive instrumentation, electrode modifications, time consuming and cumbersome operational techniques. Therefore, improvement in developing sensitive, selective, user-friendly and inexpensive hydrazine sensor still reserve a space to be explored.

2.5.2 Application of PAni in hydrazine detection

Among the various types of materials proposed for hydrazine detection, PAni is extensively studied due to its unique electrochemical behaviors towards reducing agent (hydrazine). Thus, several efforts, techniques and modifications have been made in past decades on PAni sensors in order to provide a sensitive and durable chemical sensor for hydrazine detection.

Lyutov and Tsakova (2011) have used commercially available Pd for the preparation of Pd-modified polysulfonic acid (PAMSA)-doped PAni in hydrazine detection that showed a limit of detection (LOD) value of 0.013 ppm. In another study, Ivanov and co-workers (2010) have prepared the metal-like palladium (Pd) nanoparticles (NPs)-PAni sensor for hydrazine detection. The sensor was applied by electrochemical and conductance measurements. The detection of hydrazine was measured by chronoamperometry technique that gave a low LOD value of 0.0019 ppm. However, the preparation of Pd doped PAni seems to be cumbersome due to the tedious preparation steps and complicated electrochemical synthesis of PAni.

Recently, the flat carbon nano sheets which are typically known as graphene has received viable attention due to its large specific area (Stoller et al., 2008), low manufacturing cost (Wang et al., 2014), good mechanical properties (Ren et al., 2014) and most importantly high electrical conductivity (Du et al., 2008). Ameen and co-workers (2012) have synthesized PAni/graphene sensor for hydrazine detection and it has been evaluated in terms of sensitivity, reliability and reproducibility. However, the PAni/graphene sensor exhibited poor coefficient correlation of 0.7858 in its calibration plot with high detection limit of 492 ppm. The sensor showed extremely higher LOD

than the LOD set up by Occupational Safety and Health Administration (OSHA) (1 ppm) and Chinese National Standard GB 18061-2000 (0.2 ppm) (Gao et al., 2013).

On the other hand, Paulraj and his co-workers (2011) have performed interfacial polymerization to produce PAni protected by silver nanoparticles as a sensor for hydrazine detection. Simple and cost-effective approach (without the aid of any chemical species other than silver nitrate ($AgNO_3$) and aniline dimer) was used to synthesize the PAni sensor. Differential pulse voltammetry (DPV) technique was employed to detect hydrazine in an appropriate concentration range of 0.64 – 2.88 ppm. The authors claimed that DPV technique significantly improved the detection limit of PAni-Ag composite modified glassy carbon electrode (GCE) yet the data of LOD was not shown in their article.

In general, conducting form of PAni (emeraldine salt-ES) will be converted into a non-conducting form of PAni (leucoemeraldine-LE) by showing a decrease in conductivity due to the interaction of ES with hydrazine. However, Virji and co-workers (2005) have changed this perception with their discovery of PAni incorporated with fluorinated alcohols such as hexafluoroisopropanol (HFIP) and hexafluoro-2-phenylisopropanol (HFPP) that showed an increase in conductivity upon the interaction of PAni-HFIP or PAni-HFPP with hydrazine (Yano et al., 1998). This phenomenon can be explained by the reaction between HFIP or HFPP with hydrazine had yielded an acid, which in turn doped the PAni and made it to be conductive. Although Virji and co-workers (2004) have introduced a contrary concept in the detection of hydrazine compare to the conventional ideology, this sensor showed a high LOD of 3 ppm in comparison to the limits set by authorities.

The development of one-dimensional (1D) conducting nanomaterials held an important role in the field of sensing technology. Ding and co-workers (2011) have demonstrated the excellent sensing response of single wall carbon nanotubes (SWCNT)/PAni in hydrazine detection. Apart from monitoring the sensor performance by using conductance value and cyclic voltammetry, the researchers also studied the chemical interactions between SWCNT/PAni and hydrazine. Ding and co-workers reported that, the response of SWCNT/PAni towards hydrazine was due to the charge transfer effects between SWCNT and PAni. However, the SWCNT/PAni sensor exhibited longer recovery time (over-night) which is not a practical application for PAni sensors in hydrazine detection.

Since gold (Au) nanoparticles have attracted much attention of scientific community due to the electronic, optical and catalytic activities of noble metals, Xin and co-workers (2014) have prepared PAni/Au_0 nanocomposites for hydrazine detection. These PAni/Au_0 nanocomposites possessed unique features such as enhanced mechanical, electrical and catalytic properties that cause it to become the promising sensor material. The PAni/Au_0 nanocomposite sensor showed significant response in hydrazine detection with LOD of 0.03 ppm. It also showed satisfactory results in real sample such as tap and river water with recovery and relative standard deviation (RSD) of 94 – 101 % and 3.1 – 4.9 %, respectively. Table 2.4 shows the selected PAni sensors with their hdyrazine detection technique, linear range and LOD.

In conclusion, PAni and PAni/nanocomposites were extensively studied and applied in hydrazine detection. However, most of the techniques possessed some drawbacks such as expensive electrode modification, complicated sensor set-ups and tedious preparation methods. Thus, simple and inexpensive preparation of PAni without

compromising the sensitivity, selectivity and durability PAni sensor is still open a space for an improvement.

Table 2.4 PAni sensors in hydrazine detection and their performances

PAni sensor	**Detection Technique**	**Linear range (ppm)**	**LOD (ppm)**	**References**
Palladium nanoparticle-PAni	Chronoamperometry	0.300 – 9.600	0.0019	(Ivanov et al., 2010)
Palladium modified polysulfonic acid-doped PAni	Chronoamperometry	1.282 – 32.00	0.0135	(Lyutov and Tsakova, 2011)
Palladium nanoparticle embedded PAni	Cyclicvoltametry	0.006 – 11.22	0.0016	(Lin et al., 2013)
PAni/graphene	Cyclicvoltametry	0.0003 – 3.200	493.0	(Ameen et al., 2012)
PAni/silver composites	Differential pulse voltametry	0.640 – 2.880	-	(Paulraj et al., 2011)
PAni nanofiber	Resistance measurement	-	-	(Virji et al., 2004)
PAni/Fluorinated alcohol	Resistance measurement	-	-	(Virji et al., 2005)
PAni/single wall carbon nanotube	Cyclicvoltametry/UV-Vis NIR	-	-	(Ding et al., 2011)
PAni/gold nanoparticles	Electrochemical impedance spectroscopy	0.3200 – 192.0	0.0300	(Xin et al., 2014)

Key:

' - ' The values of linear range and LOD was not reported in the literature.

CHAPTER 3 METHODOLOGY

3.1 Chemicals

In this study, aniline (Ani) (99.5%), ammonium persulfate (APS) (98%), sodium dioctyl sulfosuccinate (AOT) (96%) and titanium dioxide nanopowder (TiO_2) with diameter of 21 nm (99.5%) were used as monomer, oxidant, dopant and n-type semiconductor, respectively. These chemicals were purchased from Sigma Aldrich. Hydrochloric acid (HCl) with 12 M that purchased from R & M chemicals was diluted to 1 M and used to initiate anilium cations for polymerization. Toluene (99.5%) was used as organic solvent to dissolve PAni. Ethylene glycol:water with weight ratio of 4:6 was used in circulating cooling bath to achieve subzero temperature (-5 and -10 ˚C) for polymerization. Both toluene and ethylene glycol were purchased from Systerm. Lithium chloride monohydrate ($LiCl.H_2O$, 96.5%) was purchased from Friendmann Schmidt Chemicals was added into the reaction mixture to prevent the freezing of polymer solution during polymerization at subzero temperature.

Hydrazine (80%) and ammonium hydroxide (NH_4OH, 25%) were purchased from Merck while other interfering species used in selectivity study such as 2-propanol (99.7%), formic acid (FA, 98%) and sodium hydroxide (NaOH, 99%) were purchased from Systerm. Distilled water was used throughout the study for any dilution and dissolution of acids and alkalis except the dissolution of PAni samples that was done with toluene.

3.2 Apparatus

Glasswares as shown in Figure 3.1 such as beakers, measuring cylinder, petri dish, dropping funnel, glass rods, droppers, sample vials, stirrer bars and retort stands were used for PAni polymerization in this study. Polystyrene box filled with ice cubes that sprinkled with salt were used for polymerization at low temperature. Round bottom flask equipped with stirrer and stirrer guide were immersed in circulating cooling bath for polymerization at subzero temperatures (Figure 3.2).

Figure 3.1 Glasswares and apparatus used for polymer synthesis.

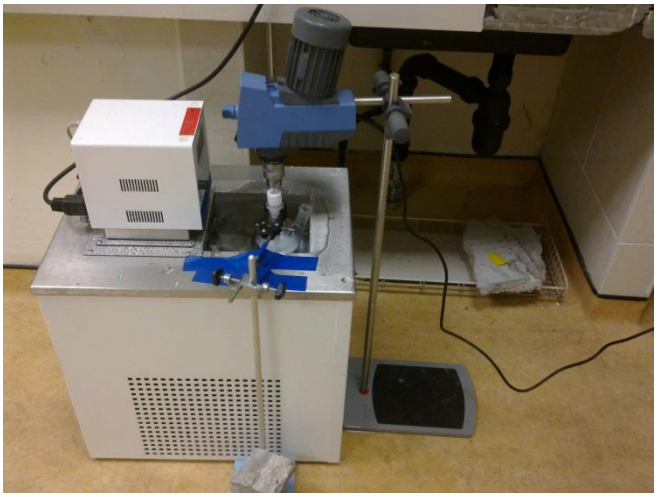

Figure 3.2 Circulating cooling bath set up used for polymerization at subzero temperature.

Aspirator pump (model: Eyela) attached to Buchner funnel was used for washing purposes after polymerization (Figure 3.3). Ultrasonic bath was used to disperse the PAni precipitates in toluene. Finally, PAni solution was spin coated by using Spin-150 spin coater at 2000 rpm to yield a uniform film on a glass substrate prior to hydrazine detection.

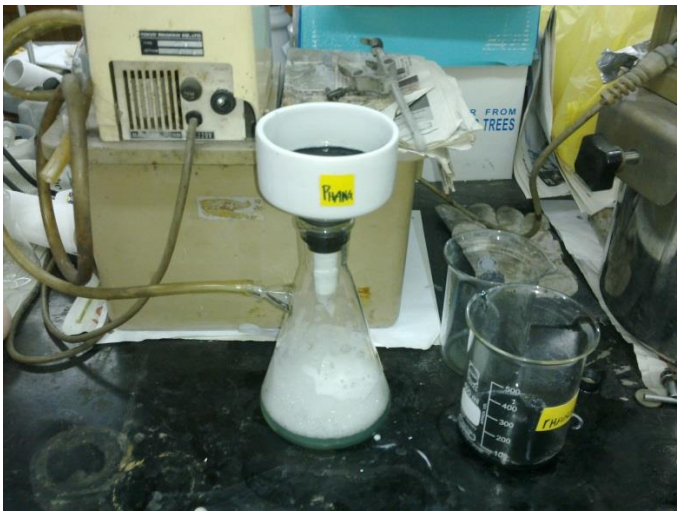

Figure 3.3 Aspirator pump set up used for washing purpose after polymerization.

3.3 Synthesis of PAni

3.3.1 Synthesis of PAni/AOT (different dopant ratio)

PAni/AOT was synthesized by chemical oxidation at 0 ˚C for 24 h. Equimolar ratio of Ani monomer to oxidant (APS) (5:5) were used throughout this study and dopant's ratio was varied in an ascending order of 9 - 27 mmol. In a typical procedure, small pieces of AOT (9 mmol, 4.00 g) were added into HCl solution (1 M) under stirring condition at room temperature. AOT is a sticky anionic surfactant which possesses symmetrical alkyl chains as shown in Figure 3.4. Therefore, it is necessary to

split the bulky AOT surfactant into small pieces to increase the surface area for dissolution in HCl solution.

Then, 5 mmol (1.40 g) of Ani was added slowly into the AOT reaction mixture and stirred for 2 h inside a polystyrene box that contain ice cubes. After that, precooled APS solution was slowly added into the reaction mixture by using dropping funnel for 2 h (Figure 3.5). This slow step is vital, as the APS is a strong oxidant that will create exothermic heat during its addition. After that, the polymer mixture was stirred for 24 h and the final product is labelled as PAni **1**.

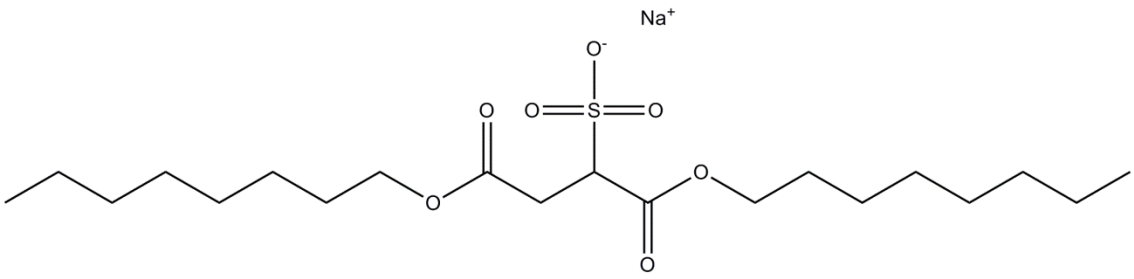

Figure 3.4 Chemical structure of sodium dioctyl sulfosuccinate (AOT).

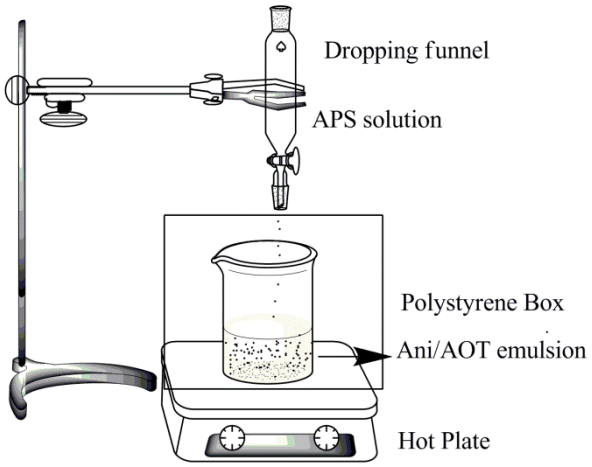

Figure 3.5 Polymerization set up for PAni synthesis.

After that, polymer mixture was filtered by using the aspirator pump (Figure 3.3) to get the PAni precipitates. This step was followed by the washing process using distilled water (100 – 200 mL) for at least three times (or until the filtrate turn colourless) to remove unreacted monomers, oxidants or dopants. Then, the PAni precipitate was dispersed into toluene in separating funnel (Figure 3.6). The top part consists of green PAni in toluene solution while the bottom part of separating funnel consists of aqueous layer with unreacted monomer, oxidants, dopants or oligomers were removed. The green PAni solution was then concentrated by using rotavapor in order to get 3% of PAni in toluene. The percentage of PAni in toluene was calculated based on Equation 3.1;

$$\%\ of\ PAni\ in\ toluene = \frac{(y-x)}{(z-x)} \times 100\% \quad \text{.....Equation 3.1}$$

where, $\varkappa$ is the mass of empty petri dish and z is the mass of 1 g of PAni solution + petri dish while y is the mass of PAni (after dried in oven) + petri dish.

For the preparation of PAni film, 140 µL of PAni (3%) in toluene was deposited on a well-cleaned glass substrate prior to spin coating technique. This was done in a three-step process (acceleration for 10 s at 1000 RPM, steady-state coating for 10 s at 5000 RPM followed by deceleration for 10 s at 1000 RPM) on a spin coater (Model: Spin 150, Germany). This technique yield PAni thin film with a uniform coating and subject to 30 min drying in an oven to remove remaining toluene solvent from the thin film. The thickness of PAni film was measured by using Mitutoyo digital micrometer with 4 decimal places (d.p.). The average thickness of film that used in this study was ~1 µm.

Figure 3.6 Dispersion of PAni precipitate into toluene solution using separating funnel.

Similar procedure was repeated for PAni **2** and PAni **3** with Ani:AOT molar ratio of 5:5 and 5:7, respectively. PAni **2** was synthesized in the presence of 15 mmol of AOT (6.60 g) while PAni **3** was added with 21 mmol of AOT (9.34 g) (Table 3.1).

Table 3.1 Chemical compositions of PAni synthesized at different dopant ratio

Chemical compositions	PAni **1**	PAni **2**	PAni **3**
Molar ratio of Ani:AOT	5:3	5:5	5:7
Amount of AOT (mmol)	9	15	21
Mass of AOT (g)	4.00	6.60	9.34

3.3.2 Synthesis of PAni/AOT (different polymerization temperatures)

From previous Section 3.3.1, Ani:AOT ratio of 5:7 (PAni **3**) was found to be the optimum ratio for PAni/AOT synthesis. Thus, in this section PAni/AOT with Ani:AOT ratio of 5:7 at different polymerization temperatures were synthesized by employing the similar procedures as discussed in Section 3.3.1 at 25 ˚C, 0 ˚C, -5 ˚C and 10 ˚C. For the synthesis temperature at 25 ˚C, polymerization was done at room temperature without any ice cubes. APS solution was precooled before adding into Ani/AOT mixture and the polymerization was preceded as discussed earlier. On the other hand, 3 % and 7.14 % of LiCl monohydrate was added in AOT/HCl emulsion for PAni/AOT that synthesized at -5 ˚C and -10 ˚C, respectively, as anti-freezing agent during subzero polymerization (Stejskal et al., 1998).

3.3.3 Synthesis of PAni/TiO_2 nanocomposites (different TiO_2 ratio)

PAni/TiO_2 nanocomposites were synthesized via chemical oxidation method using TiO_2 nanoparticles (~21 nm) which acted as n-type semiconductor with Ani:AOT ratio of 5:7 (PAni **3**) at 0 ˚C. In a typical procedure, 21 mmol of AOT (9.34 g) was dispersed in 200 mL of HCl (1 M) solution. Then, Ani was added drop by drop into AOT/HCl emulsion in ice bath for 2 h. After that, the whole reaction medium was transferred into an ultrasonicator (Figure 3.7). 10 % of TiO_2 (0.14 g) nanoparticles were then added slowly into the Ani/AOT reaction mixture inside the ultrasonicator for 1 h in order to disperse the TiO_2 nanoparticles in the reaction mixture. Ultrasonication step is necessary because TiO_2 nanoparticles will aggregate with a normal hotplate stirring method, thus it may block and distort the growth of PAni chains during polymerization (Li et al., 2013).

Then, APS solution was added slowly for 2 h. Gradual colour changes was observed during the addition of APS that indicates the growth of PAni chains. The reaction mixture was then preceded for 24 h at 0 ˚C. Similar procedures were repeated for the synthesis of PAni with different TiO_2 ratio such as 20% (0.28 g) and 40% (0.56 g).

Figure 3.7 Ultrasonication set up for dispersion of TiO_2 nanoparticles in Ani/AOT reaction mixture.

3.3.4 Synthesis of PAni/Ti20 nanocomposites (different polymerization temperatures)

PAni with 20% of TiO_2 was found to be the optimum ratio from Section 3.3.3. Thus, in this final part, all PAni/TiO_2 nanocomposites were synthesized with Ani:AOT ratio of 5:7 and 20% of TiO_2 nanoparticles under different polymerization temperatures (-5 ˚C, 0 ˚C and 25 ˚C). Hence, all PAni/TiO nanocomposites were denoted as PAni/Ti20 followed by the respective polymerization temperatures such as PAni/Ti20, -5 ˚C, PAni/Ti20, 0 ˚C and PAni/Ti20, 25 ˚C.

Typically, PAni/Ti20, -5 ˚C was synthesized by employing similar procedure as discussed in Section 3.3.3 up to the addition of TiO_2 nanoparticles. After that, the whole reaction media was transferred into the circulating cooling bath for subzero polymerization temperature (-5 ˚C) with the addition of LiCl (3%) and followed by dropwise addition of APS for 2 h. Then, 24 h polymerization was preceeded under -5 ˚C. PAni/Ti20, 0 ˚C was the similar PAni used in Section 3.3.3. PAni/Ti20, 25 ˚C was synthesized by employing the similar procedure as discussed for PAni/Ti20, -5 ˚C in this Section 3.3.4 but the polymerization was carried out at room temperature which was about ~25 ˚C.

3.4 Characterizations of PAni

3.4.1 Fourier transform infrared (FTIR) spectrometer

Almost any compound having covalent bonds, whether organic or inorganic will absorb various frequencies of electromagnetic radiation in the infrared region of the electromagnetic spectrum. In this study, PAni were characterized by Perkin Elmer RX1 FT-IR equipped with Pike GladiATR Technologies attenuated total reflectance (ATR) spectrometer in the wavenumber range of 400 – 4000 cm^{-1}. PAni was pressed using diamond internal reflection element at ambient temperature. Infrared (IR) light was varied by monochromator and guided through an interferometer after passing the sample and the signal was produced in the interferogram at 4 scans. Finally, the interferograms were analyzed by Spectrum software.

3.4.2 Ultraviolet-visible (UV-Vis) spectrometer

In this study, UV-Vis, UV-1650 PC (Shimadzu) was used to characterize the PAni in the wavelength range of 300 – 900 nm with scan rate of 1.0 nm intervals. The UV-Vis spectrometer consists of two lamps as light source; tungsten lamp that covers from 350 – 1100 nm and deuterium lamp that covers from 190 – 350 nm. Non-coated glass substrate was used in the reference position while PAni coated-glass substrate was used in the sample position. The data acquisition was monitored by Shimadzu UV-Probe Software.

3.4.3 X-ray Diffractometer (XRD)

Non-destructive structural analysis of a material can be done by a diffractometer from the scattering pattern produced when a beam of radiation or particles interacts with the sample. In this study, XRD patterns were obtained using Empyrean X-ray diffractometer, equipped with a Cu target at 40 kV and 40 mA. Vertical goniometer with radius of 240 mm is used to reduce the diffracted beam radius for specific applications in the maximum usable range of $5^\circ < 2\theta < 168^\circ$ with 2θ linearity equal or better than $\pm 0.01^\circ$. PAni were coated on fluorine doped tin oxide (FTO) substrates and the measurements were performed within 2θ range of $5 – 60^\circ$ at scan speed of 2° /min.

3.4.4 Field emission scanning electron microscope (FESEM)

FESEM is one of the first surface analysis instruments that approached near atomic resolution. FESEM is used to investigate molecular surface structures and their electronic properties. Typically, FESEM is a microscope that works with electrons

instead of light. These electrons are liberated by a field emission source and accelerated in a high electrical field gradient. The object is scanned by electrons according to a zig-zag pattern.

The morphology of PAni were investigated by FESEM (Jeol JSM-7600F) with magnification of 20,000 × at an acceleration voltage of ~5 kV. PAni samples were dried in an oven at 60 ˚C (overnight) prior to use in FESEM.

3.4.5 Energy dispersive x-ray spectrometer (EDX)

Energy dispersive x-ray (EDX) analysis which is also known as EDS or EDAX, is an x-ray technique used to identify the elements in a sample. In general, EDX spectrometers are attached to electron microscopy instruments such as scanning electron microscope (SEM), FESEM or transmission electron microscope (TEM). Therefore, EDX can be performed simultaneously with any electron microscopes. In this study, EDX (Oxford Instrument, 50 mm^2) measurements for the elements present in PAni/AOT and PAni/TiO_2 nanocomposites were done in the range of 0 – 6 keV.

3.4.6 Resistivity meter

In this study, Mitsubishi Loresta GP MCP-T600 was used to evaluate the electronic conductivity of PAni. Typically, electronic conductivity of a material is inversely proportional to the resistivity. Anyhow, the electronic conductivity was directly obtained from the resistivity meter as it possesses multiple unit system. In this study, a specific four point probe known as PSP probe with interspin distance of 1.5 mm was used to record the electrical conductivity of PAni. The PSP probe was

pressed gently on three different positions of PAni thin film and the average electrical conductivity was recorded.

3.5 Responses of PAni in hydrazine detection

In this study, all PAni were investigated in hydrazine detection by using UV-Vis responses as main study. Conductivity responses and FTIR structural analysis were used as supporting elements to study the interaction between between PAni and hydrazine.

3.5.1 UV-Vis responses

UV-Vis responses for all PAni were recorded in terms of the effect of time (0 – 5 min) and the effect of hydrazine concentrations (1 – 100 ppm). All measurements were done before and after immersion of PAni in hydrazine solution that carried out in cuvette cells as shown in Figure 3.8.

For the effect of time, UV-Vis absorbances of PAni were monitored in hydrazine detection (1 ppm) at ~780 nm. The absorbances were recorded at 0.12 min (7 s) as immediate response then followed by 5 consecutive measurements up to 5 min.

For the effect of hydrazine concentration, UV-Vis absorbances of PAni were monitored in hydrazine detection (1 – 100 ppm) at 0.12 min. The normalized UV-Vis absorbances were calculated based on Equation 3.2;

$$Normalized\ UV-Vis\ Absorbance = \frac{A_f}{A_i} \quad \text{.....Equation 3.2}$$

where, A_i is the intial absorbance of PAni before immersion in hydrazine solution while A_f is the time dependent absorbance of PAni after immersion in hydrazine. The absorbance values were monitored at π – polaron peak of PAni (~780 nm).

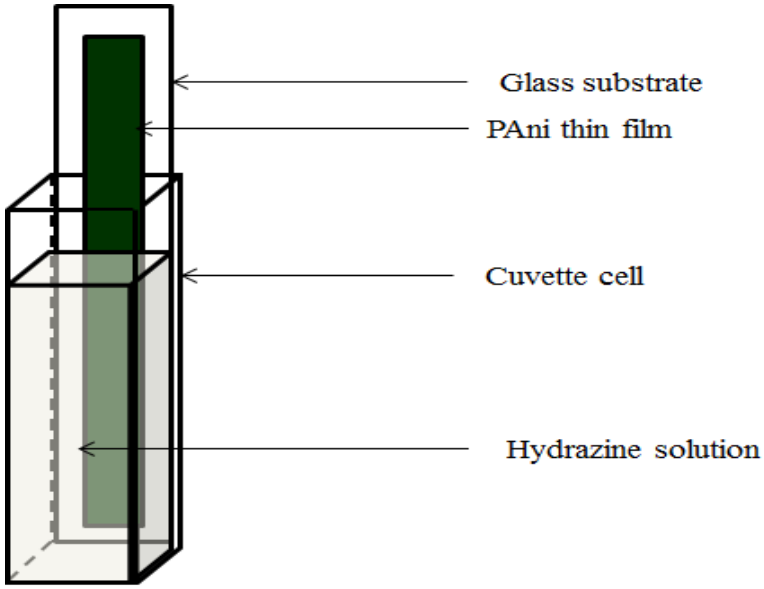

Figure 3.8 Simple PAni sensor setup for hydrazine detection.

3.5.2 Conductivity responses

Conductivity response is one of the supporting elements in this research work to support the UV-Vis response or in other words to understand the interaction between PAni and hydrazine. Conductivity responses were monitered by using resistivity meter equipped with PSP probe. Initially, conductivity responses were done on the effect of immersion time and then followed by effect of hydrazine concentration (1 – 100 ppm) as discussed earlier (Section 3.5.1). The response of PAni in hydrazine detection was evaluated based on equation 3.3;

$$Normalized\ conductivity = \frac{\sigma_f}{\sigma_i}$$ .....Equation 3.3

where, σ_i is the initial conductivity of PAni before immersion in hydrazine while, σ_f is the time dependent conductivity of PAni after immersion in hydrazine. Each measurement was done by employing new PAni thin film to avoid any contamination from the hydrazine residues.

3.5.3 FTIR structural analysis

FTIR structural analysis was performed as another supporting measurement to understand the structural changes that occured during the interaction between PAni and hydrazine. The changes in terms of chemical structure for conducting form of PAni (before immersion) (ES) and non-conducting form of PAni (after immersed in hydrazine) (LE) was evaluated based on equation 3.4;

$$Intensity\ ratio\ of\ \frac{quinoid}{benzenoid} = \frac{I_{\sim 1565}}{I_{\sim 1468}}$$ ……...…Equation 3.4

where, the decrease in the intensity ratio of quinoid/benzenoid shows that ES has transformed into LE upon interaction with hydrazine.

3.6 Sensor performances of PAni/Ti20, -5 ˚C in hydrazine detection

Sensor performances of PAni/Ti20, -5 ˚C (effect of film thickness, reusability, selectivity and long term stability) in hydrazine detection were studied by using UV-Vis spectrometer.

3.6.1 Effect of film thickness

PAni/Ti20, -5 ˚C with various films thicknesses were obtained by multilayer spin coating technique. The first layer was prepared by spin coating ~140 µL of PAni/Ti20, -5 ˚C on a pre-cleaned glass substrate that yielded ~1 µm of film thickness. Similar procedure was repeated for the preparation of multiple film layers such as 2, 3, 4 and 5 layers that possessed average film thicknesses of 3, 5.5, 7 and 9 µm, respectively.

UV-Vis responses of PAni/Ti20, -5 ˚C with different film thicknesses were evaluated by monitoring its absorbance at π – polaron peak (~780 nm) before and after immersion in hydrazine (1 ppm). Equation 3.5 was employed to calculate the response of PAni/Ti20, -5 ˚C with different film thicknesses in hydrazine detection;

$$UV - Vis\ response\ of\ PAni/Ti20, -5\ ^{\circ}C = \frac{A_i}{A_f} \quad \text{.....Equation 3.5}$$

where, A_i is the initial absorbance of PAni/Ti20, -5 ˚C at the π – polaron peak (~780 nm) before immersion in hydrazine while A_f is the absorbance of PAni/Ti20, -5 ˚C after immersion in hydrazine within 0.12 min.

3.6.2 Reusability study

Hereafter, the other sensor performances of PAni/Ti20, -5 ˚C (reusability, selectivity and long term stability) were investigated with film thickness of 1 µm. Reusability study on PAni/Ti20, -5 ˚C was carried out in the presence of 1 ppm of

hydrazine (dedope) and 1 M of HCl (redope). In this reusability study, dissimilar concentration of hydrazine and HCl were selected because 1 ppm of hydrazine is the concentration of hydrazine that needs to be detected. On the other hand, 1 M of HCl was used because; this is the concentration of HCl that used during the polymerization of aniline. Besides, 1M of HCl has resulted in rapid recovery of PAni/Ti20, -5 ˚C in order to be reused in hydrazine detection. Equation 3.2 was used to calculate the normalized UV-Vis absorbance in reusability study.

3.6.3 Selectivity study

The selectivity study of PAni/Ti20, -5 ˚C in hydrazine detection was carried out in the presence of interfering compounds such as 2-propanol, formic acid, ammonia and sodium hydroxide. Similar concentrations of interfering compounds (1 ppm) were used in this selectivity study. Initially, the UV-Vis spectra of PAni/Ti20, -5 ˚C before immersion and after immersion in each interfering compounds were recorded in the range of 450 – 900 nm. Finally, the UV-Vis spectrum of PAni/Ti20, -5 ˚C after immersion in the mixed interfering compounds (with hydrazine) solution was recorded.

3.6.4 Long term stability

Long term stability of PAni/Ti20, -5 ˚C was investigated up to 60 days in hydrazine detection (1 ppm). PAni/Ti20, -5 ˚C was redoped by 1 M of HCl (after each detection) and then stored in an air-tight container. Equation 3.2 was employed to calculate the normalized UV-Vis absorbance.

3.7 Method validation

Method validation is the process used to justify the analytical procedure employed for a specific test or real sample analysis. In this section method validatios of PAni (all best PAni from each section) such as linear range (calibration plot), sensitivity, limit of detection (LOD), limit of quantitation (LOQ), recovery and relative standard deviation (RSD), were incorporated.

Linear ranges of PAni were demonstrated in calibration curves that have been plotted as –log Absorbance versus hydrazine concentration range of 0.05 – 5.00 ppm. In this section, –log Absorbance was used as a response in order to obtain a positive gradient (slope) in the calibration plot. Besides, the slope of linear equation showed the sensitivity of PAni that studied in hydrazine detection (0.05 – 5.00 ppm) (Chakraborty and Raj, 2010).

The standard deviation (SD) was calculated based on the absorbance value of blank (non-coated glass substrate) at ~780 nm in the UV-Vis spectrum. Ten measurements (absorbances) of distinctive glass substrated were taken and applied in Equation 3.6;

$$\mathrm{SD} = \sqrt{\frac{\sum(\times - \bar{\times})^2}{\mathrm{n}-1}} \quad \text{..... Equation 3.6,}$$

Where, $\times$ and $\bar{\times}$ is the absorbance of non-coated glass substrate at ~780 nm and average reading of ten measurements, respectively. ‘n’ shows the sample size (n = 10) of the measurements. Distilled water was used as blank for the SD measurement. The SD that obtained in this study is 0.000857.

Low range of hydrazine concentration (0.05 – 5.00 ppm) was selected to achieve lower limit of detection (LOD) and limit of quantitation (LOQ). LOD and LOQ of PAni/Ti20, -5 ˚C were calculated based on Equation 3.7 and 3.8, respectively (Mahmoudian et al., 2013);

$$LOD = \frac{(3 \times SD)}{slope\ of\ calibration\ curve} \quad \text{Equation 3.7}$$

$$LOQ = \frac{(10 \times SD)}{slope\ of\ calibration\ curve} \quad \text{Equation 3.8}$$

3.8 Real sample analysis

Real sample analysis of PAni/Ti20, -5 ˚C in hydrazine detection was done with two different water samples that collected from polymer research laboratory and river (Sungai Batu) that passess by rubber factory, heavy construction and some residential areas. Known concentration of hydrazine (0.50, 1.00 and 4.00 ppm) was spiked into the real sample and the recoveries were calculated by using UV-Vis analysis. Recoveries and relative standard deviation (RSD) were calculated based on Equations 3.9 and 3.10, respectively (Yanling Gao et al., 2008);

$$Rocovery = \frac{Amount\ of\ hydrazine\ found}{Amount\ of\ hydrazine\ spiked} \times 100\% \quad \text{Equation 3.9}$$

$$RSD = \left(\frac{SD}{\bar{x}}\right) \times 100\% \quad \text{Equation 3.10}$$

CHAPTER 4 RESULTS AND DISCUSSION

4.1 PAni/AOT (different dopant ratio) in hydrazine detection

Among all CPs, polyaniline (PAni) has received widespread attraction due to its ease of synthesis (Wang et al., 2013), high conductivity, low cost and good environmental stability (Wang et al., 2009). However, the great potential of PAni was masked by its serious disadvantages such as insolubility, infusibility and hence, poor processability (Saïdi et al., 2014). Attempts have been made to improve its solubility, by doping PAni with suitable surfactants, such as sodium dodecyl sulfate (SDS), dodecylbenzenesulphonic acid (DBSA), camphor sulphonic acid (CSA) (Cao et al., 1992) and etc. Among all surfactants, sodium dioctyl sulfosuccinate (AOT) dopant has been chosen in this study due to the presence of alkyl chain and sulphonyl group (SO_4^{2-}) that will enhance the solubility of PAni in both aqueous medium (Sayyed and Maldar, 2010) and organic solvents (Zou et al., 2013), respectively. Besides, fewer reports are found on the incorporation of PAni with AOT dopant up to date.

4.1.1 Characterizations of PAni/AOT (different dopant ratio)

PAni/AOT was synthesized at different Ani:AOT ratio of 5:3, 5:5 and 5:7 as described in Table 3.1 that labelled as PAni **1**, PAni **2** and PAni **3**, respectively. The chemical structure, morphology and conductivity of PAni/AOT with different dopant ratio were characterized by using FTIR and UV-Vis spectrometers, XRD, FESEM coupled with EDX analyser and resistivity meter.

4.1.1 (a) FTIR analysis

FTIR spectra of PAni **1**, PAni **2** and PAni **3** that measured in the wavenumber range of 400 – 4000 cm^{-1} were shown in Appendix A1. In general, all PAni exhibited broad transmission band at wavenumbers higher than 2000 cm^{-1} which indicate the typical form of conducting state of PAni. Similar phenomenon was observed by Epstein et al., (1987) and Ping (1996). Thus, the discussion for FTIR spectra of PAni **1**, PAni **2** and PAni **3** in this study was focused at wavenumber range of 400 – 2000 cm^{-1} as shown in Figure 4.1.

In general, FTIR spectra of PAni **1** – **3** exhibited almost identical peaks in the wavenumber range of 400 – 2000 cm^{-1}. The peaks at 773 – 788 cm^{-1} and 895 – 899 cm^{-1} attributed to the C-H bending vibration of para substituted aromatic ring and C=C vibration, respectively. The peak at 1178 – 1183 cm^{-1} explicated S=O of symmetric and asymmetric stretching from AOT dopant (Cao et al., 1992; Wang et al., 2009). The peaks observed at 1217 – 1228 cm^{-1} were attributed to C-N stretching (Gupta et al., 2011) while the peaks at 1544 – 1574 cm^{-1} and 1612 – 1630 cm^{-1} were corresponded to benzenoid and quinoid vibration mode of PAni, respectively (Choudhury, 2009). The peaks observed at 1740 – 1742 cm^{-1} were due to the C=O from AOT dopant (Park et al., 2009). The distinctive peaks corresponding to each functional group for all PAni are summarized in Table 4.1.

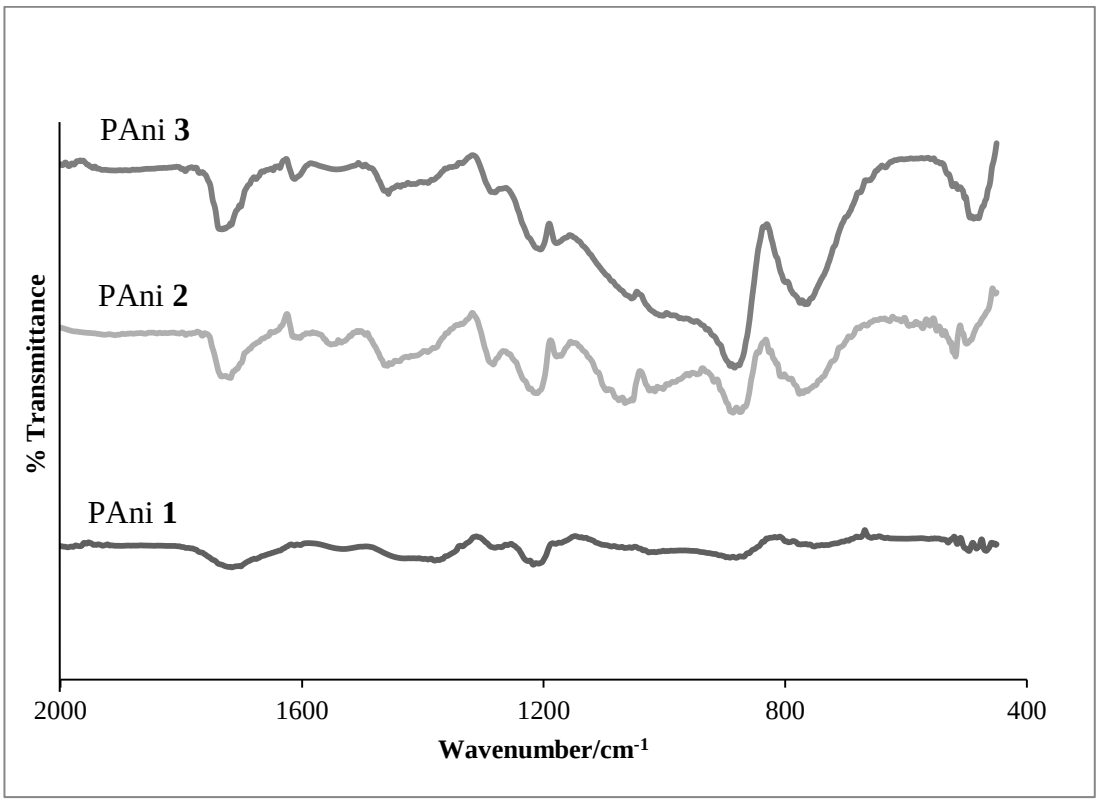

Figure 4.1 FTIR spectra of PAni **1**, PAni **2** and PAni **3**.

Table 4.1 Distinctive peaks of PAni synthesized with different dopant ratio.

Functional groups	Wavenumber (cm^{-1})		
	PAni **1**	PAni **2**	PAni **3**
C-H vibration	773	787	788
C=C vibration	895	898	899
S=O vibration	1183	1188	1178
C-N stretching	1217	1220	1228
Benzenoid	1544	1570	1574
Quinoid	1612	1620	1630
C=O	1740	1742	1742

4.1.1 (b) UV-Vis analysis

Figure 4.2 shows the UV-Vis spectra of PAni **1**, PAni **2** and PAni **3** in the wavelength range of 300 – 900 nm. In general, PAni **1** – **3** exhibits similar characteristic peaks at ~347 – 354 nm, ~428 – 432 nm and ~776 – 790 nm as shown in Table 4.2. The absorbance peak at ~347 – 354 nm is attributed to π – π* conjugation that found in benzenoid units of PAni. Shoulder peak at ~415 nm is credited to polaron – π* that shows the PAni exist in conducting form (emeraldine salt-ES) (Yang et al., 2007). Both peaks at ~347 – 354 nm and ~428 – 432 nm are overlapped and created a flat or distorted peak that indicates high level of doping (Moulton et al., 2004). Finally, the last peak at ~776 – 790 nm is ascribed to π – polaron that resembles the doped state of quinoid cations (Zheng and Song, 2009).

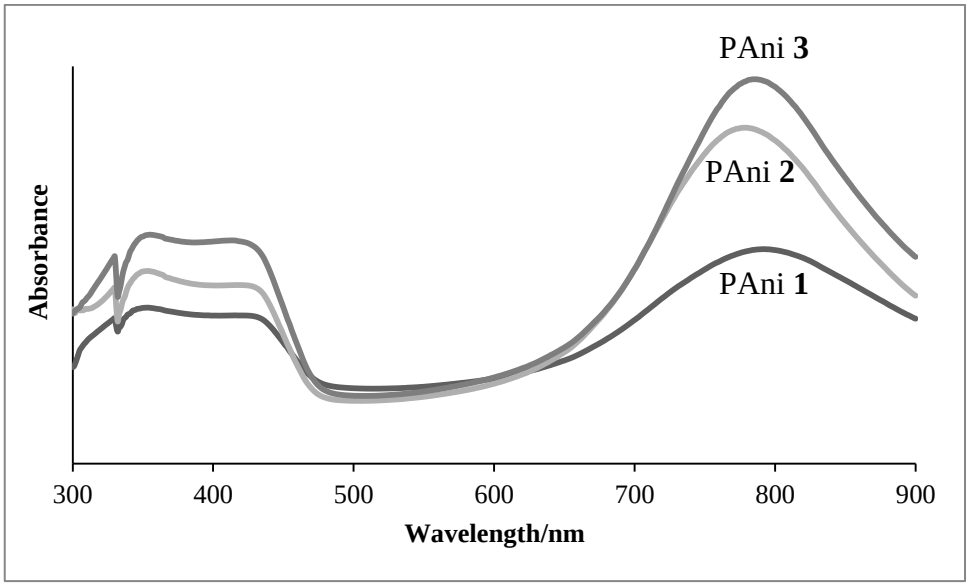

Figure 4.2 UV-Vis spectra of PAni **1**, PAni **2** and PAni **3**.

Table 4.2 The assignments of UV-Vis absorbance peaks for PAni synthesized with different dopant ratio.

PAni	$\pi - \pi^*$ (nm)	polaron – π^* (nm)	π – polaron (nm)
PAni **1**	347	432	790
PAni **2**	350	428	776
PAni **3**	354	425	780

4.1.1 (c) XRD analysis

X-ray diffractograms of PAni **1**, PAni **2** and PAni **3** doped with different dopant ratio are shown in Figure 4.3. In general, all PAni exhibited similar amorphous behavior in 2θ range of 5 – 65˚. PAni **1** – **3** show two broad peaks at 2θ = 14.4˚ and 25.1˚ that corresponding to the repetition units of Ani monomers and the densely packed phenyl rings, respectively (Chaudhari and Kelkar, 1997; Wu et al., 2005). Besides, another broad peak centered at 2θ = 19.7˚ indicates the effective doping of AOT dopant (Amrithesh et al., 2008; Trchová et al., 2006). Among all PAni, PAni **3** possesses the highest peak at 19.7˚ that explicate the most efficient doping in the emeraldine salt (ES) state of PAni which is in good agreement with the conductivity data (Table 4.3).

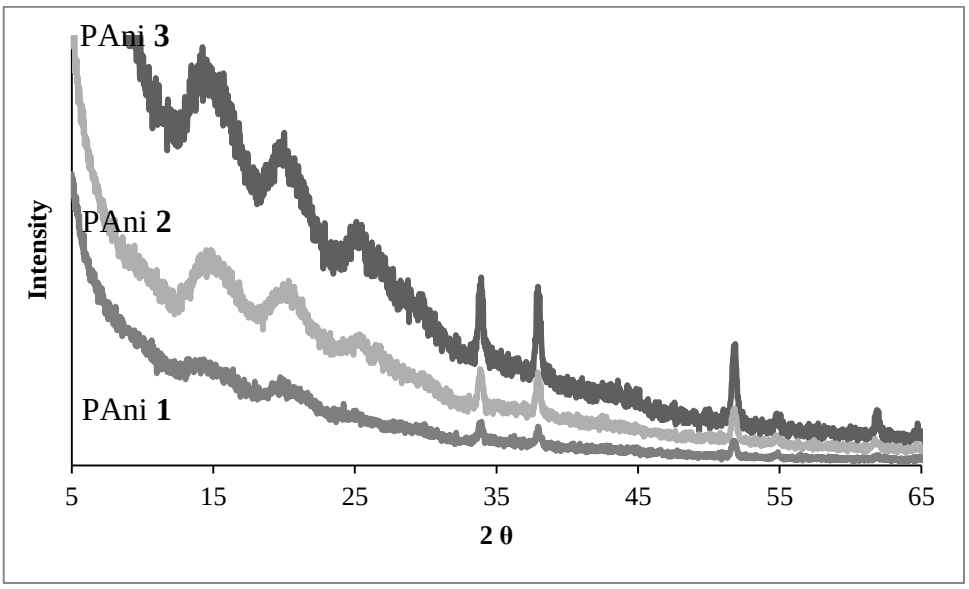

Figure 4.3 X-ray diffractograms of PAni **1**, PAni **2** and PAni **3**.

4.1.1 (d) FESEM analysis

Figure 4.4 (a)-(c) shows the FESEM images of PAni **1**, PAni **2** and PAni **3**, respectively with magnification of 20,000 × while Figure 4.4 (d) shows the morphology of PAni **3** from a distant-view with magnification of 2,500 ×. PAni **1** shows an irregular granular shape with dimensions of 100 – 600 nm. Based on previous study, granular shape is the most common morphology of PAni that prepared in a typical polymerization (Mazerolles et al., 1999). However, PAni **2** (Figure 4.4 (b)) and PAni **3** (Figure 4.4 (c)) exhibited the fibrillar structure that interconnects the PAni chains, thus reduce the electron hopping distance along the PAni backbone. Moreover, the stacking of PAni layers (PAni **3**) as shown in Figure 4.4 (d) will significantly produce the efficient electron hopping (Mi et al., 2014) that will induce higher conductivity (Table 4.3) compare to others PAni.

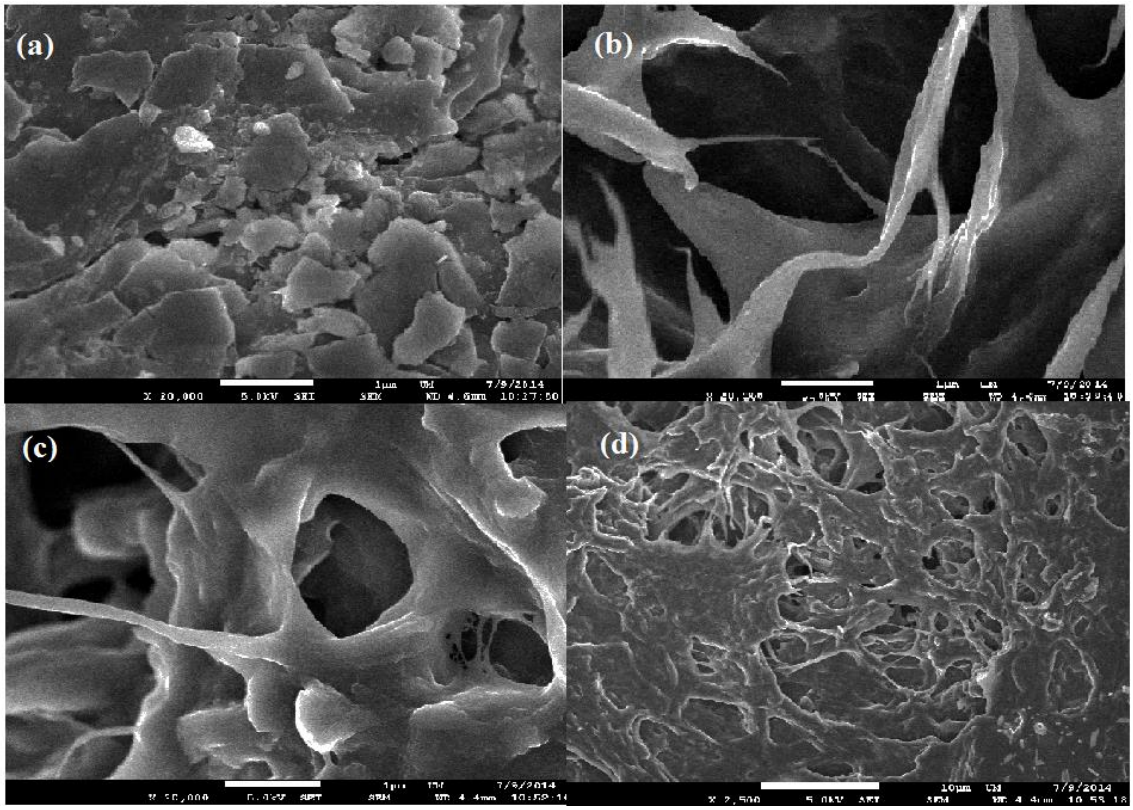

Figure 4.4 FESEM images of (a) PAni **1**, (b) PAni **2** and (c) PAni **3** at magnification of 20,000 × and (d) PAni **3** with magnification of 2,500 ×.

4.1.1 (e) EDX analysis

In this study, PAni **1** – **3** possess the similar EDX spectra in the range of 0 – 6 keV as shown in Figure 4.5. In general, all PAni show the signal of Carbon (C) at 0.25 keV and Nitrogen (N) at 0.40 keV as the characteristic peaks. The signals of Oxygen (O) at 0.53 keV and Sulphur (S) at 2.34 keV indicates that the PAni has been successfully doped by the AOT dopant (Abaci et al., 2011). However, the weak signal of Chlorine (Cl) at 2.62 keV indicates the impurities from the polymerization medium (HCl).

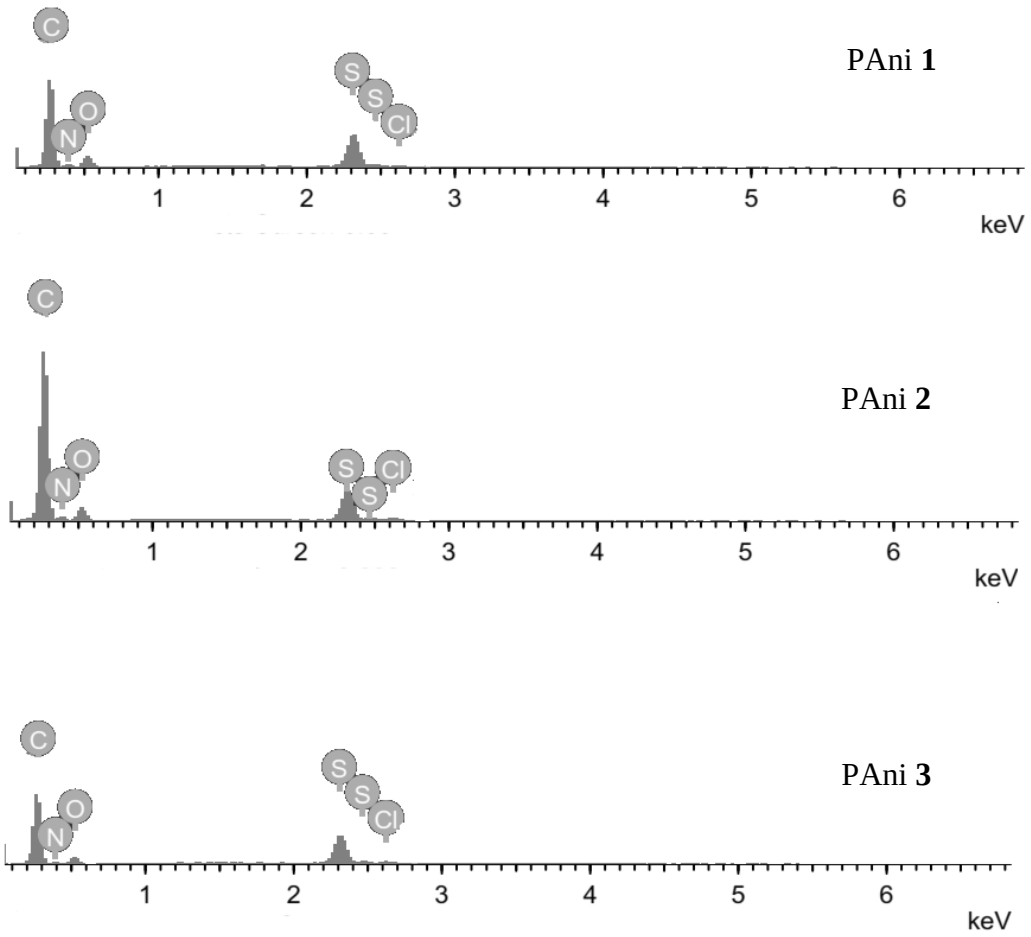

Figure 4.5 EDX spectra of PAni **1**, PAni **2** and PAni **3** synthesized at 0 ˚C.

4.1.1 (f) Conductivity analysis

The conductivities of PAni **1**, PAni **2** and PAni **3** synthesized with different dopant ratio were 0.420 S/cm, 0.580 S/cm and 0.820 S/cm, respectively (Table 4.3). In general, conductivity of PAni increase with the increase in AOT dopant ratio from PAni **1** to PAni **3**. It is because, PAni doped with higher dopant ratio significantly enhanced the mobility of charge carriers (delocalization of polarons) along the PAni chains, thus increased the conductivity of the resulting PAni (Bhadra et al., 2007).

Based on the FTIR spectra in Figure 4.1, the intensity of quinoid peak increased with ascending order of PAni **1** < PAni **2** < PAni **3** suggesting that the number of quinoid rings along the PAni chain increases with respect to the dopant ratio. Hence, there may be a greater chance for PAni with higher dopant ratio exist in the conducting state (ES) (Tung et al., 2010). Besides, sulphonyl group from AOT dopant that used in this study not only improve the solubility of PAni in toluene but also enhanced the conductivity of PAni obtained (Cao and Smith, 1993; Zou et al., 2013). This phenomenon is in good agreement with previous research done by Qiang and co-workers (2014). In addition, the stacking of PAni layers in PAni **3** as shown in Figure 4.4 (d) has led to the efficient electron hopping along the PAni backbone that resulted in the highest conductivity.

Table 4.3 Conductivities of PAni/AOT synthesized with different dopant ratio.

Polymer	Conductivity (S/cm)
PAni **1**	0.420
PAni **2**	0.580
PAni **3**	0.820

4.1.2 Responses of PAni/AOT (different dopant ratio) sensors in hydrazine detection

In this part, PAni/AOT with different dopant ratio are monitored in hydrazine detection by using UV-Vis responses as main study. Conductivity responses and FTIR structural analysis were used as the supporting element to investigate the interaction between PAni and hydrazine. All measurements were taken before and after immersion of PAni in hydrazine (1 – 100 ppm).

4.1.2 (a) UV-Vis responses

Figure 4.7 shows the normalized UV-Vis absorbance of PAni in hydrazine detection (1 ppm) between 0 – 5 min. The optimum immersion time or in another word, the shortest response time of hydrazine detection by using PAni/AOT with different dopant ratio were investigated between 0 – 5 min. From the normalized UV-Vis absorbance, A_i is the initial absorbance of PAni before immersion in hydrazine, while A_f is the time dependent absorbance of PAni after immersion in hydrazine. The normalized UV-Vis absorbance as shown in Figure 4.6 are calculated based on the absorbance of PAni (polaron – π^*) peak at ~776 – 790 nm (Inset of Figure 4.6) before and after immersion in hydrazine by employing Equation 3.2.

In general, the normalized UV-Vis absorbances of all PAni with different dopant ratio decrease with increasing of time in hydrazine detection. It is because, before immersion in hydrazine, PAni exists in the conducting state (ES) that possess numerous free charge carriers. However, the free charge carriers along the PAni backbone will be removed after the dedoping process by hydrazine (reducing agent). Therefore, the decrease in polaron absorbance peak (~776 – 790 nm) from UV-Vis spectra (Figure 4.6) can be expected as the ES will be converted into non-conducting form of PAni (leucoemeraldine-LE) as shown in Figure 4.7 (Yoon et al., 2011).

All PAni show decrease in normalized UV-Vis absorbance at 0.12 min (immediate response time) followed by gradual decrease (after 0.12 min) in hydrazine detection. Typically, PAni **3** shows significant decrease in the normalized UV-Vis absorbance at 0.12 min compare to PAni **1** and PAni **2**.

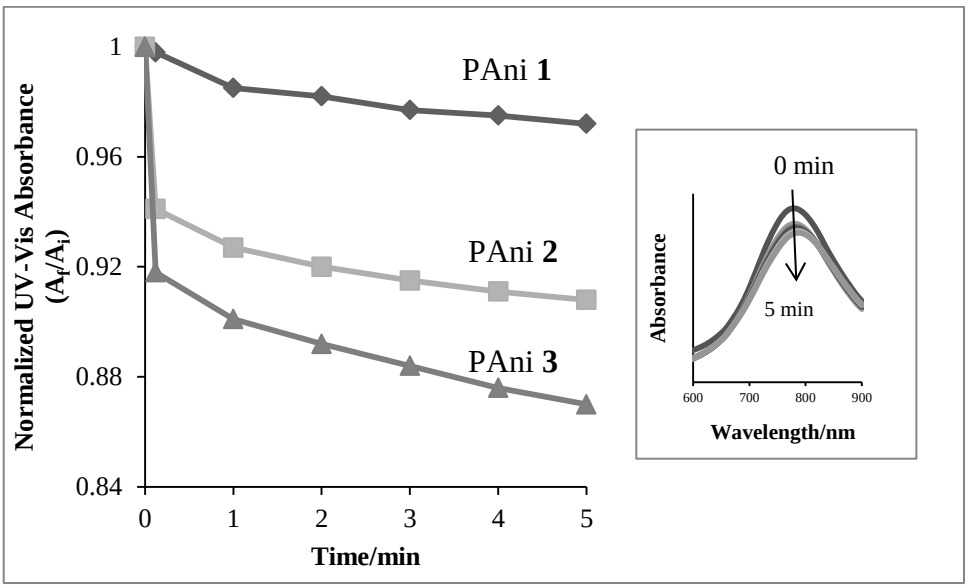

Figure 4.6 Normalized UV-Vis absorbance of PAni **1**, PAni **2** and PAni **3** for hydrazine detection (1 ppm) between 0 – 5 min. (Inset: The absorbance peak of PAni **3** at ~780 nm in hydrazine detection).

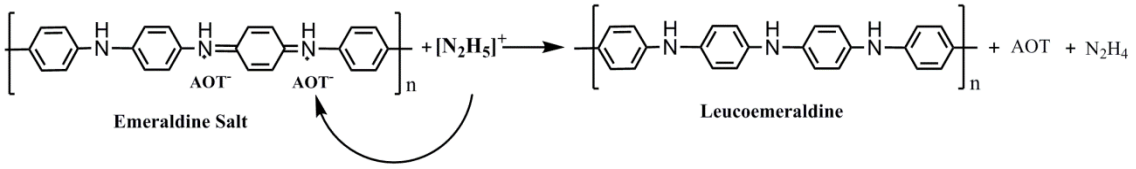

Figure 4.7 Interaction of ES with hydrazine to form LE.

Figure 4.8 shows the normalized UV-Vis absorbance of PAni **1**, PAni **2** and PAni **3** in different concentration of hydrazine (1 – 100 ppm). Among all PAni, PAni **3** exhibits the significant decrease in normalized UV-Vis absorbance because higher amount of dopant ratio possess higher amount of reactive sites for the interaction of hydrazine, thus improve the sensitivity in hydrazine detection (Kar and Choudhury, 2013). Hence, it can be said, higher degree of doping in PAni will eventually improve the sensitivity of PAni in hydrazine detection. On the other hand, PAni was effectively

dedoped at highest concentration (100 ppm) of hydrazine due to the presence of prominent amount of hydrazinium species in the reaction media (Ameen et al., 2012).

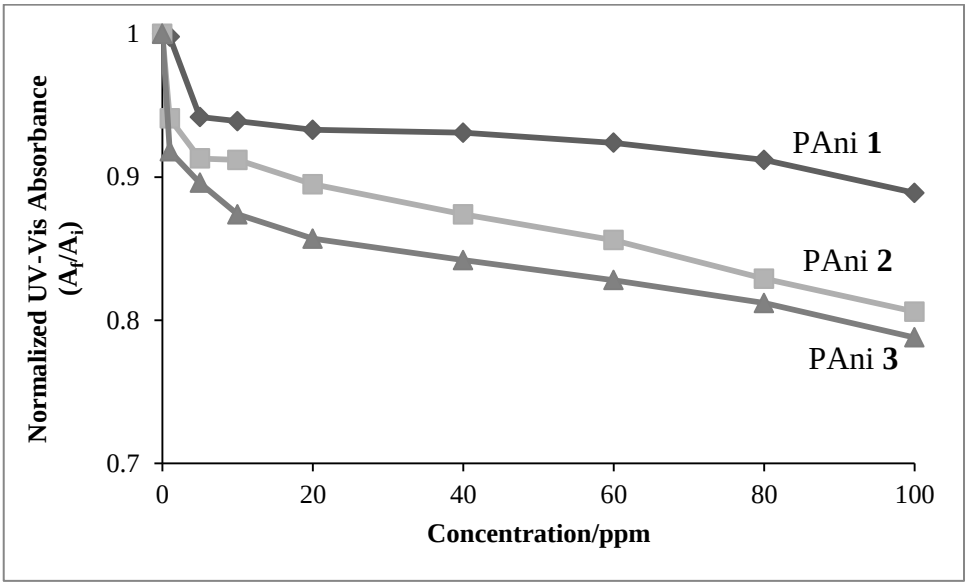

Figure 4.8 Normalized UV-Vis absorbance of PAni **1**, PAni **2** and PAni **3** in different concentration of hydrazine detection (1 – 100 ppm).

4.1.2 (b) Conductivity responses

The optimum immersion time for hydrazine detection (1 ppm) in terms of conductivity response by using PAni **1**, PAni **2** and PAni **3** were investigated between 0 – 5 min as shown in Figure 4.9. σ_i is the conductivity of PAni before immersion in hydrazine, while σ_f is time dependent conductivity of PAni after immersion in hydrazine. Normalized conductivity is calculated based on Equation 3.3. In essence, all PAni exhibit decrease in normalized conductivity within 0 – 5 min due to the removal of free charge carriers from ES backbone by hydrazine to produce LE (Figure 4.7) (Qi et al., 2014; Virji et al., 2004).

In Figure 4.9, it seems the decrements at 0.12 min are 0.02, 0.10 and 0.50 for PAni 1, PAni 2 and PAni 3, respectively. Among all PAni, PAni **3** showed significant decrease in normalized conductivity upon immersion in 1 ppm of hydrazine due to the higher number of charge carriers that can be readily dedoped by hydrazine to transform ES to LE (Figure 4.7). In addition, the presence of large number of AOT dopant as surfactant would bring the conducting islands more closely which will minimize the electron hopping band gap and thus eventually improve the interaction between PAni **3** and hydrazine (Gill et al., 2010).

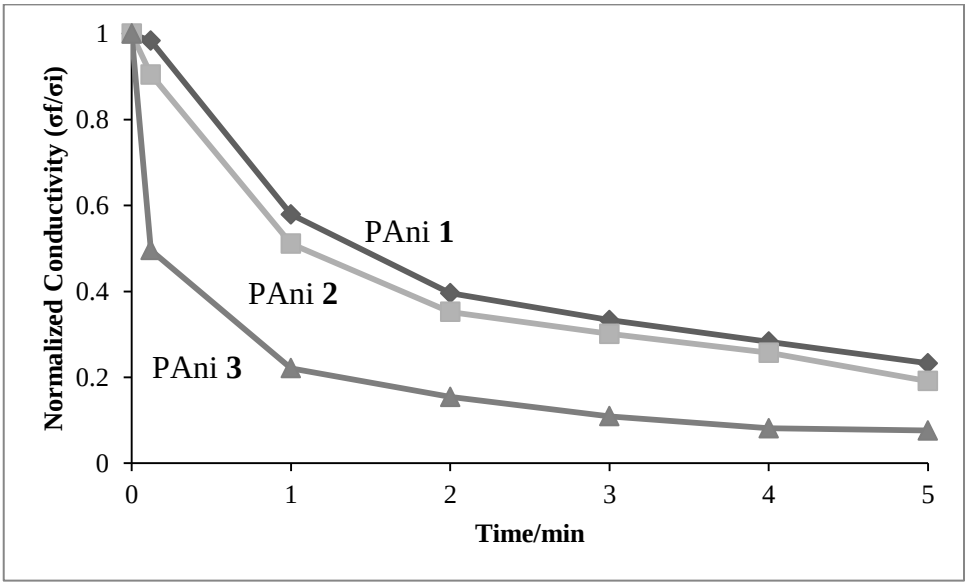

Figure 4.9 Normalized conductivity of PAni **1**, PAni **2** and PAni **3** for hydrazine detection (1 ppm).

Other than that, Figure 4.10 shows the normalized conductivity of PAni **1** – PAni **3** in different concentration of hydrazine (1 – 100 ppm) that recorded at 0.12 min (immediate response). Figure 4.10 mimicked almost similar pattern as shown by Figure 4.9 where PAni **3** underwent significant decrease in normalized conductivity compare to the PAni **1** and PAni **2** when the concentration of hydrazine increased. PAni **1** and PAni **2** that composed of less amount of AOT dopant could not perform as well as

PAni **3** due to the limited reactive sites that present in the PAni **1** and PAni **2** backbone for the interaction with hydrazine (Virji et al., 2005).

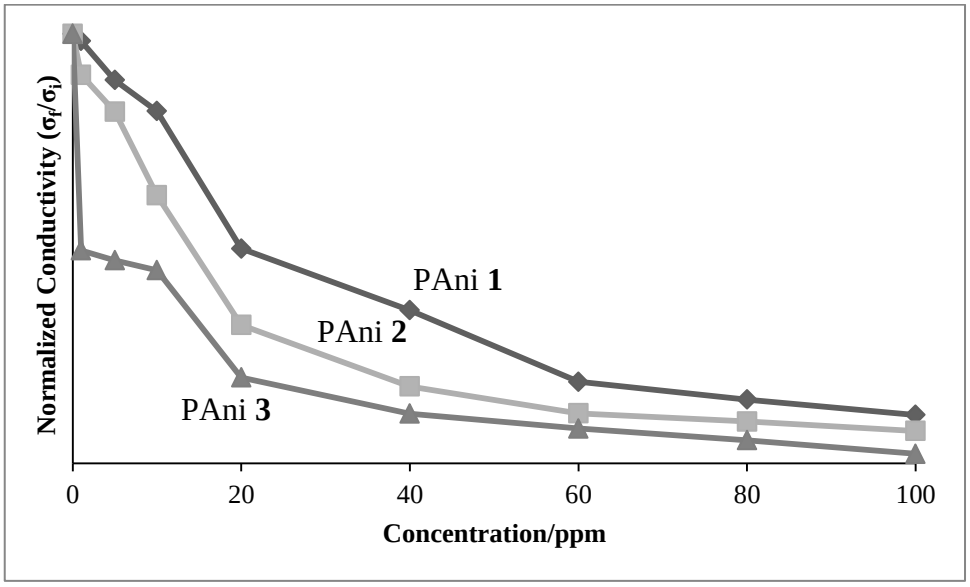

Figure 4.10 Normalized conductivity of PAni **1**, PAni **2** and PAni **3** in detection of hydrazine (1 – 100 ppm) at 0.12 min (immediate response).

4.1.2 (c) FTIR structural analysis

Among all PAni synthesized with different dopant ratio, PAni **3** was chosen to study the structural changes that occurred between PAni and hydrazine due to its excellent performance in hydrazine detection. Besides showing the functional groups present in a compound, FTIR also can be a useful tool in determining the structural changes that take place during a chemical interaction. Figure 4.11 demonstrates the FTIR spectra of PAni **3** before and after immersion in 1 ppm of hydrazine. The FTIR spectra were measured at 0.12 min (response time) to observe the structural changes of PAni **3** upon immediate interaction with hydrazine. In addition, ES possess equivalent benzenoid and quinoids units in the half oxidized state. Once the ES reacts with hydrazine, the quinoids will be converted into benzenoids to form the LE.

Predominating benzenoid (Figure 4.7) units can be indicated by the decrease in intensity ratio of I_Q/I_B (I_{1612}/I_{1520}) (Yoon et al., 2011).

The intensity ratio of quinoid and benzenoid stretching at 1612 cm^{-1} and 1544 cm^{-1}, respectively were taken into consideration to get a better understanding in its structural changes upon interaction with hydrazine (Choi et al., 2008). The intensity ratio of I_Q/I_B was calculated based on the equation 3.5 (Section 3.5.3).

The intensity ratio of PAni **3** before immersion was recorded to be 1.00 and after immersion in 1 ppm of hydrazine was 0.98. The slight decrease in I_{1612}/I_{1520} was caused by the structural changes of ES to LE (Figure 4.7).

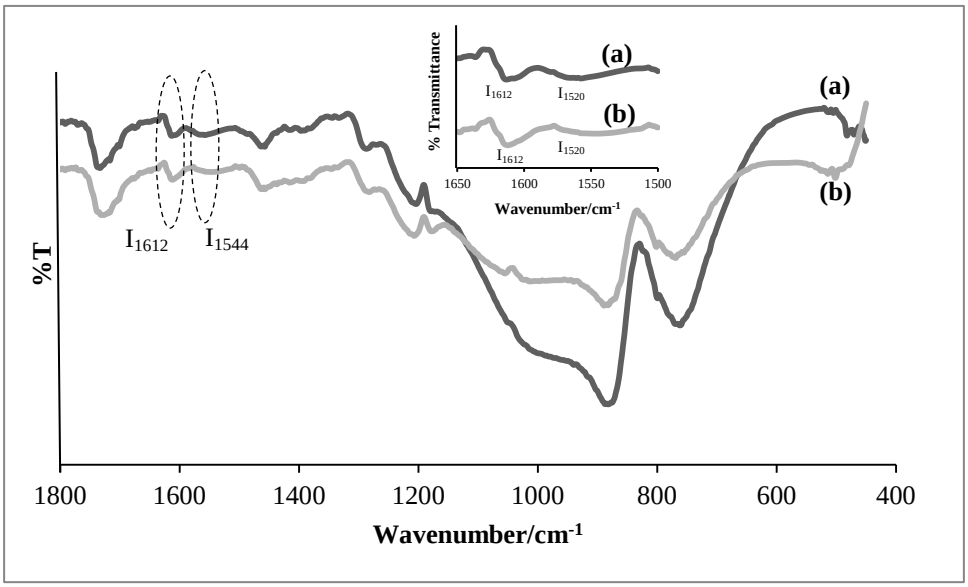

Figure 4.11 FTIR spectra of PAni **3** (a) before and (b) after immersion in 1 ppm of hydrazine (Inset: Intensity of I_{1612} and I_{1520}).

Figure 4.12 depicts the schematic diagram of PAni/AOT that synthesized with different dopant ratio. PAni **3** contains numerous reactive sites (AOT dopant) compare

to PAni **1** and PAni **2** as proved by the highest polaron peak at ~780 nm in Figure 4.2. Thus, the best sensor response of PAni **3** as shown in UV-Vis (Figure 4.7 and Figure 4.8) and conductivity (Figure 4.9 and Figure 4.10) measurements are due to the highest reactive sites (AOT dopant) that induce more interaction between the hydrazine and PAni.

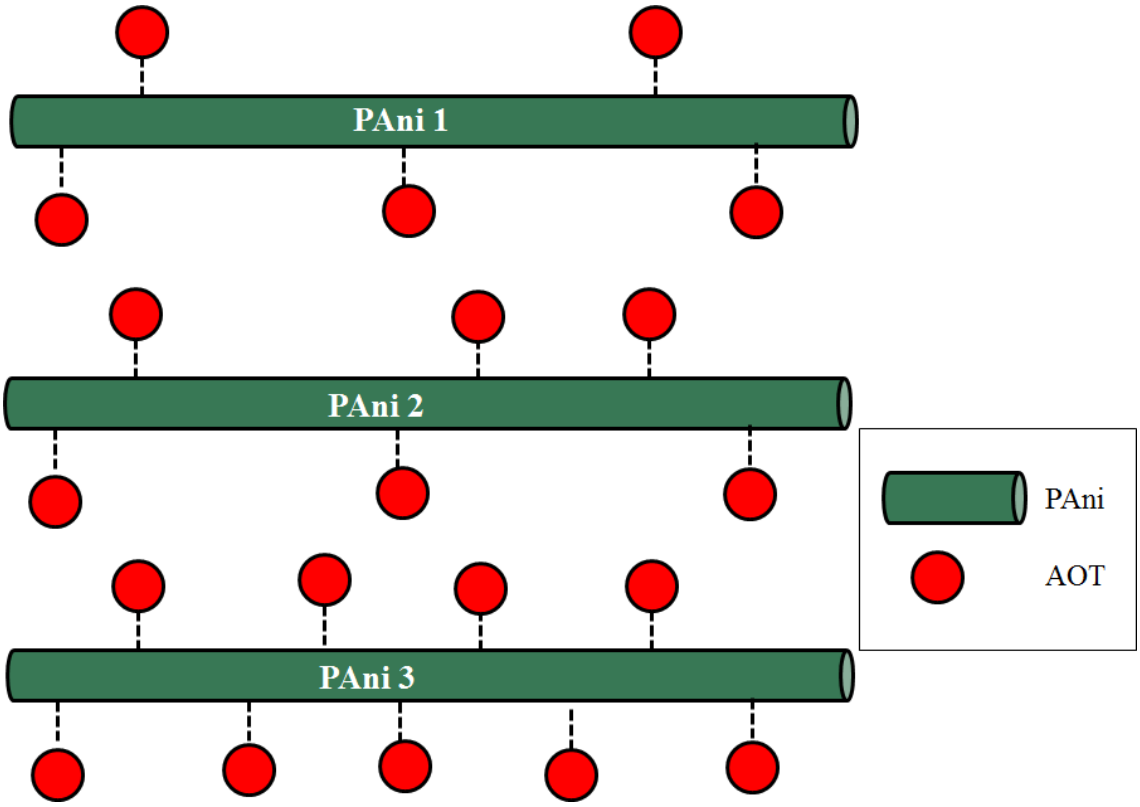

Figure 4.12 Schematic diagram of PAni/AOT that synthesized with different dopant ratio.

4.2 PAni/AOT (different polymerization temperature) in hydrazine detection

In principle, polymerization of Ani by chemical oxidation in the presence of APS would release heat that can influence the structure and properties of PAni (Fu and Elsenbaumer, 1994). However, investigation on the effect of polymerization temperature on the performance of PAni chemical sensor is rarely reported (Bláha et al, 2013). Thus, manipulation of polymerization temperature in producing PAni with crystalline and long chained structure is the paramount interest of this section.

4.2.1 Characterizations of PAni/AOT (different polymerization temperature)

In this part, PAni has been synthesized at various polymerization temperatures such as -10, -5, 0 and 25 ˚C with Ani:AOT ratio of 5:7. The Ani:AOT ratio of 5:7 was chosen since PAni **3** has shown the best performance in hydrazine detection among the PAni **1** and PAni **2**. PAni, 0 ˚C is similar as the PAni **3** that prepared in the section 4.1. In this section, PAni synthesized with different polymerization temperatures were labelled as PAni, -10 ˚C, PAni, -5 ˚C, PAni, 0 ˚C and PAni, 25 ˚C.

4.2.1 (a) FTIR analysis

Figure 4.13 shows the FTIR spectra of PAni that synthesized at various polymerization temperatures. In general, all PAni showed similar functional groups as PAni with different dopant ratio in Figure 4.1. Thus, characteristic peaks of PAni with different polymerization temperatures are not discussed in this section. However, the distinctive peaks for PAni synthesized at different polymerization temperatures are summarized in Table 4.4.

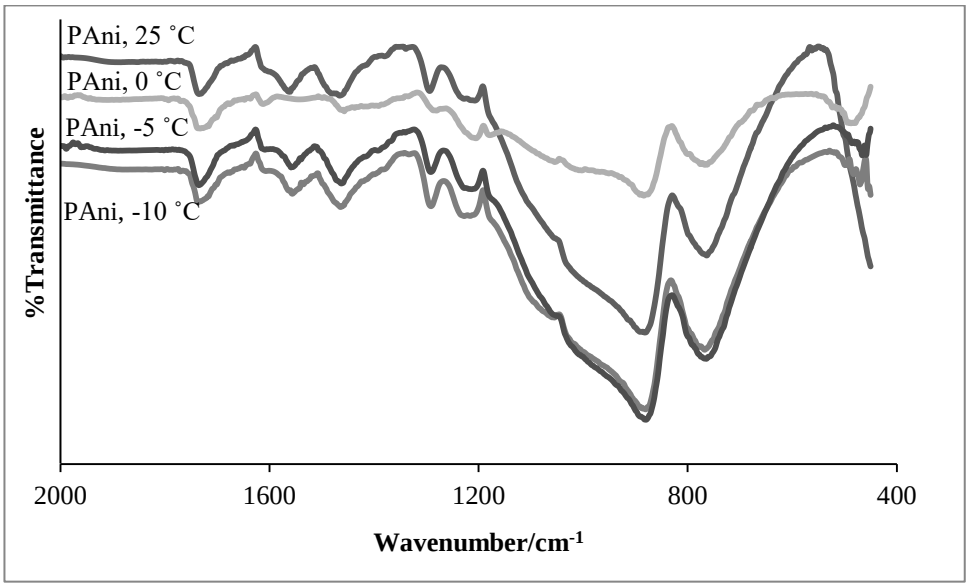

Figure 4.13 FTIR spectra of PAni, -10 ˚C, PAni, -5 ˚C, PAni, 0 ˚C and PAni, 25 ˚C.

Table 4.4 Distinctive peaks of PAni synthesized at different polymerization temperatures

Functional groups	Wavenumber (cm^{-1})			
	PAni, -10 ˚C	PAni, -5 ˚C	PAni, 0 ˚C	PAni, 25 ˚C
C-H vibration	782	772	788	756
C=C vibration	875	880	899	896
S=O vibration	1183	1183	1178	1180
C-N stretching	1230	1217	1228	1236
Benzenoid	1457	1468	1574	1483
Quinoid	1563	1565	1630	1572
C=O	1727	1752	1742	1740

4.2.1 (b) UV-Vis analysis

UV-Vis spectra of PAni that synthesized at various polymerization temperatures are demonstrated in Figure 4.14. In principle, all PAni have shown similar pattern as PAni with different dopant ratio (Figure 4.2). The distinctive peaks of PAni synthesized at various polymerization temperatures are summarized in Table 4.5.

According to the previous research, the higher the absorbance value at π – polaron (~779 – 786 nm) peak, the higher the doping level in the ES state (Xia and Wang, 2001). It can be clearly seen that PAni, -5 ˚C possessed the highest degree of doping extension followed by PAni, 0 ˚C, PAni, -10 ˚C and PAni, 25 ˚C. In essence, doping level will increase with the decrement of polymerization temperature during the PAni synthesis. Altough PAni, -10 ˚C was synthesized at the lowest sub-zero temperature, the addition of LiCl in excess during polymerization (to prevent the freezing) may caused the significant ring chlorination along the PAni backbone, thus reduced the doping level (Yang et al., 2009). Meanwhile, PAni, 25 ˚C that synthesized at higher temperature presumably contained numerous defect sites and thus less eventually decreased the conductivity of PAni, 25 ˚C (Table 4.6) (Bláha et al., 2013).

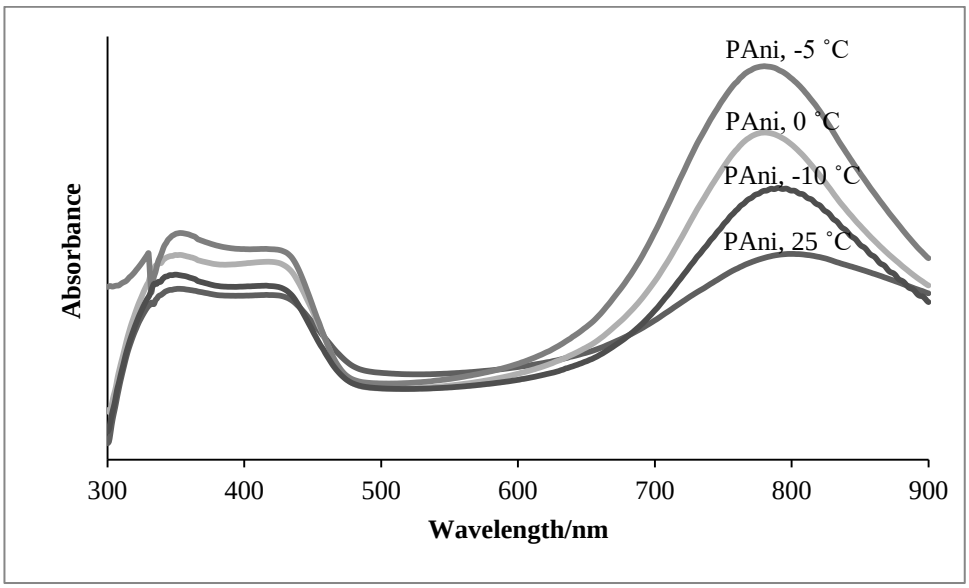

Figure 4.14 UV-Vis spectra of PAni, -10 ˚C, PAni, -5 ˚C, PAni, 0 ˚C, and PAni, 25 ˚C.

Table 4.5 The assignments of UV-Vis absorption peaks for PAni synthesized at different polymerization temperature

PAni	π – π* (nm)	polaron – π* (nm)	π – polaron (nm)
PAni, -10 ˚C	347	430	779
PAni, -5 ˚C	350	428	786
PAni, 0 ˚C	354	425	780
PAni, 25 ˚C	340	430	782

4.2.1 (c) XRD analysis

Figure 4.15 shows the x-ray diffractograms of PAni, -10 ˚C, PAni, -5 ˚C, PAni, 0 ˚C and PAni, 25 ˚C. PAni synthesized with different polymerization temperatures possess similar peaks as PAni in Section 4.1.1 (c) except for the absence of two crystalline peaks at 2θ = 34˚ and 38˚ in PAni, 25 ˚C. However, the sharp peaks at 2θ =

34˚ and 38˚ for PAni, -10 ˚C, PAni, -5 ˚C and PAni, 0 ˚C show crystalline phases meanwhile PAni, 25 ˚C shows amorphous behavior in x-ray diffractogram.

The sharp peaks as indicated by PAni, -10 ˚C, PAni, -5 ˚C and PAni, 0 ˚C could display a metallic-like conductive state when synthesized at subzero polymerization temperatures (Li et al., 1993). Therefore, understanding on the relationship between XRD patterns and polymerization temperature are important to draw the conclusion on the conductivity of PAni. The obtained x-ray diffractogram is well supported by the conductivity analysis as shown by Table 4.6.

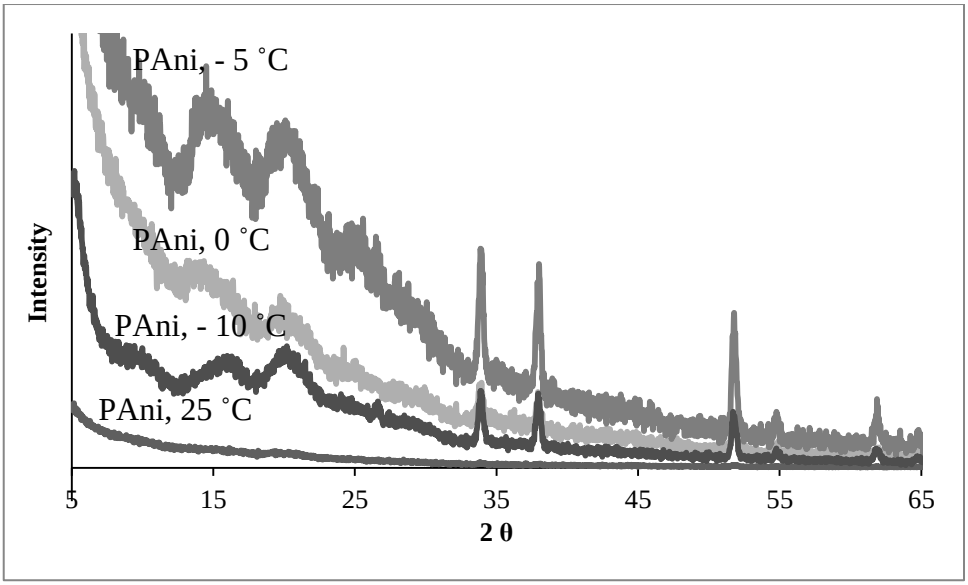

Figure 4.15 XRD patterns of PAni, -10 ˚C, PAni, -5 ˚C, PAni, 0 ˚C and PAni, 25 ˚C.

4.2.1 (d) FESEM analysis

In general, morphology studies may provide better understanding on the growth of PAni chains during polymerization. Temperature directed polymerization of PAni would play an important role in determining the physical properties of PAni such as

crystallinity and conductivity that can affect the performance of PAni sensor. Figure 4.16 depicts the morphology of PAni, -10 ˚C, PAni, -5 ˚C, PAni, 0 ˚C and PAni, 25 ˚C with magnification of 20,000 ×. PAni, 25 ˚C and PAni, -10 ˚C showed the rough surface structure while PAni, 0 ˚C exhibits porous nature (similar as in Figure 4.4). On the other hand, PAni, -5 ˚C explicates the tiny nanofibers that interconnects the conducting islands of PAni matrix thus enhanced the conductivity (Konyushenko et al., 2008). This phenomenon can be supported by the higher degree of crystallinity and highest conductivity of PAni, -5 ˚C as shown in Figure 4.15 and Table 4.6, respectively.

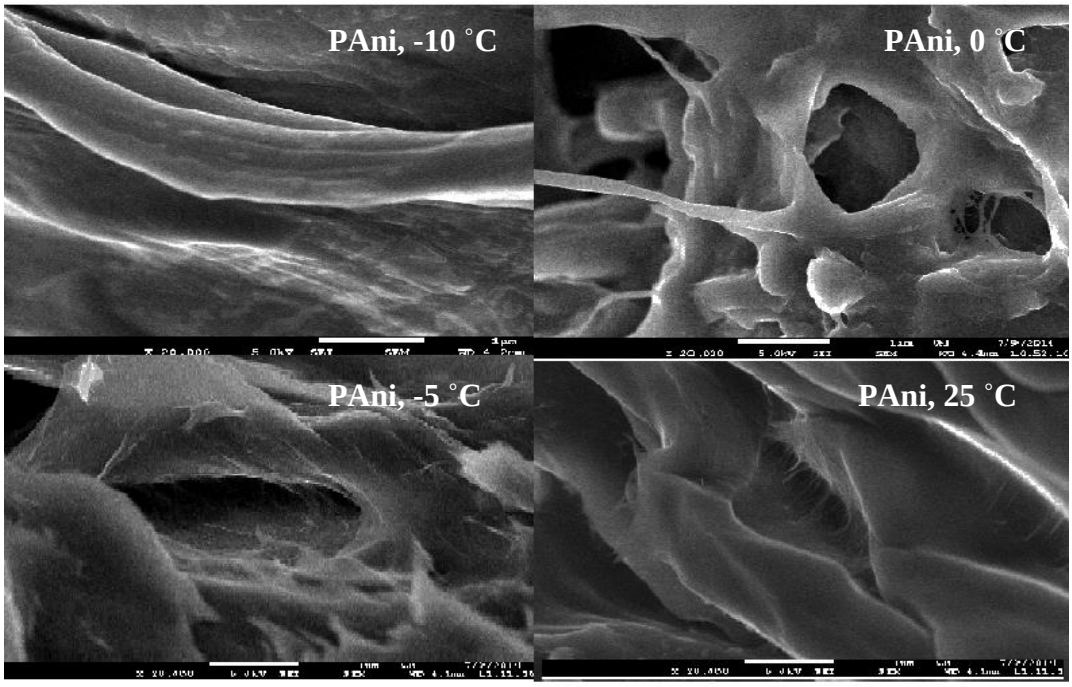

Figure 4.16 FESEM images of PAni, -10 ˚C, PAni, -5 ˚C, PAni, 0 ˚C and PAni, 25 ˚C with magnification of 20,000 ×.

4.2.1 (e) EDX analysis

Figure 4.17 depicts the EDX spectra of PAni, -10 ˚C, PAni, -5 ˚C, PAni, 0 ˚C and PAni, 25 ˚C. Typically, all EDX spectra of PAni synthesized with different

polymerization temperatures exhibited similar trend with PAni synthesized with different dopant ratio as shown in Section 4.1.1 (e) (Figure 4.5). Thus, the typical characteristic peaks were not discussed in this section.

However, the intensity of Carbon peak at 0.25 keV increases as the polymerization temperature decreases from 25 ˚C to -10 ˚C that indicates the formation of longer PAni chain upon subzero polymerization temperatures. Besides, an extra chlorine peak at 2.82 keV is observed in PAni, -10 ˚C due to the addition of LiCl in excess (to avoid freezing) during subzero polymerization temperature. The presence of extra Chlorine peak at 2.82 keV for PAni, -10 ˚C further proves the ring chlorination phenomenon as discussed earlier in UV-Vis analysis (Section 4.2.1 (b)).

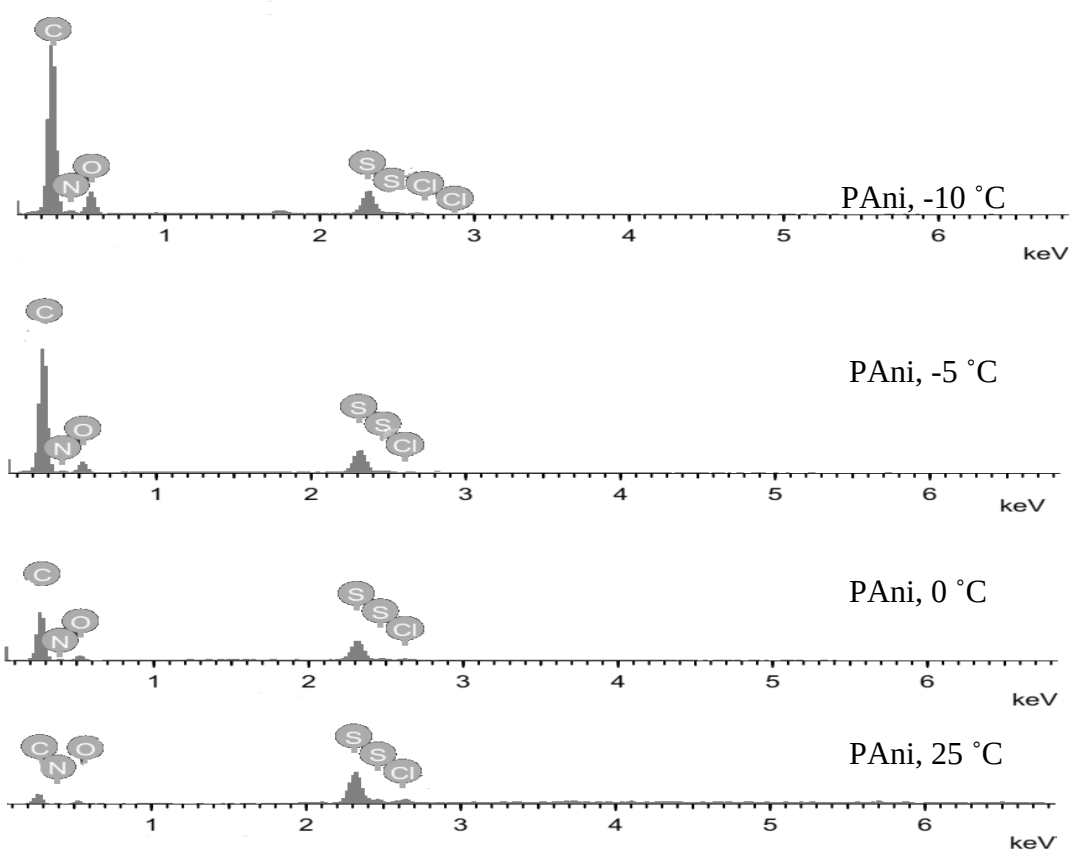

Figure 4.17 EDX spectra of PAni, -10 ˚C, PAni, -5 ˚C, PAni, 0 ˚C and PAni, 25 ˚C.

4.2.1 (f) Conductivity analysis

The conductivities of PAni synthesized at various polymerization temperatures are recorded in Table 4.6. In this study, PAni, -5 ˚C recorded the highest conductivity (1.813 S/cm) followed by PAni, 0 ˚C, PAni -10 ˚C and PAni 25 ˚C with conductivity of 0.820, 0.232 and 0.006 S/cm, respectively.

PAni, -5 ˚C showed the highest conductivity due to several factors such as it possesses less defect sites due to the subzero polymerization temperature and long polymer chain with numerous polarons that consists of high inter or intrachain interactions (UV-Vis in Figure 4.14). Besides, the high crystallinity (XRD in Figure 4.15) and interconnected fibers (FESEM in Figure 4.16) also enhances the conductivity of PAni, -5 ˚C (Jiang et al., 1997; Stejskal et al., 1998).

However, PAni -10 ˚C that synthesized at even lower subzero temperature exhibited poor conductivity due to the addition of excess LiCl during polymerization that caused the ring chlorination (Yang et al., 2009). As discussed earlier, polymer synthesis at higher temperature would contain more defect sites, less conjugation and polarons (Table 4.5), thus PAni, 25 ˚C recorded the lowest conductivity in Table 4.6 (Bláha et al., 2013).

Table 4.6 Conductivities of PAni/AOT synthesized with different polymerization temperatures

Polymer	Conductivity (S/cm)
PAni, 25 ˚C	0.006
PAni, 0 ˚C	0.820
PAni, -5 ˚C	1.813
PAni, -10 ˚C	0.232

4.2.2 Responses of PAni/AOT (different polymerization temperatures) sensors in hydrazine detection

In this part, PAni with Ani:AOT ratio of 5:7 that synthesized at different polymerization temperatures were monitored in hydrazine detection by using UV-Vis response as main study. Conductivity and FTIR analysis were used as supporting element to investigate the interaction between PAni and hydrazine. All measurements were taken before and after immersion in hydrazine (1 – 100 ppm).

4.2.2 (a) UV-Vis responses

Figure 4.18 shows the UV-Vis response of PAni, -10 ˚C, PAni, -5 ˚C, PAni, 0 ˚C and PAni, 25 ˚C in hydrazine detection (1 ppm) from 0 – 5 min. In general, all PAni synthesized with different polymerization temperatures show decrease in normalized UV-Vis absorbance (~780 nm) with increasing of time upon exposure to hydrazine. Among all PAni, PAni -5 ˚C exhibited the most significant decrease in

normalized absorbance at 0.12 min (7 s). It is because, PAni, -5 ˚C that synthesized at subzero temperature will produce PAni with extended conjugation (polarons) that attributed to the highest response in hydrazine detection.

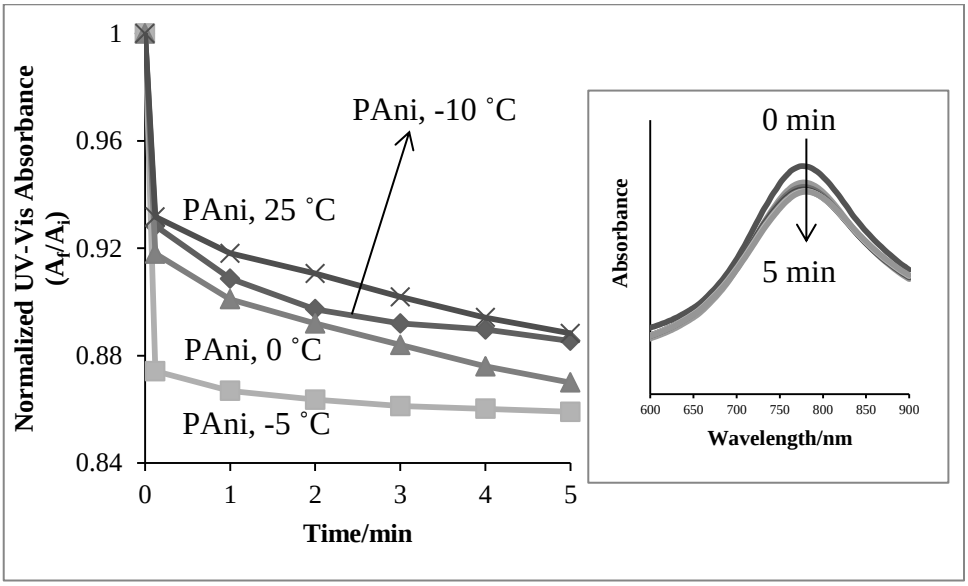

Figure 4.18 Normalized UV-Vis absorbance of PAni, -10 ˚C, PAni, -5 ˚C, PAni, 0 ˚C and PAni, 25 ˚C in hydrazine detection (1 ppm). (Inset: The absorbance peak of PAni, -5 ˚C at ~780 nm in hydrazine detection).

The normalized UV-Vis absorbances of PAni/AOT synthesized at different polymerization temperature in different concentration of hydrazine (1 – 100 ppm) were shown in Figure 4.19. In general, all PAni showed dramatic decrease in normalized UV-Vis absorbance (~780 nm) as the concentration of hydrazine increased. Among all PAni, PAni, -5 ˚C exhibited the significant response in hydrazine detection due to the longer PAni chain that provides more reactive sites for the interaction with hydrazine (Qi et al., 2014).

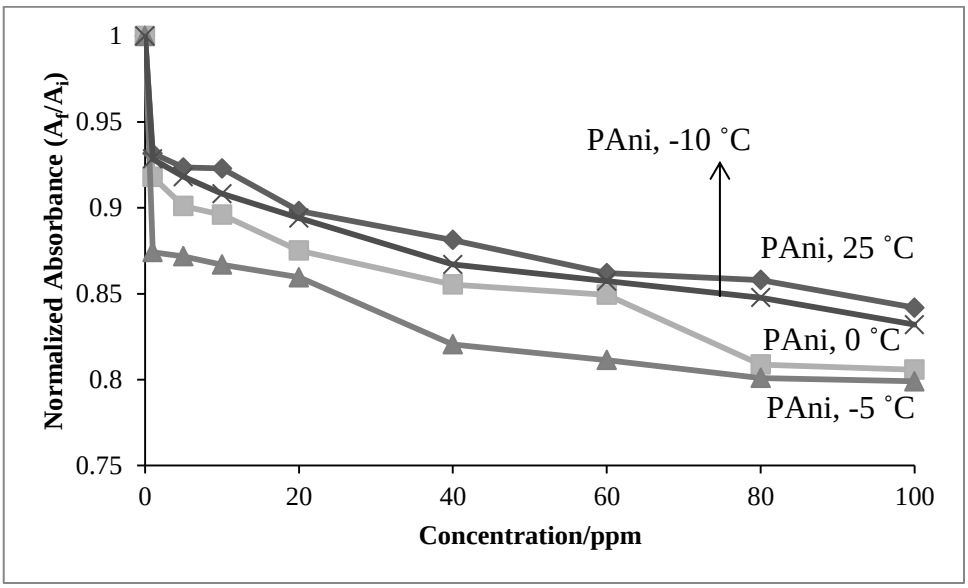

Figure 4.19 Normalized UV-Vis absorbance of PAni, -10 ˚C, PAni, -5 ˚C, PAni, 0 ˚C and PAni, 25 ˚C in different concentration of hydrazine (1 – 100 ppm).

4.2.2 (b) Conductivity responses

Figure 4.20 demonstrates the normalized conductivity of PAni, -10 ˚C, PAni, -5 ˚C, PAni, 0 ˚C and PAni, 25 ˚C in hydrazine detection (1 ppm) from 0 – 5 min. In general, normalized conductivity of all PAni decrease with respect to the immersion time in hydrazine. Among all PAni, significant decrease in normalized conductivity was observed in PAni, -5 ˚C due to its higher electrical conductivity (Table 4.6) (Jiang et al., 1997).

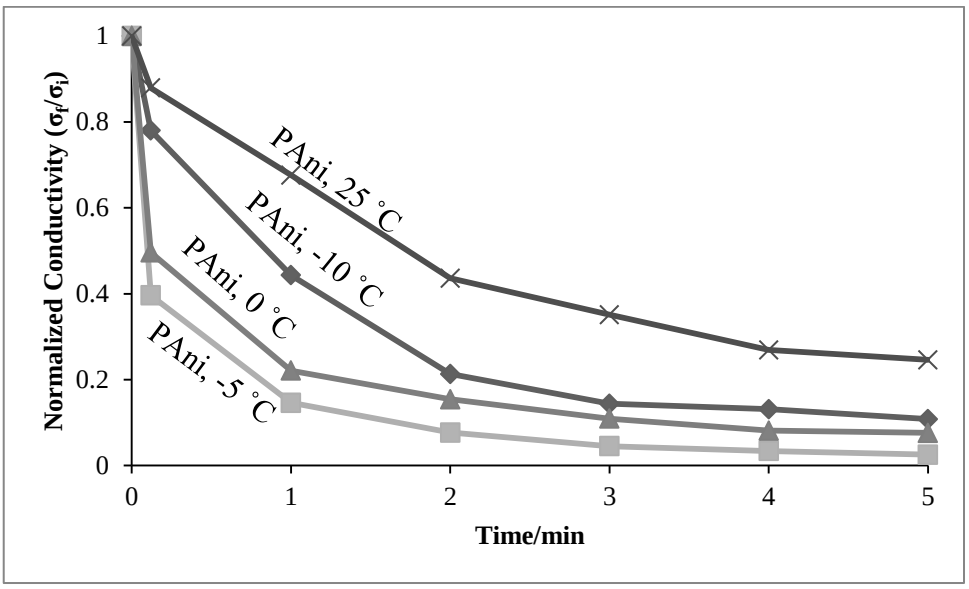

Figure 4.20 Normalized conductivity of PAni, -10 ˚C, PAni, -5 ˚C, PAni, 0 ˚C and PAni, 25 ˚C in hydrazine detection (1 ppm) between 0 – 5 min.

The normalized conductivity of PAni, -10 ˚C, PAni, -5 ˚C, PAni, 0 ˚C and PAni, 25 ˚C in different concentration of hydrazine (1 – 100 ppm) were demonstrated in Figure 4.21. In principle, all PAni exhibited decrease in normalized conductivity due to the transformation of ES state to LE state upon interaction with hydrazine (Figure 4.7).

Among all PAni, both PAni, -5 ˚C (Figure 4.20 and Figure 4.21) showed excellent decrease in normalized conductivity upon immersion in different concentrations of hydrazine. It is because, subzero polymerization temperature would result in a longer PAni chain that possess numerous active sites for the interaction with hydrazine (Stejskal et al., 1998). However, both PAni, -10 ˚C (Figure 4.20 and Figure 4.21) that supposed to possess similar characteristics as PAni, -5 ˚C exhibited a contrary poor response. This is because, addition of excess LiCl during subzero polymerization has given an adverse effect (ring chlorination) to the PAni, -10 ˚C chains, thus reduce the performance of PAni, -10 ˚C in hydrazine detection (Tai et al., 2008; Yang et al., 2009).

On the other hand, PAni, 25 ˚C exhibited the lowest response in normalized conductivity upon interaction with hydrazine. Theoritically, PAni synthesized at higher temperature would possess many defect sites (less reactive sites) within the PAni chains (Sambasevam et al., 2015) that would result in poor sensor response. The normalized conductivities of PAni synthesized at different polymerization are in good agreement with normalized absorbance of PAni (Figure 4.19) in various concentration of hydrazine detection (1 – 100 ppm).

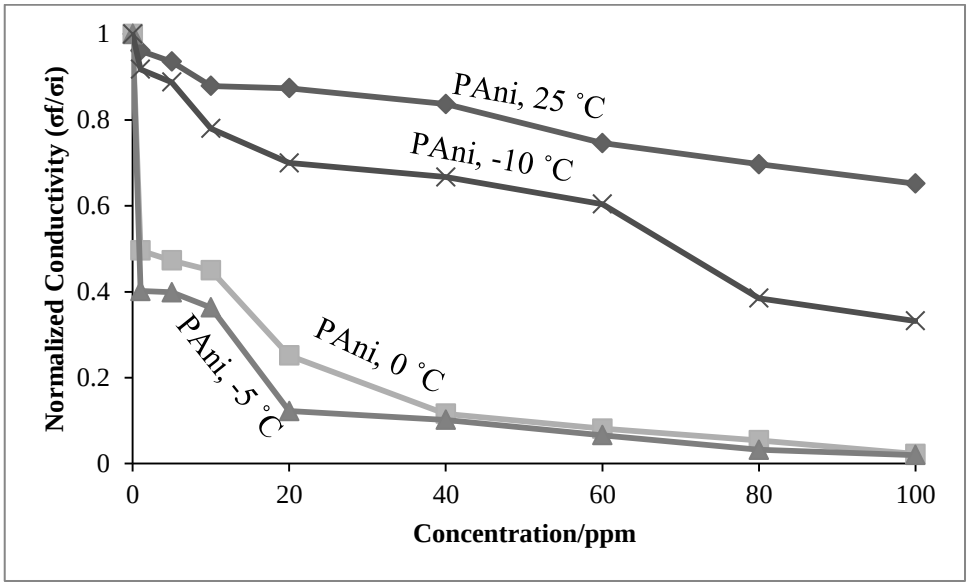

Figure 4.21 Normalized conductivity of PAni, -10 ˚C, PAni, -5 ˚C, PAni, 0 ˚C and PAni, 25 ˚C in different concentration of hydrazine (1 – 100 ppm).

4.2.2 (c) FTIR structural analysis

Among all PAni synthesized with different polymerization temperatures, PAni, -5 ˚C was chosen to study the structural changes that occurred between PAni and hydrazine due to its excellent performance in hydrazine detection. Figure 4.22 shows the FTIR spectra of PAni, -5 ˚C before and after immersion in hydrazine (1 ppm) with response time of 0.12 min.

The I_{1565}/I_{1468} ratio of ES (before) and LE (after) were recorded as 1.00 and 0.89, respectively. The decrease in I_{1565}/I_{1468} ratio indicates that PAni backbone possess predominant benzenoid moieties. This observation confirmed the transformation of PAni from ES state to LE state (Choi et al., 2008; Yoon et al., 2011) as shown by Figure 4.7 (Cataldo and Maltese, 2002; Furukawa et al., 1988; Huang et al., 2003).

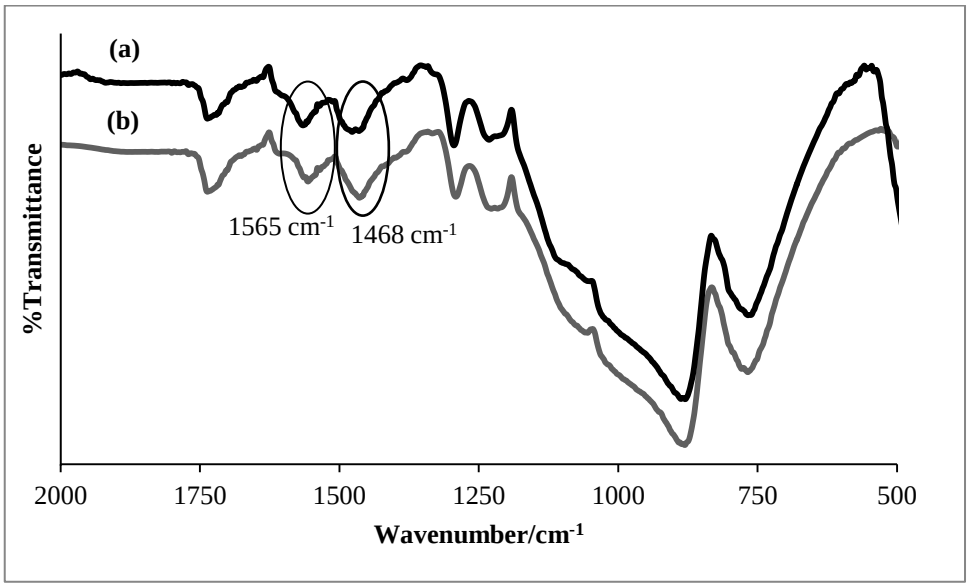

Figure 4.22 FTIR spectra of PAni, -5 ˚C (a) before and (b) after immersion in hydrazine (1 ppm).

Figure 4.23 shows the schematic diagram of PAni synthesized at different polymerization temperatures with Ani:AOT ratio of 5:7. In principle, PAni chains elongate as the polymerization temperature decreased (Yang et al., 2009). Thus, elongated PAni chain would possess numerous reactive sites which will enhance the sensing properties of PAni. According to Yang and co-workers (2009), the rate of polymerization would become slower with the decrement of polymerization temperature, thus produce the PAni that possess longer chain and with less/no defect sites. In this study, similar behavior was observed for PAni synthesized at subzero

temperatures such as PAni, -10 ˚C and PAni, -5 ˚C which contains defect free sites and high conductivity.

Although, PAni, -10 ˚C possessed longer polymer chain, it contained fair amount of ring chlorinated sites that restrict the electron delocalization, thus significantly reduce the conductivity of PAni, -10 ˚C (MacDiarmid and Huang, 1999). Eventhough, PAni, -5 ˚C possessed shorter chain length than PAni, -10 ˚C, addition of optimum amount of LiCl during polymerization process, did not affect the PAni, -5 ˚C chains in terms of ring chlorination and yielded PAni with the highest conductivity (1.81 S/cm) in this study.

On the other hand, PAni, 25 ˚C that synthesized at higher temperature possess the shortest polaron chain and numerous defect sites. This sort of retardation at PAni chains would decrease the conductivity (0.006 S/cm) and sensitivity of PAni chains in hydrazine detection as shown by Table 4.6 and Figure 4.21.

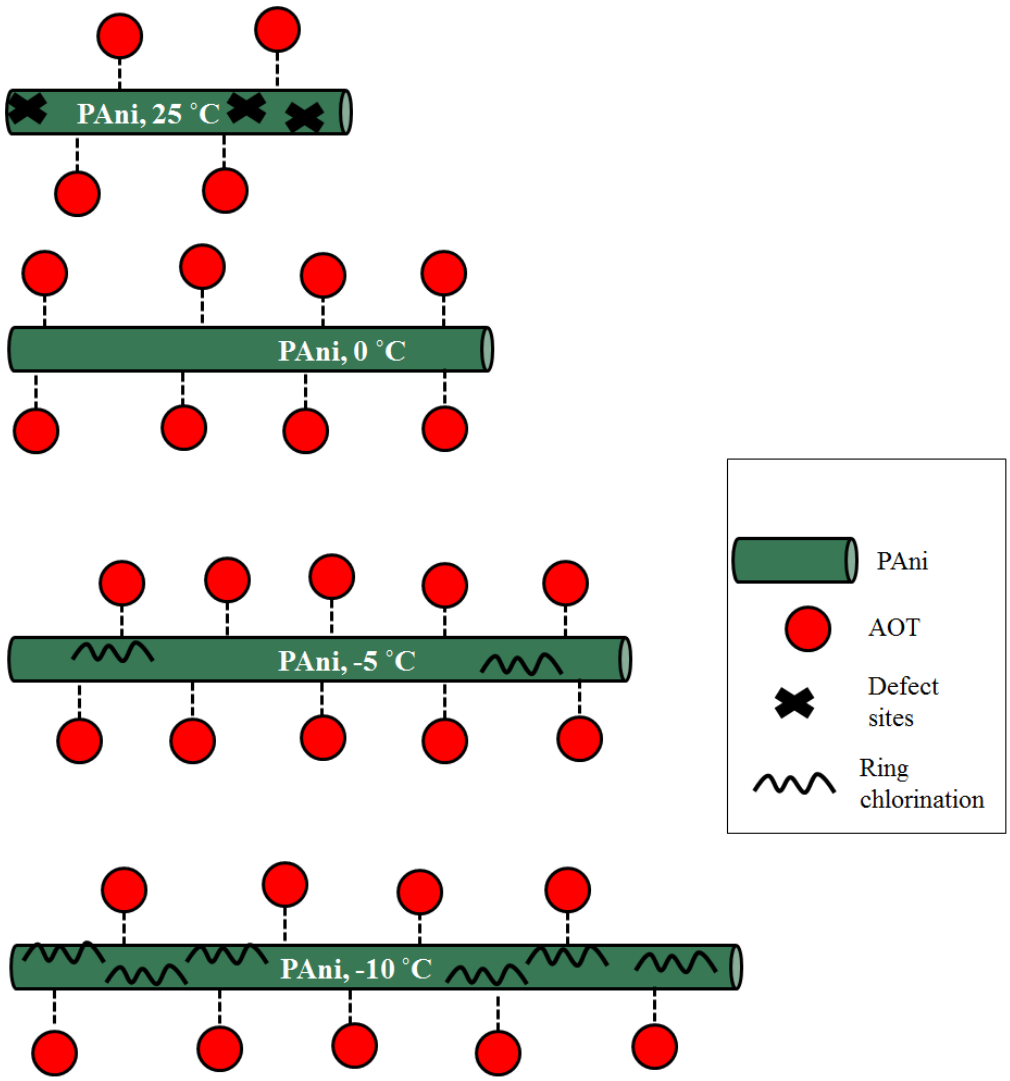

Figure 4.23 Schematic diagram of PAni/AOT that synthesized at various polymerization temperatures.

4.3 PAni/TiO_2 nanocomposites (different TiO_2 ratio) in hydrazine detection

The synergetic behavior between PAni (p-type) and TiO_2 (n-type) nanoparticles would yield a conducting polymer with unique properties (Zhang et al., 2006; Liu and Hwang, 2000). In this study, nano-sized TiO_2 particles (~21 nm) were chosen due to its high surface area to improve the sensing performance in hydrazine detection. Besides, TiO_2 nanoparticles are more favored compared to other inorganic metal oxides due to

its special features including non-toxicity, chemical inertness and low cost (Olad et al., 2013; Chatterjee and Islam, 2008; Zhang et al., 2005). This section discusses about the synergetic effect between PAni and different ratio of TiO_2 nanoparticles in hydrazine detection.

4.3.1 Characterizations of PAni/TiO_2 nanocomposites (different TiO_2 ratio)

In this section, PAni has been synthesized at 0 ˚C with different ratio of TiO_2 nanoparticles (10 – 40 %) with Ani:AOT ratio of 5:7. Ani:AOT ratio of 5:7 was chosen due to the optimum monomer:dopant ratio that optimized from Section 4.1. PAni/TiO_2 nanocomposites with 10%, 20% and 40% of TiO_2 nanoparticles were labelled as PAni/Ti10, PAni/Ti20 and PAni/Ti40, respectively.

4.3.1 (a) FTIR analysis

Figure 4.24 shows the FTIR spectra of pristine PAni and PAni/TiO_2 nanocomposites synthesized with different TiO_2 ratios. The distinctive FTIR peaks of pristine PAni and PAni/TiO_2 nanocomposites were tabulated in Table 4.7. In principle, PAni/TiO_2 nanocomposites exhibit similar PAni characteristic peaks in the wavenumber region of 400 – 2000 cm^{-1} as discussed in Section 4.1.1 (a) (FTIR analysis). However, there is an evidence of peak displacement when TiO_2 nanoparticles were added to PAni due to the interaction between PAni and TiO_2 nanoparticles (Yavuz and Gök, 2007).

Besides, all PAni/TiO_2 nanocomposites exhibit a significant peak at 1280 – 1297 cm^{-1} that corresponds to the Ti-O-C stretching as evident for the interactions between PAni and TiO_2 nanoparticles (Hübert et al., 2011; Nasirian and Milani Moghaddam,

2014). Among all PAni/TiO_2 obtained, PAni/Ti20 possessed the sharpest peak at benzenoid (1418 – 1475 cm^{-1}) and quinoid (1612 – 1540 cm^{-1}) regions due to the effective and optimum incorporation of TiO_2 (20%) into the PAni matrix (Yavuz and Gök, 2007).

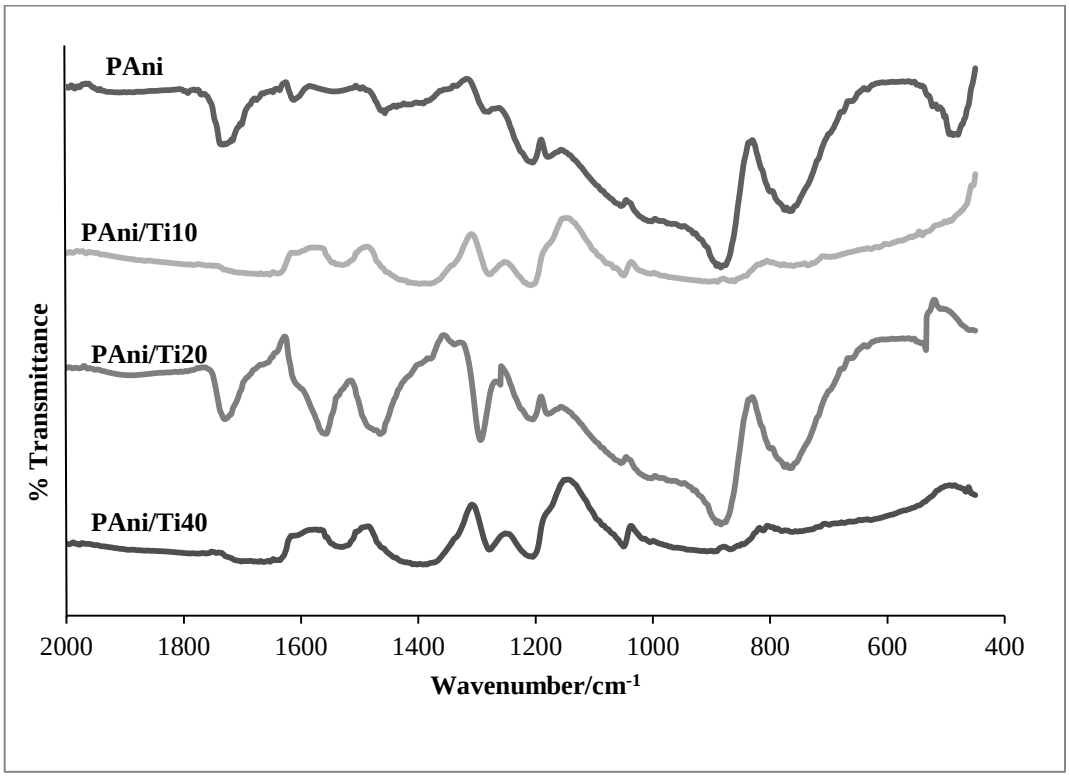

Figure 4.24 FTIR spectra of pristine PAni and PAni/TiO_2 nanocomposites with different TiO_2 ratio.

Table 4.7 Distinctive peaks of pristine PAni and PAni/TiO_2 nanocomposites synthesized with different TiO_2 ratio.

Functional groups	Wavenumber (cm^{-1})			
	PAni	PAni/Ti10	PAni/Ti20	PAni/Ti40
C-H vibration	773	781	775	781
C=C vibration	899	895	899	896
S=O vibration	1178	1175	1183	1190
C-N stretching	1217	1210	1232	1214
Ti-O-C stretching	1289	1284	1297	1280
Benzenoid	1468	1418	1475	1420
Quinoid	1612	1548	1565	1540
C=O	1736	1702	1755	1709

4.3.1 (b) UV-Vis analysis

Figure 4.25 shows the UV-Vis spectra of pristine PAni and PAni/TiO_2 nanocomposites with different TiO_2 ratio. In general, pristine PAni and PAni/TiO_2 nanocomposites exhibit similar absorption peaks in the wavelength range of 300 – 900 nm. The distinctive UV-Vis peaks of pristine PAni and PAni/TiO_2 nanocomposites are shown in Table 4.8.

It can be noted that both PAni and PAni/TiO_2 nanocomposites possess almost similar UV-Vis spectra with slight shifts due to the encapsulation of TiO_2 nanoparticles (Li et al., 2004). Besides, the absorption intensity of PAni/TiO_2 nanocomposites are

lower compare to pristine PAni due to the effective hydrogen bonding in the form of NH•••O-Ti (Xu et al., 2005; Yavuz and Gök, 2007).

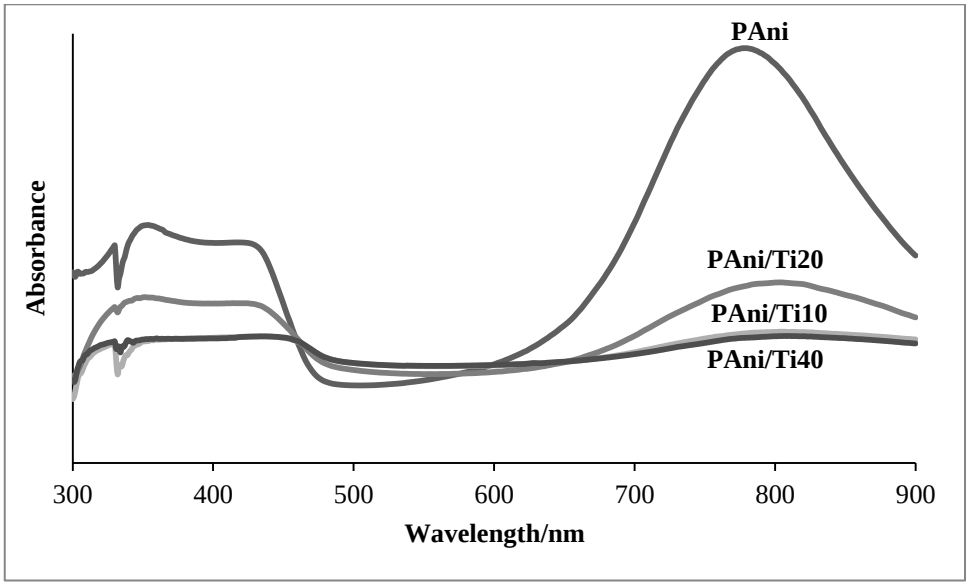

Figure 4.25 UV-Vis absorption spectra of pristine PAni and PAni/TiO_2 nanocomposites with different TiO_2 ratios.

Table 4.8 The assignments of UV-Vis absorption peaks for pristine PAni and PAni/TiO_2 nanocomposites synthesized with different TiO_2 ratio

Polymer	$\pi - \pi^*$ (nm)	polaron – π^* (nm)	π – polaron (nm)
PAni	354	426	774
PAni/Ti10	348	450	807
PAni/Ti20	350	428	795
PAni/Ti40	343	445	798

4.3.1 (c) XRD analysis

X-ray difractogram of pristine PAni and PAni/TiO_2 nanocomposites are shown in Figure 4.26. In principle pristine PAni and PAni/TiO_2 nanocomposites diffractograms exhibited similar PAni characteristic peaks in the 2θ range of 5 – 25˚ that already discussed in Section 4.1.1 (c) (XRD analysis). However, PAni/TiO_2 nanocomposites exhibited sharp and distinct peaks at 33.4˚, 37.8˚, 47.9˚, 51.3˚ and 61.6˚ indicating the presence of TiO_2 nanoparticles in the PAni matrix (Deivanayaki et al., 2013; Li et al., 2013).

In conclusion, pristine PAni and PAni/TiO_2 nanocomposites exhibit almost similar PAni characteristic peaks in FTIR, UV-Vis spectra and X-ray diffractogram, thus confirmed the PAni present in the doped ES form.

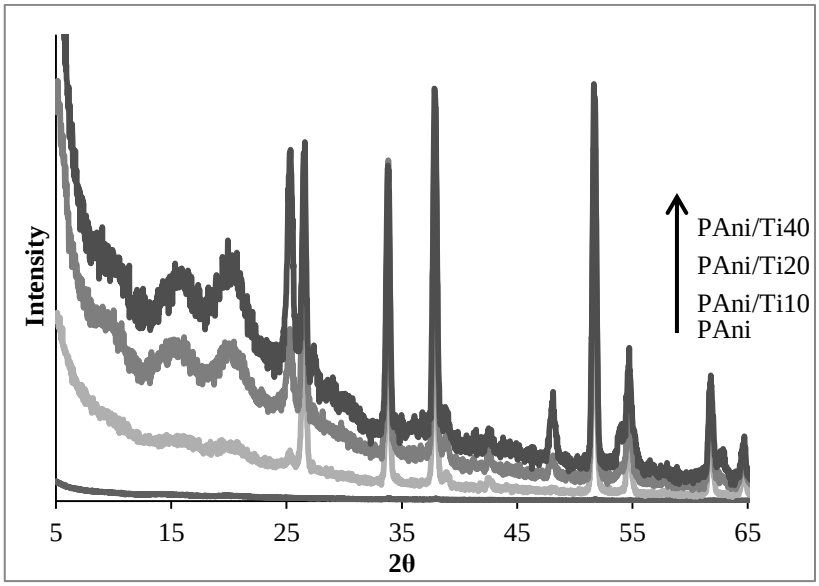

Figure 4.26 X-ray diffractograms of pristine PAni and PAni/TiO_2 nanocomposites with different TiO_2 ratios.

4.3.1 (d) FESEM analysis

Figure 4.27 shows the FESEM micrographs of pristine PAni and PAni/TiO_2 nanocomposites (different TiO_2 ratios) with magnification of 20,000 ×. The micrographs give a clear evident on the incorporation of TiO_2 nanoparticles as white coloured spots on the PAni/TiO_2 nanocomposites (Figure 4.27) compare with pristine PAni. Besides, PAni/Ti10 and PAni/Ti20 exhibit fibrilar structures (act as bridge) that interconnect the conducting islands of PAni matrices (circle part). This morphology indicates the efficient electron hopping of PAni/Ti10 and PAni/Ti20 that will significantly improve the sensing mechanism in hydrazine detection. On the other hand, PAni/Ti40 does not exhibit fibrilar structure, thus restrict the electrons mobility along the PAni backbone and results in poor conductivity (Table 4.9).

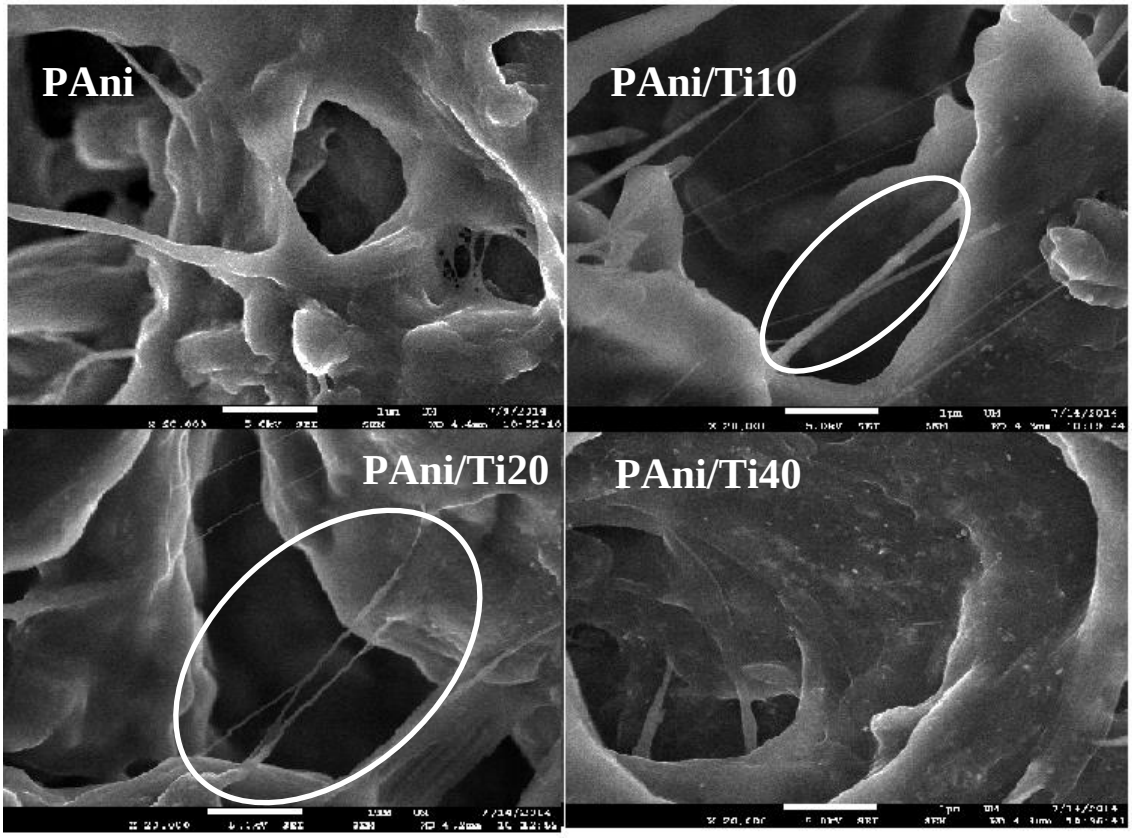

Figure 4.27 FESEM images of pristine PAni, PAni/Ti10, PAni/Ti20 and PAni/Ti40 at magnification of 20,000 ×.

4.3.1 (e) EDX analysis

Elemental compositions of pristine PAni and PAni/TiO_2 nanocomposites with different TiO_2 ratios are shown in Figure 4.28. PAni/TiO_2 nanocomposites exhibit similar EDX spectra as pristine PAni as discussed in Section 4.1.1 (e). However, two new TiO_2 peaks at 4.5 keV and 4.9 keV appeared in all PAni/TiO_2 nanocomposites that indicates the effective incorporation of TiO_2 nanoparticles in PAni matrix (Ghavami et al., 2014; Su and Gan, 2012).

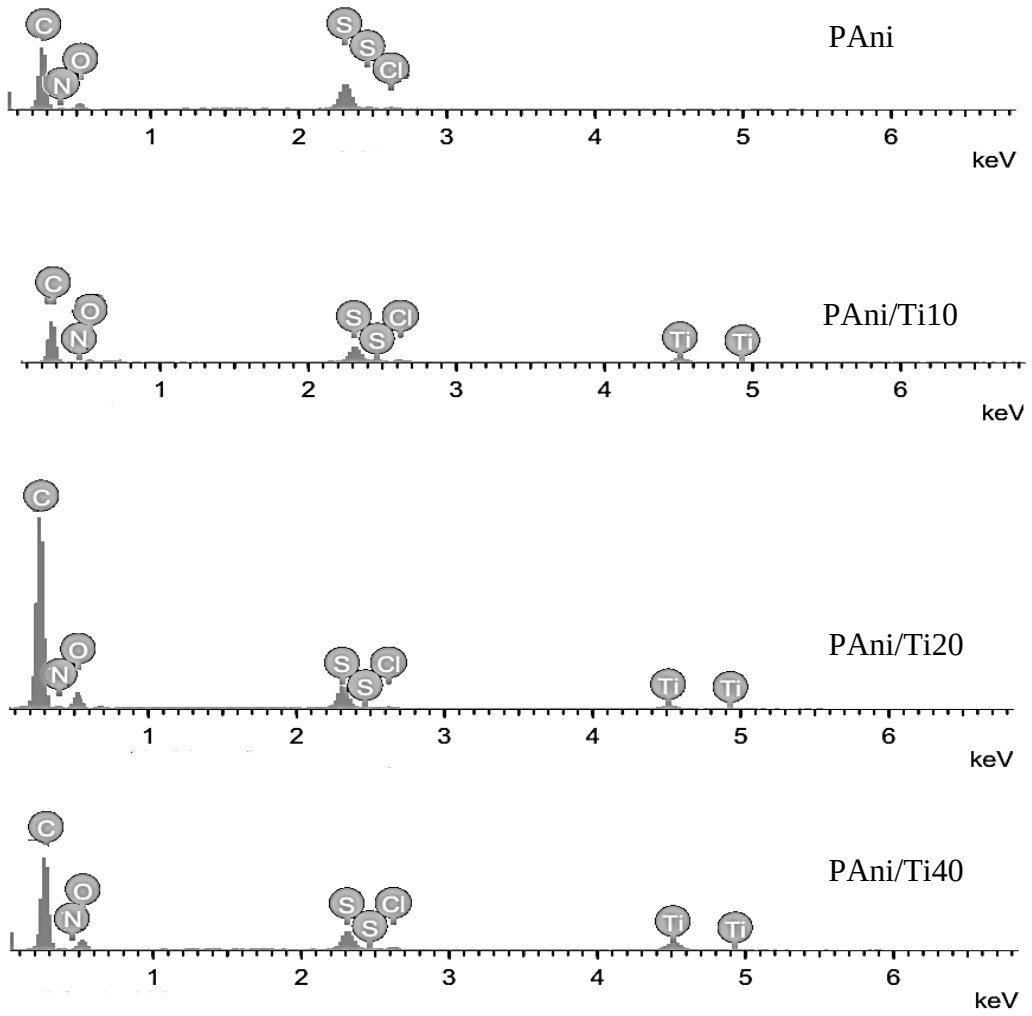

Figure 4.28 EDX spectra of pristine PAni and PAni/TiO_2 nanocomposites with different ratio of TiO_2.

4.3.1 (f) Conductivity analysis

Table 4.9 shows the conductivities of pristine PAni and PAni/TiO_2 nanocomposites with different TiO_2 ratio. Pristine PAni recorded the conducitivity of 0.800 S/cm while PAni/Ti10, PAni/Ti20 and PAni/Ti40 showed the conductivities of 0.900, 1.600 and 0.600 S/cm, respectively. In general, the conductivities of PAni/Ti10 and PAni/Ti20 nanocomposites increase with increasing the TiO_2 ratio at 10% and 20%. However, PAni/Ti40 with 40% of TiO_2 exhibited the poorest conductivity.

In this conductivity study, two phenomena have occurred upon the addition of different TiO_2 ratios in pristine PAni. Phenomenon A is the increment in conductivity when 10% and 20% of TiO_2 were added in PAni. This phenomenon A is due to the adsorption of anilinium ions on the surface of TiO_2 grains, (O^- anions) during the oxidative polymerization of PAni nanocomposites. The interaction between anilinium ions and O^- anions caused the trapped electrons to return to the surface of the TiO_2 grains. This process has decreased the potential barrier between PAni and TiO_2 nanoparticles and resulted in an increase in charge carrier mobility that eventually increased the relative conductivity of PAni/Ti10 and PAni/Ti20 (Nasirian and Moghaddam, 2014).

On the other hand, phenomenon B is the decrement in conductivity of PAni/Ti40 (0.600 S/cm) upon the addition of 40% of TiO_2. This phenomenon is due to the possible charge blockage at conductive pathway of PAni that caused by the excessive addition of TiO_2 nanoparticles in PAni matrix. Moreover, the absent of fibrillar structure in PAni/Ti40 could be another factor for decrement in conductivity (Figure 4.27) (Cao et al., 1992; Gu et al., 2012; Yang and Heeger, 1994).

Table 4.9 Conductivities of pristine PAni and PAni/TiO_2 nanocomposites

Polymer	Conductivity (S/cm)
PAni	0.800
PAni/Ti10	0.900
PAni/Ti20	1.600
PAni/Ti40	0.600

4.3.2 Responses of pristine PAni and PAni/TiO_2 nanocomposites (different TiO_2 ratio) sensors in hydrazine detection

In this section, pristine PAni was included for comparison purpose. The primary sensor study was focused on PAni/TiO_2 nanocomposites with different TiO_2 ratios that prepared at 0 ˚C with Ani:AOT ratio of 5:7 were monitored in hydrazine detection by using UV-Vis as main study. Conductivity responses and FTIR structural analysis were used as supporting element to investigate the interaction between PAni/TiO_2 nanocomposites and hydrazine. All measurements were taken before and after immersion in hydrazine (1 – 100 ppm).

4.3.2 (a) UV-Vis responses

The UV-Vis responses of pristine PAni and PAni/TiO_2 nanocomposites in hydrazine detection (1 ppm) were investigated as shown in Figure 4.29. All PAni showed significant decrease in normalized UV-Vis absorbance at 0.12 min and it reached equilibrium from 1 – 5 min. Among all PAni, PAni/Ti20 showed the largest decrease in normalized UV-Vis absorbance followed by PAni/Ti10, PAni/Ti40 and pristine PAni (Zheng et al., 2008). In principle, the decreased normalized UV-Vis

absorbance is directly proportional to the intensity of electron delocalization along the PAni backbone (Anitha and Subramanian, 2003; Kar and Choudhury, 2013).

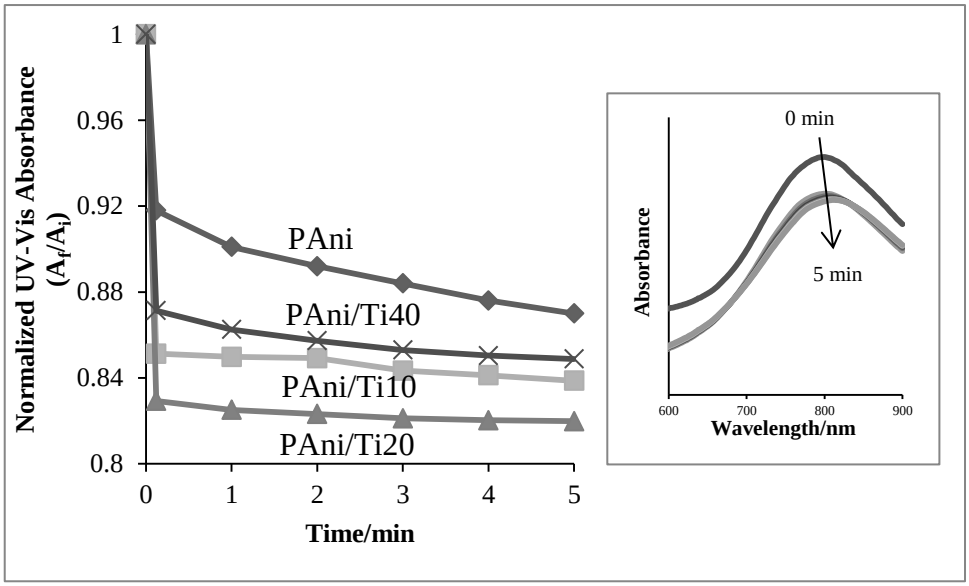

Figure 4.29 Normalized UV-Vis absorbance of pristine PAni, PAni/Ti10, PAni/Ti20 and PAni/Ti40 for hydrazine detection (1 ppm) between 0 – 5 min. (Inset: The absorbance peak of PAni/Ti20 at ~795 nm in hydrazine detection).

Figure 4.30 demonstrates normalized UV-Vis absorbance of pristine PAni and PAni/TiO_2 nanocomposites with different TiO_2 ratio in different concentrations of hydrazine (1 – 100 ppm). All pristine PAni and PAni/TiO_2 nanocomposites show similar pattern in the normalized UV-Vis response as shown in Figure 4.29. Hence, optimum amount of TiO_2 in PAni matrix has improved the sensing mechanism of PAni/Ti20 as discussed by phenomenon A in Figure 4.34. Meanwhile, PAni/Ti40 demonstrates poorer response than PAni/Ti10 and PAni/Ti20 but greater response compare to pristine PAni. It is because, even though addition of TiO_2 (40%) in PAni slightly improved the sensing mechanism than PAni, the remaining excess TiO_2 nanoparticles has created the charge blocking mechanism along the PAni backbone (Figure 4.34), thus it demonstrates a low response in hydrazine detection (Ansari and Mohammad, 2011).

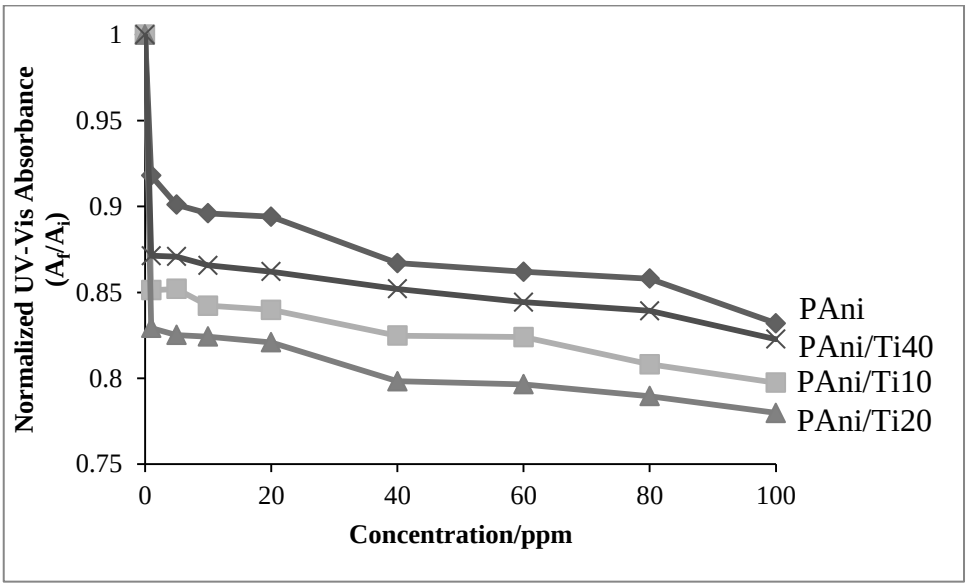

Figure 4.30 Normalized UV-Vis absorbance of pristine PAni, PAni/Ti10, PAni/Ti20 and PAni/Ti40 in different concentration of hydrazine detection (1 – 100 ppm).

4.3.2 (b) Conductivity responses

Figure 4.31 shows the response of pristine PAni and PAni/TiO_2 nanocomposites in hydrazine detection (1 ppm) with respect to time. In essence, all PAni exhibited similar pattern as shown in normalized UV-Vis absorbance (Figure 4.29). Among all PAni obtained, PAni/Ti20 showed the significant decrease in normalized conductivity followed by PAni/Ti10, PAni/Ti40 and pristine PAni which is in good agreement with Figure 4.29 (normalized UV-Vis response).

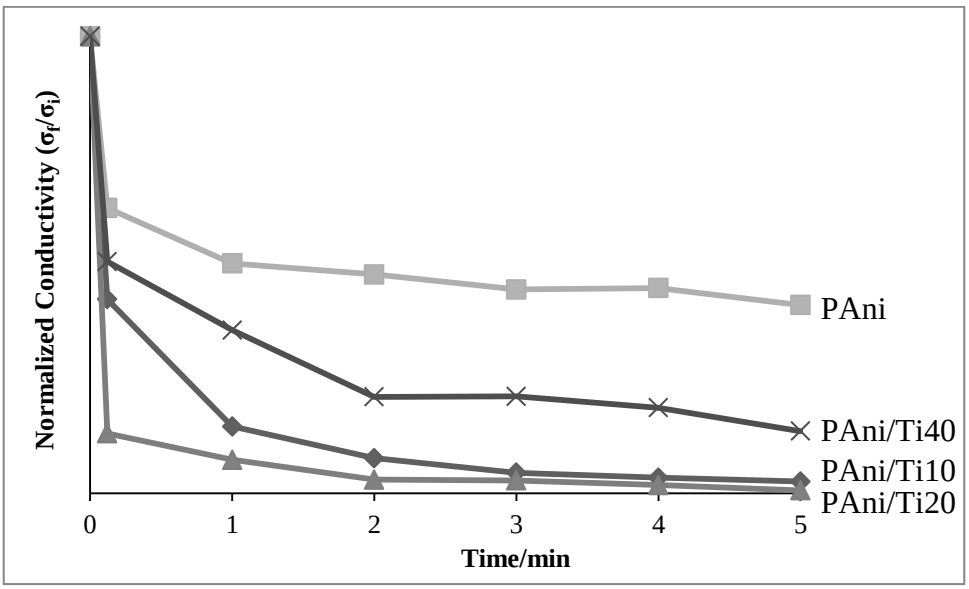

Figure 4.31 Normalized conductivity pristine of PAni, PAni/Ti10, PAni/Ti20 and PAni/Ti40 in hydrazine detection (1 ppm) with respect to time.

Figure 4.32 depicts the normalized conductivity of pristine PAni and PAni/TiO_2 nanocomposites in different concentrations of hydrazine (1 – 100 ppm). In general, pristine PAni and all PAni/TiO_2 nanocomposites exhibit decrease in normalized conductivity upon immersion in different concentrations of hydrazine at 0.12 min. Pristine PAni and PAni/TiO_2 nanocomposites in both Figure 4.31 and Figure 4.32 exhibit similar trend in hydrazine detection in the order of PAni/Ti20 > PAni/Ti10 > PAni/Ti40 > PAni.

As explained in phenomenon A (Figure 4.34), PAni/Ti20 with excellent conducting mechanism that provided by bridging of TiO_2 nanoparticles between PAni chains will significantly improve the interaction of PAni and hydrazine. The similar phenomenon was also observed by Dhawale et al., (2008). On the other hand, PAni/Ti40 shows poor response in normalized conductivity due to the charge blocking mechanism that explained in phenomenon B (Figure 4.34).

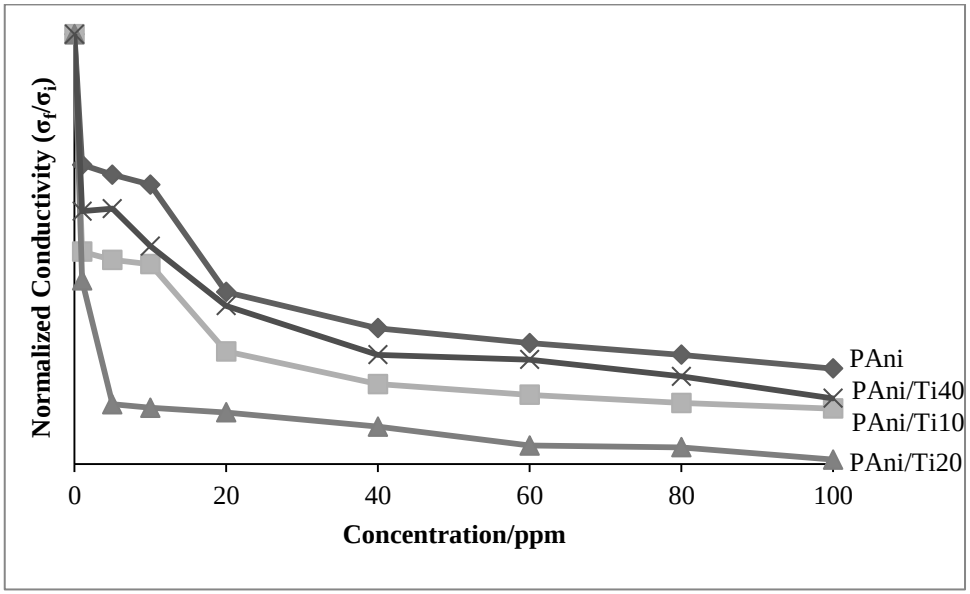

Figure 4.32 Normalized conductivity of pristine PAni, PAni/Ti10, PAni/Ti20 and PAni/Ti40 in hydrazine detection (1 – 100 ppm).

4.3.2 (c) FTIR structural analysis

Section 4.3.2 (a) and 4.3.2 (b) clearly demonstrates that PAni/Ti20 performed the best in hydrazine detection. Thus, PAni/Ti20 is chosen to investigate the FTIR response (structural changes) of PAni/Ti20 before immersion and after immersion in 1 ppm of hydrazine is shown in Figure 4.33. The I_{1565}/I_{1475} ratio of PAni/Ti20 (ES) was recorded as 1.00 before immersion in hydrazine. After immersion in hydrazine, the I_{1565}/I_{1475} ratio of PAni/Ti20 (LE) was recorded as 0.89 that indicates the PAni backbone held predominant benzenoid moieties (Choi et al., 2008; Yoon et al., 2011). Hence, Figure 4.33 further supports the interaction and structural changes that occur for PAni/Ti20 nanocomposite upon immersion in 1 ppm of hydrazine (Figure 4.7).

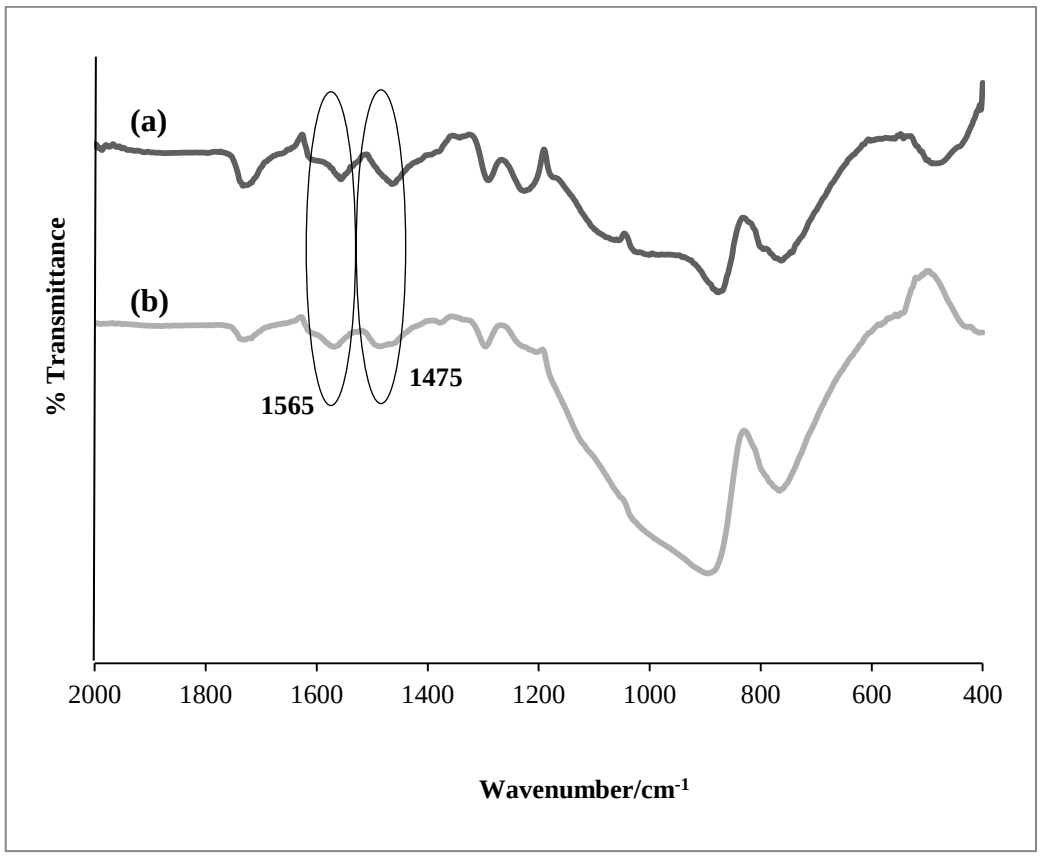

Figure 4.33 FTIR response of PAni/Ti20 (a) before and (b) after immersion in hydrazine (1 ppm).

As shown in Figure 4.34 all PAni/TiO_2 nanocomposites may possess almost equal length of PAni chains but the presence of TiO_2 nanoparticles at different ratio would exhibit significant changes in PAni sensor mechanism. As discussed in conductivity analysis (Table 4.9), UV-Vis (Figure 4.29 and Figure 4.30) and conductivity responses (Figure 4.31 and Figure 4.32), the incorporation of TiO_2 (10% and 20%) has enhanced the conductivity properties in sensitive hydrazine detection. This is due to the phenomenon A, where the electron affinity of TiO_2 grains (n-type) well matched with the electron donating behavior of PAni (p-type) that enhanced the electron delocalization. This significantly reduced the potential barrier that occurs between TiO_2 grains and PAni backbone. This phenomenon A has made the PAni/Ti20 nanocomposite as competitive sensor in hydrazine detection (Gonçalves et al., 2010).

However, addition of TiO_2 nanoparticles with 40%, served as blocking charge carriers and thus reduced the conductivity of PAni (phenomenon B) (Ansari and Mohammad, 2011). Hence, it could not perform as well as PAni/Ti10 and PAni/Ti20.

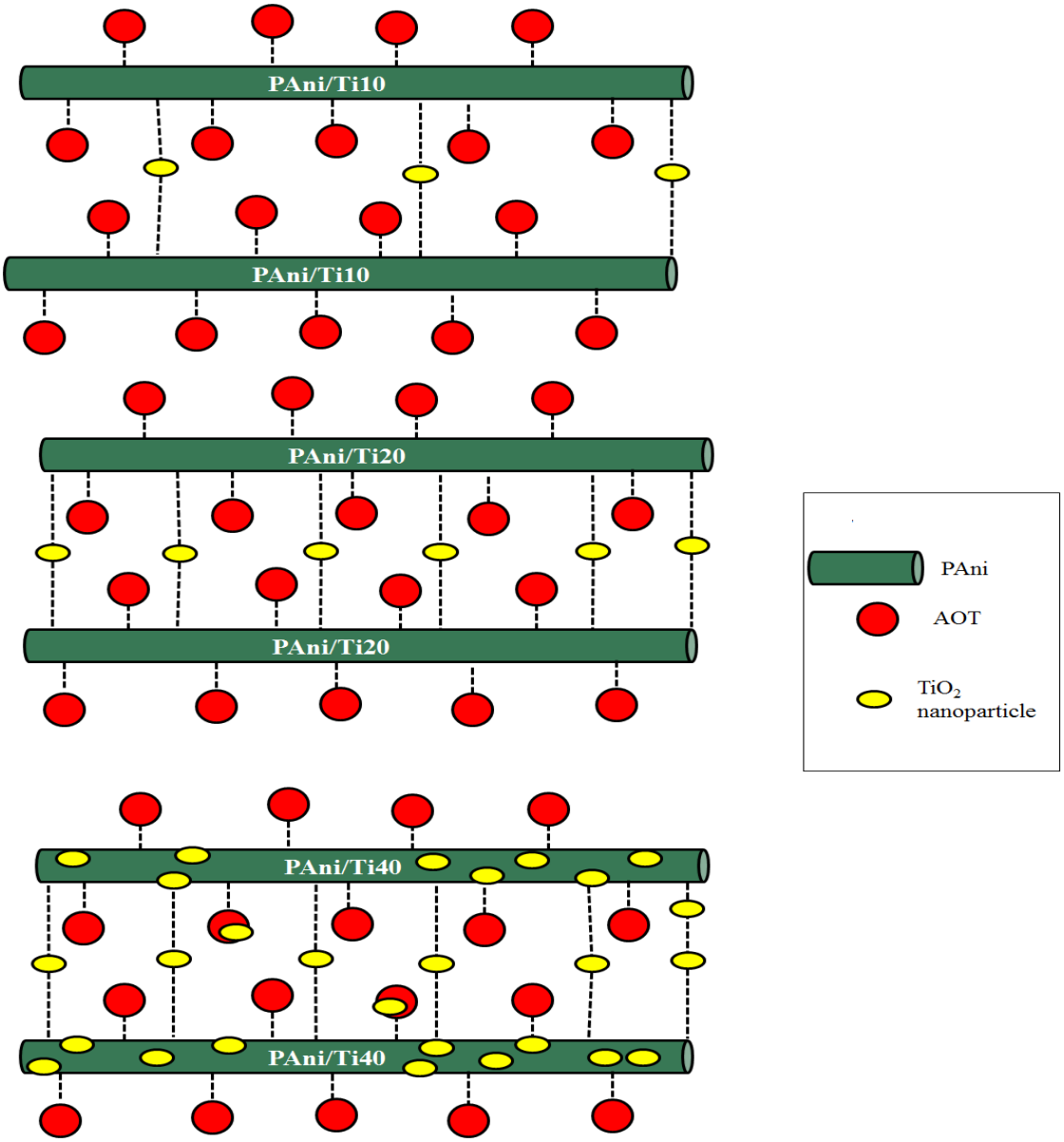

Figure 4.34 Schematic digram of PAni/TiO_2 nanocomposites with different TiO_2 ratios in PAni matrices.

4.4 PAni/Ti20 nanocomposites (different polymerization temperatures) in hydrazine detection

Section 4.3 clearly demonstrated the improved performance of PAni/Ti20 nanocomposites in hydrazine detection due to the optimum ratio of TiO_2 (20%) nanoparticles in PAni/TiO_2 nanocomposites in terms of enhanced electron delocalization via decrease in potential barrier between PAni and TiO_2 nanoparticles. PAni/Ti20 nanocomposites provide better electrical properties due to the direct interfacial interaction of PAni with 20% of TiO_2, where the polymer act as electron donors (p-type semiconductor) and TiO_2 act as electron acceptors (n-type semiconductor). Besides, the results in section 4.2 significantly showed that manipulation of polymer chain length by different polymerization temperature will produce a hybrid PAni with improved sensitivity (more reactive sites) for hydrazine interaction (Stejskal, et al., 1998). Thus, final part of this study focuses on the synthesis of PAni/Ti20 nanocomposites at different polymerization temperatures in hydrazine detection.

4.4.1 Characterizations of PAni/Ti20 nanocomposites (different polymerization temperatures)

In this final section, PAni with Ani:AOT ratio of 5:7 was synthesized in the presence of 20% of TiO_2 nanoparticles under different polymerization temperatures such as -5 ˚C, 0 ˚C and 25 ˚C and labelled as PAni/Ti20, -5 ˚C, PAni/Ti20, 0 ˚C, PAni/Ti20, 25 ˚C, respectively. PAni, -10 ˚C was not investigated in this section because addition of excess LiCl during the synthesis of PAni at -10 ˚C would produce

ring chlorination that will reduce the performance of PAni in hydrazine detection (Section 4.2).

4.4.1 (a) FTIR analysis

Figure 4.35 depicts the FTIR spectra of PAni/Ti20, -5 ˚C, PAni/Ti20, 0 ˚C and PAni/Ti20, 25 ˚C that measured in the wavenumber range of 400 – 2000 cm^{-1}. The characteristic peaks of the PAni/Ti20 nanocomposites with various polymerization temperatures were similar to PAni/Ti20 nanocomposites in Section 4.3.1 (a), thus characteristic peaks of PAni/Ti20 nanocomposites were summarized in Table 4.10.

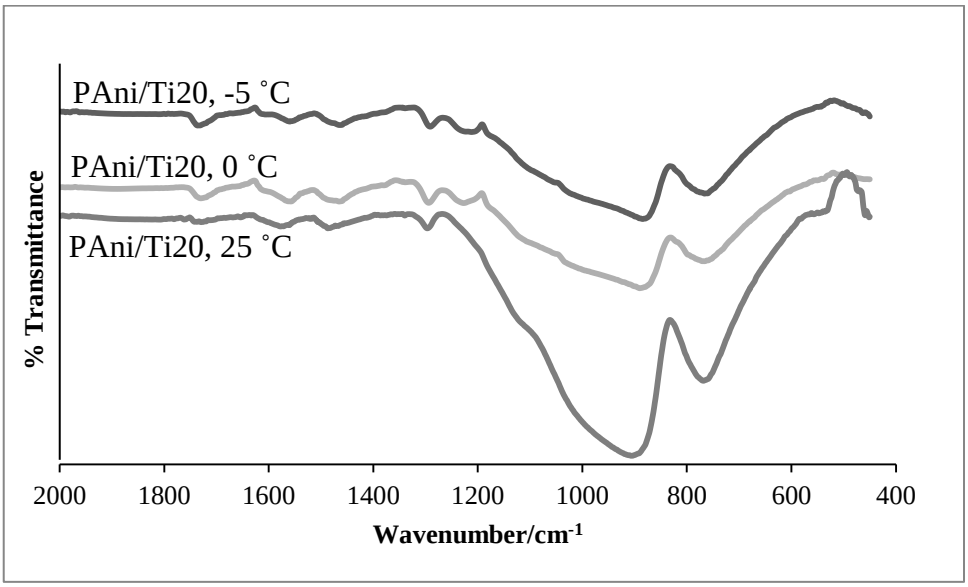

Figure 4.35 FTIR spectra of PAni/Ti20, -5 ˚C, PAni/Ti20, 0 ˚C and PAni/Ti20, 25 ˚C.

Table 4.10 Functional groups present in PAni/Ti20 that synthesized at different polymerization temperatures

Functional groups	Wavenumber (cm^{-1})		
	PAni/Ti20, -5 ˚C	PAni/Ti20, 0 ˚C	PAni/Ti20, 25 ˚C
C-H vibration	780	780	780
C=C vibration	880	885	907
S=O vibration	1110	1115	1122
C-N stretching	1230	1232	1222
Ti-O-C stretching	1297	1297	1297
Benzenoid	1466	1475	1478
Quinoid	1564	1565	1566
C=O	1755	1755	1755

4.4.1 (b) UV-Vis analysis

Figure 4.36 depicts the UV-Vis spectra of PAni/Ti20, -5 ˚C, PAni/Ti20, 0 ˚C and PAni/Ti20, 25 ˚C. In general, PAni/Ti20 nanocomposites exhibit similar absorption peaks in the wavelength range of 300 – 900 nm. Table 4.11 summarizes the distintive peaks of PAni/Ti20 with different polymerization temperatures. Among all PAni/Ti20 nanocomposites, PAni/Ti20, -5 ˚C and PAni/Ti20, 0 ˚C possess the apparent polaron peak at 777 – 804 nm that indicates the high conductivity nature due to the low (0 ˚C) and subzero (-5 ˚C) polymerization temperatures for both PAni (Table 4.12) (Xia and Wang, 2001).

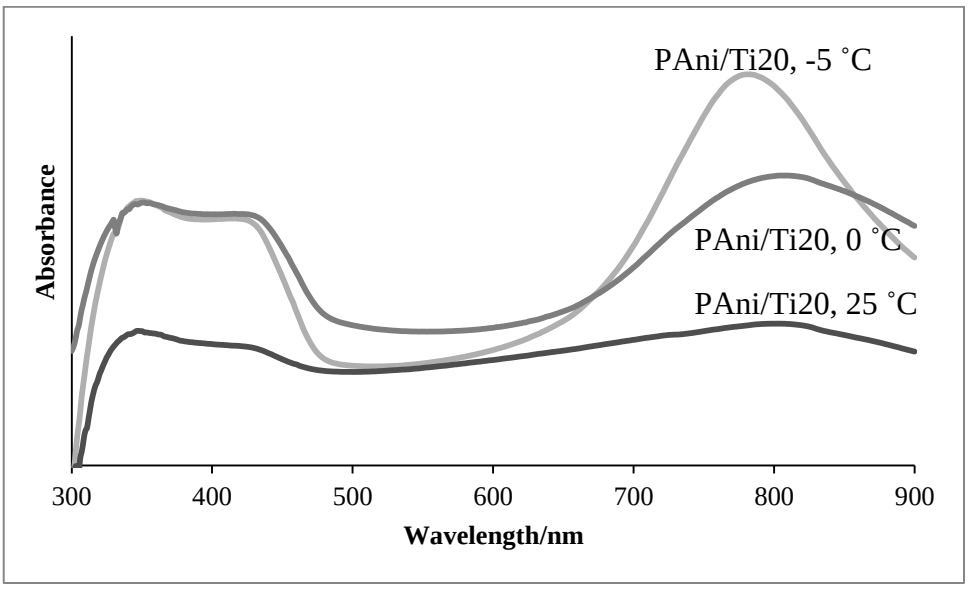

Figure 4.36 UV-Vis spectra of PAni/Ti20, -5 ˚C, PAni/Ti20, 0 ˚C and PAni/Ti20, 25 ˚C.

Table 4.11 The assignments of UV-Vis absorption peaks for PAni/TiO_2 nanocomposites synthesized with different polymerization temperatures

Polymer	π – π* (nm)	polaron – π* (nm)	π – polaron (nm)
PAni/Ti20, -5 ˚C	348	452	777
PAni/Ti20, 0 ˚C	345	452	795
PAni/Ti20, 25 ˚C	343	450	804

4.4.1 (c) XRD analysis

XRD diffractograms of PAni/Ti20 that synthesized at various polymerization temperatures (-5 ˚C, 0 ˚C and 25 ˚C) were shown in Figure 4.37. In general, all PAni/Ti20 nanocomposites exhibited almost similar peaks in the 2θ range of 5 – 25˚ as discussed in Section 4.1.1 (c) (XRD analysis). PAni/Ti20 nanocomposites synthesized at different polymerization temperatures exhibited some sharp peaks at 2θ = 47.9˚,

51.5˚, 53.8˚ and 61.5˚ that indicates degree of crystallinity due to the presence of TiO_2 nanoparticles in PAni/Ti20 matrix. Besides, the crystallinity of PAni/Ti20 nancomposites increase as the polymerization temperature decreases.

In general, PAni/Ti20, -5 ˚C, PAni/Ti20, 0 ˚C and PAni/Ti20, 25 ˚C exhibited almost identical trend in FTIR, UV-Vis and X-ray spectra (Figure 4.35 – 4.37) that significantly prove that all PAni/Ti20 nanocomposites obtained in this study possess similar chemical structure.

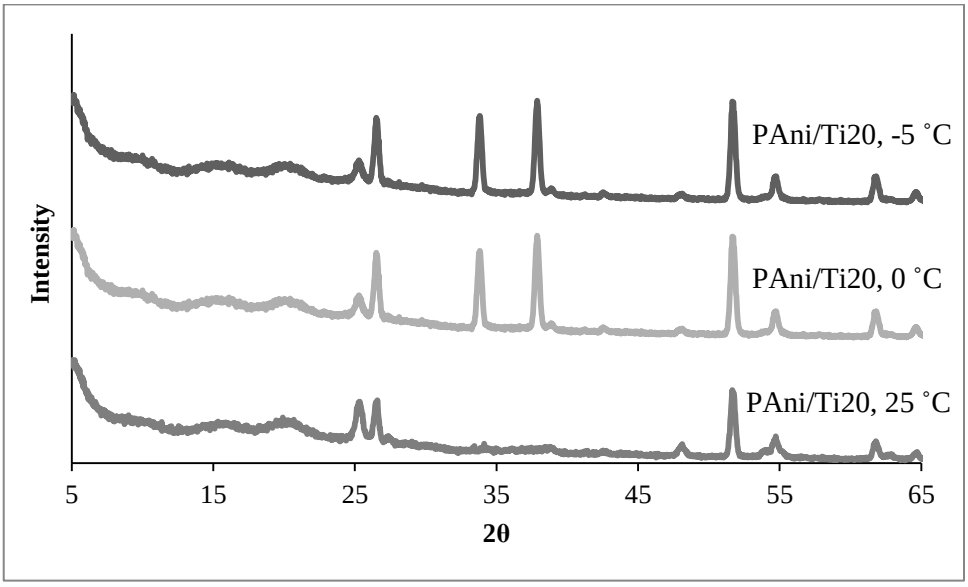

Figure 4.37 X-ray diffractograms of PAni/Ti20, -5 ˚C, PAni/Ti20, 0 ˚C and PAni/Ti20, 25 ˚C with different polymerization temperatures.

4.4.1 (d) FESEM analysis

Figure 4.38 (a)-(c) shows the FESEM images of PAni/Ti20, -5 ˚C, PAni/Ti20, 0 ˚C and PAni/Ti20, 25 ˚C, respectively with magnification of 20,000 × while Figure 4.38 (d) shows the morphology of PAni/Ti20, -5 ˚C from a distant-view with a magnification of 5,000 ×. In general, all PAni/Ti20 synthesized at different

polymerization temperatures show white coloured spots that indicates the presence of TiO_2 nanoparticles in PAni matrix (Katoch et al., 2012).

PAni/Ti20, -5 ˚C and PAni/Ti20, 0 ˚C presented thick and thin fibrillar structures, respectively that interconnects the PAni chains, thus reduce the electron hopping distance along the PAni backbone (Konyushenko et al., 2008). Besides, subzero polymerization temperature has resulted in a longer and perfect growth of PAni chain for PAni/Ti20, -5 ˚C. In addition, Figure 4.38 (d) clearly demonstrates the elongated fibrillary structure of PAni/Ti20, -5 ˚C from a distant view that will induce higher conductivity (Mi et al., 2014) (Table 4.12) compare to others PAni/Ti20 synthesized at different polymerization temperatures.

On the other hand, PAni/Ti20, 25 ˚C presumably possess irregular surface morphology due to the high polymerization temperature (Bláha et al., 2013). Besides, room temperature polymerization may cause defect sites and shorten the PAni chain that resulted in poor conductivity as shown in Table 4.12.

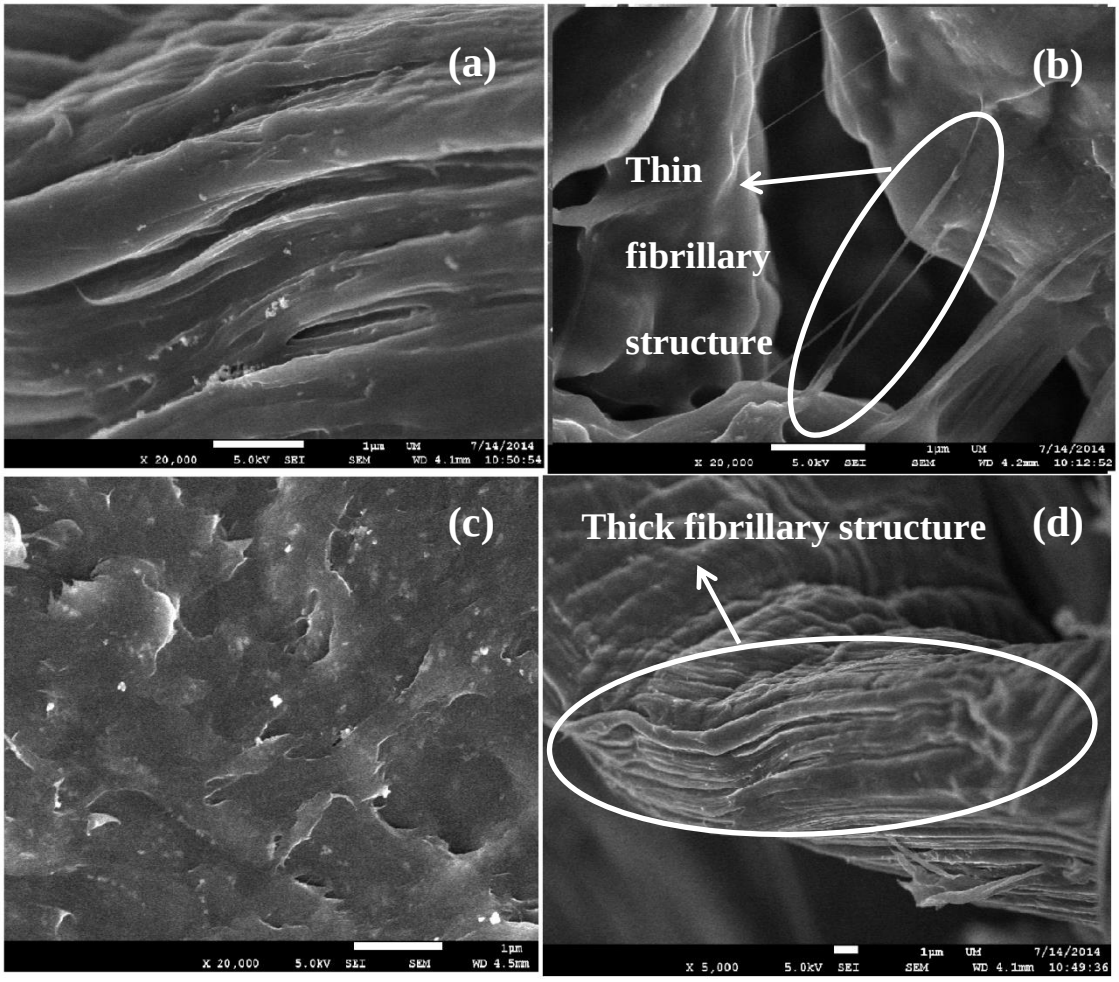

Figure 4.38 FESEM images of (a) PAni/Ti20, -5 ˚C, (b) PAni/Ti20, 0 ˚C and (c) PAni/Ti20, 25 ˚C at mangnifications of 20,000 × and (d) PAni/Ti20, -5 ˚C at magnifications of 5,000 ×.

4.4.1 (e) EDX analysis

Figure 4.39 depicts the EDX spectra of PAni/Ti20, -5 ˚C, PAni/Ti20, 0 ˚C, and PAni/Ti20, 25 ˚C. Typically, all EDX spectra of PAni/Ti20 nanocomposites synthesized at different polymerization temperature exhibited similar trend with PAni/TiO_2 nanocomposites in Section 4.3.1 (e). Thus, the typical characteristic peaks of PAni/T20 nanocomposites are not discussed in this section.

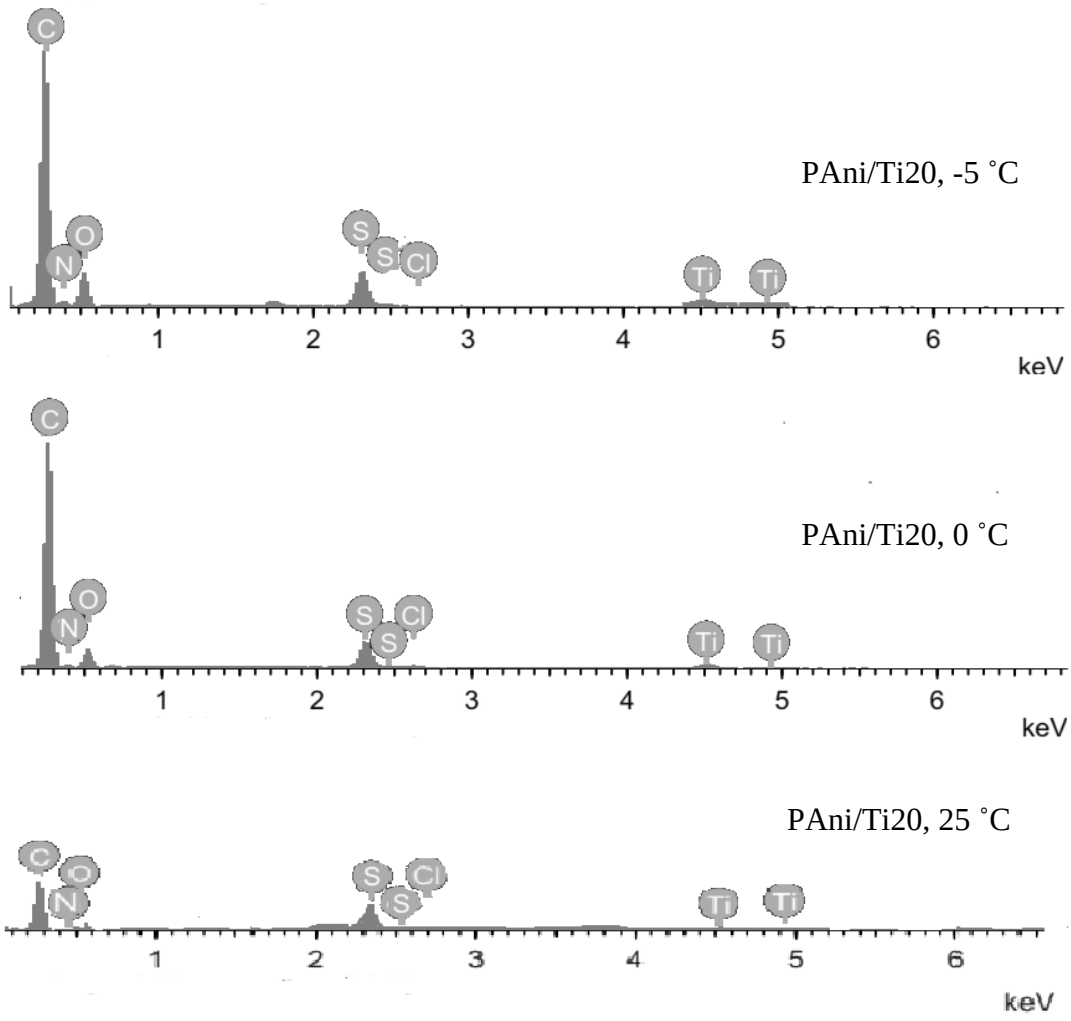

Figure 4.39 EDX spectra of PAni/Ti20 nanocomposites synthesized at different polymerization temperatures.

4.4.1 (f) Conductivity analysis

Table 4.12 shows the conductivities of PAni/Ti20 that synthesized at various polymerization temperatures. Among all PAni/TiO_2 nanocomposites, PAni/Ti20, -5 ˚C possessed the highest conductivity of 1.985 S/cm while PAni/Ti20, 0 ˚C and PAni/Ti20, 25 ˚C possessed the conductivity of 1.600 and 0.0028 S/cm, respectively.

PAni/Ti20, -5 ˚C that synthesized at subzero polymerization temperature will produce long PAni chain with less defect sites and higher crystallinity. Thus, in PAni/Ti20, -5 ˚C more delocalization of electron will appear along the PAni backbone and finally possessed the highest conductivity (Stejskal et al., 1998). On the other hand, PAni/Ti20, 25 ˚C that synthesized at higher temperature may produce PAni chains with numerous defect sites that will restrict electron hopping along the PAni backbone (Ansari and Mohammad, 2011) and resulted in poor conductivity of 0.0028 S/cm.

Table 4.12 Conductivities of PAni/Ti20 synthesized at various polymerization temperatures

Polymer	Conductivity (S/cm)
PAni/Ti20, -5 ˚C	1.9850
PAni/Ti20, 0 ˚C	1.6000
PAni/Ti20, 25 ˚C	0.0028

4.4.2 Responses of PAni/Ti20 nanocomposite (different polymerization temperature) sensors in hydrazine detection

In this part, PAni/Ti20 nanocomposites with Ani:AOT ratio of 5:7 with different polymerization temperatures (-5 ˚C, 0 ˚C and 25 ˚C) were monitored in hydrazine detection by using UV-Vis as main study. Conductivity and FTIR structural analysis were used as supporting element to investigate the interaction between PAni/Ti20 nanocomposites and hydrazine. All measurements of PAni/Ti20 nanocomposites were taken before and after immersion in hydrazine (1 – 100 ppm).

4.4.2 (a) UV-Vis responses

The UV-Vis responses of PAni/Ti20 nanocomposites synthesized at different polymerization temperatures in hydrazine detection (1 ppm) were investigated as shown in Figure 4.40. In general, all PAni/Ti20 nanocomposites showed significant decrease in normalized UV-Vis absorbance at 0.12 min and reached equilibrium from 1 – 5 min. For instance, PAni/Ti20, -5 ˚C has shown the most significant decrease in normalized UV-Vis absorbance at 0.12 min followed by PAni/Ti20, 0 ˚C and PAni/Ti20, 25 ˚C.

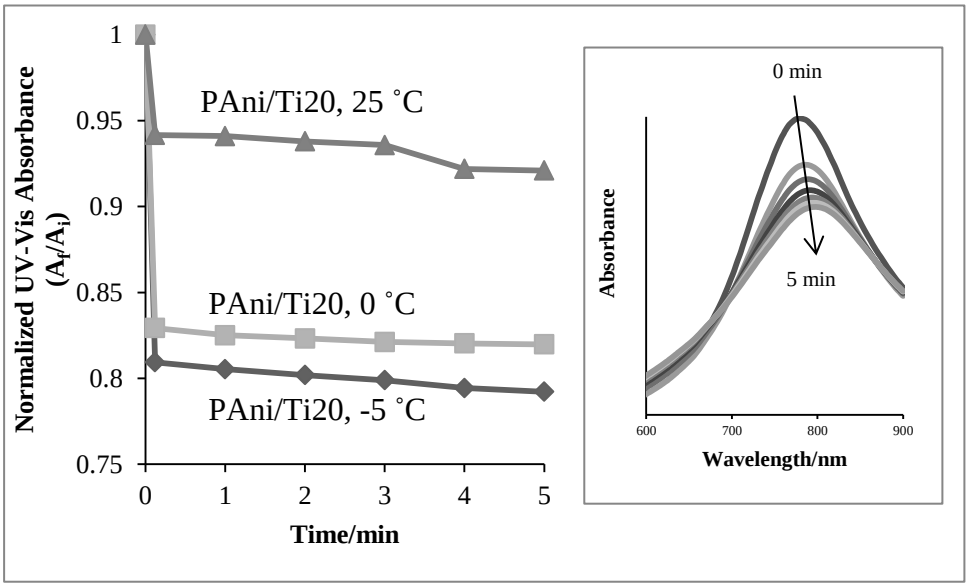

Figure 4.40 Normalized UV-Vis absorbance of PAni/Ti20, -5 ˚C, PAni/Ti20, 0 ˚C and PAni/Ti20, 25 ˚C for hydrazine detection (1 ppm) between 0 – 5 min. (Inset: The absorbance peak of PAni/Ti20 at ~795 nm in hydrazine detection).

PAni/Ti20 nanocomposites that synthesized at different polymerization temperatures were investigated in differerent concentrations of hydrazine (1 – 100 ppm) at 0.12 min as shown in Figure 4.41. In principle, all PAni/Ti20 nanocomposites exhibited decrease in normalized absorbance with increasing of hydrazine concentrations. PAni/Ti20, -5 ˚C has shown an extraordinary result by showing the

most significant decrease in normalized UV-Vis absorbance in hydrazine detection. Oppositely, PAni/Ti20, 0 ˚C and PAni/Ti20, 25 ˚C have shown a moderate and poor responses, respectively in hydrazine detection.

The sensing performance of PAni/Ti20, -5 ˚C in both Figure 4.40 and Figure 4.41 achieved the highest sensitivity in hydrazine detection because PAni/Ti20, -5 ˚C nanocomposite synthesized at subzero temperature (-5 ˚C) will produce PAni/Ti20, -5 ˚C with long conjugation length and more reactive sites in PAni/Ti20, -5 ˚C backbone as shown in UV-Vis spectrum (Figure 4.36) (Xia and Wang, 2001). Besides, PAni/Ti20, -5 ˚C possess the highest crystallinity (Figure 4.37) (Deivanayaki et al., 2013) and the highest conductivity of 1.985 S/cm (Table 4.12) that ensure PAni/Ti20, -5 ˚C possessed significant electron delocalization along the PAni backbone (Stejskal et al., 2010), thus results in the best performance in hydrazine detection. On the other hand, PAni/Ti20, 25 ˚C exhibited the poorest normalized UV-Vis absorbance in hydrazine detection due to the presence of defect sites along the PAni chain (Bláha et al., 2013).

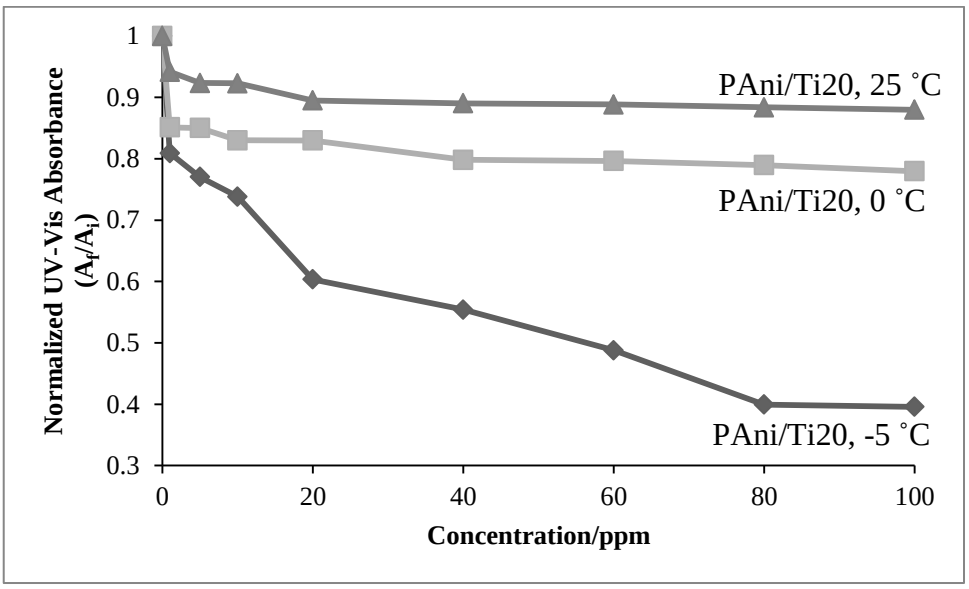

Figure 4.41 Normalized UV-Vis absorbance of PAni/Ti20, -5 ˚C, PAni/Ti20, 0 ˚C and PAni/Ti20, 25 ˚C in different concentrations of hydrazine (1 – 100 ppm).

4.4.2 (b) Conductivity responses

Normalized conductivities of PAni/Ti20 nanocomposites that synthesized under different polymerization temperatures (-5, 0 and 25 ˚C) were investigated in hydrazine detection (1 ppm) with respect to the time as shown in Figure 4.42. In essence, all PAni/Ti20 nanocomposites exhibited decrease in normalized conductivity with increase of time. Among all PAni/Ti20 nanocomposites, PAni/Ti20, -5 ˚C has shown significant decrease in normalized conductivity in hydrazine detection (1 ppm) at 0.12 min followed by PAni/Ti20, 0 ˚C and PAni/Ti20, 25 ˚C.

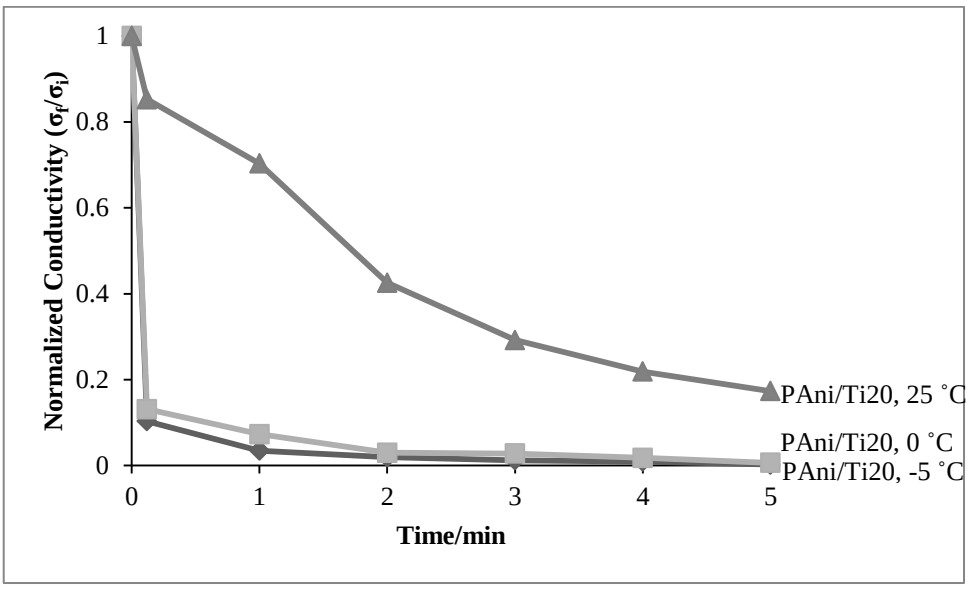

Figure 4.42 Normalized conductivity of PAni/Ti20, -5 ˚C, PAni/Ti20, 0 ˚C and PAni/Ti20, 25 ˚C in hydrazine detection (1 ppm).

Figure 4.43 shows the normalized conductivity of PAni/Ti20, -5 ˚C, PAni/Ti20, 0 ˚C and PAni/Ti20, 25 ˚C in different concentrations of hydrazine (1 – 100 ppm) at 0.12 min. In general, normalized conductivity of PAni/Ti20 nanocomposites decreased as the concentration of hydrazine increased. The normalized conductivity behaviors of all PAni/Ti20 nanocomposites are similar to the normalized UV-Vis absorbance in Section 4.4.2 (a), thus it further the prove validity of data obtained via UV-Vis response.

Among all PAni/Ti20 nancomposites that synthesized with different polymerization temperatures, PAni/Ti20, -5 ˚C in both Figure 4.42 and Figure 4.43 exhibit significant response due to the long and defect free PAni/Ti20, -5 ˚C chains and optimum amount of TiO_2 nanoparticles that forms the effective bridging between PAni/Ti20, -5 ˚C chains as shown in Figure 4.45. On the other hand, PAni/Ti20, 25 ˚C exhibited poor response in hydrazine detection due to formation of defect sites along the PAni/Ti20, -5 ˚C backbone during higher temperature polymerization.

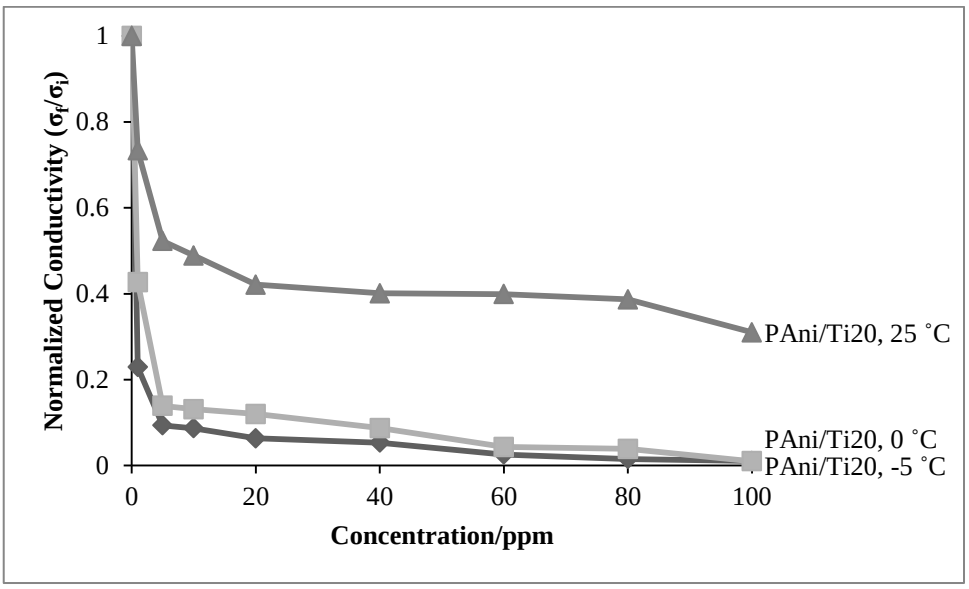

Figure 4.43 Normalized conductivity of PAni/Ti20, -5 ˚C, PAni/Ti20, 0 ˚C and PAni/Ti20, 25 ˚C Ti40 in different concentrations of hydrazine (1 – 100 ppm).

4.4.2 (c) FTIR structural analysis

Evidently, PAni/Ti20, -5 ˚C exhibited a significant response in hydrazine detection from 1 – 100 ppm as justified in UV-Vis (Section 4.4.2 (a)) and conductivity (Section 4.4.2 (b)) responses. Thus, PAni/Ti20, -5 ˚C was selected to study the structural changes that took place during the immersion in 1 ppm of hydrazine (Figure 4.44). The I_{1565}/I_{1485} ratio of PAni/Ti20, -5 ˚C (ES) before immersion was shown as 1.00 but it decreased to 0.85 after immersion (LE state) in hydrazine. Besides, decrement in I_{1565}/I_{1485} ratio depicts that PAni/Ti20, -5 ˚C in the ES state with equimolar benzenoid and quinoid rings will be converted into predominant benzenoid units in LE as shown by Figure 4.7. Therefore, FTIR structural analysis proves the successful transformation of ES to LE state upon immersion in hydrazine.

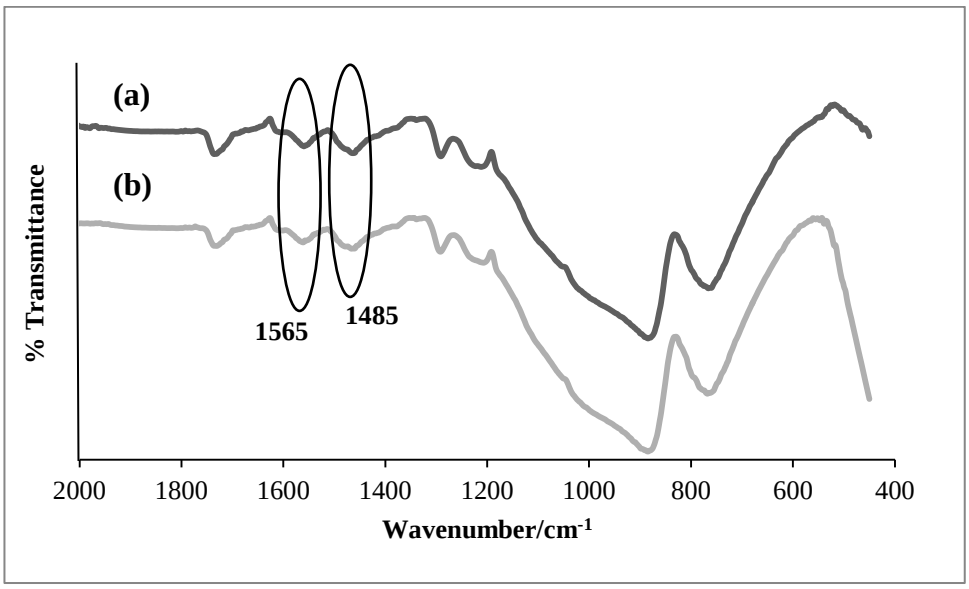

Figure 4.44 FTIR spectra of PAni/Ti20, -5 ˚C (a) before and (b) after immersion in hydrazine (1 ppm).

Schematic diagram in Figure 4.45 has been employed to discuss the sensitivity of PAni/Ti20 nanocomposites that synthesized at different polymerization temperatures (-5 ˚C, 0 ˚C and 25 ˚C) in hydrazine detection. Among all PAni/Ti20 nanocomposites, PAni/Ti20, -5 ˚C exhibited the most significant response in hydrazine detection. Eventhough, all PAni/Ti20 nanocomposites synthesized with similar Ani:AOT ratio of 5:7 and optimum amount of TiO_2 nanoparticles (20%), the manipulation on polymerization temperature has given a significant effect on the length of PAni/Ti20 nanocomposite chains. Thus, subzero polymerization temperature of PAni/Ti20, -5 ˚C has resulted in extended conjugation length that contains numerous reactive sites (Stejskal et al., 1998). Besides that, extended conjugation lead to more bridging between PAni and TiO_2 nanoparticles (Sengupta and Adhikari, 2007).

Even though, PAni/Ti20, 0 ˚C possessed almost all good characteristics as PAni/Ti20, -5 ˚C but polymerization at 0 ˚C did not help much on the performance for hydrazine detection. On the other hand, PAni/Ti20, 25 ˚C contained numerous defect

sites that restricted the electron delocalization and thus reduced the response in hydrazine detection.

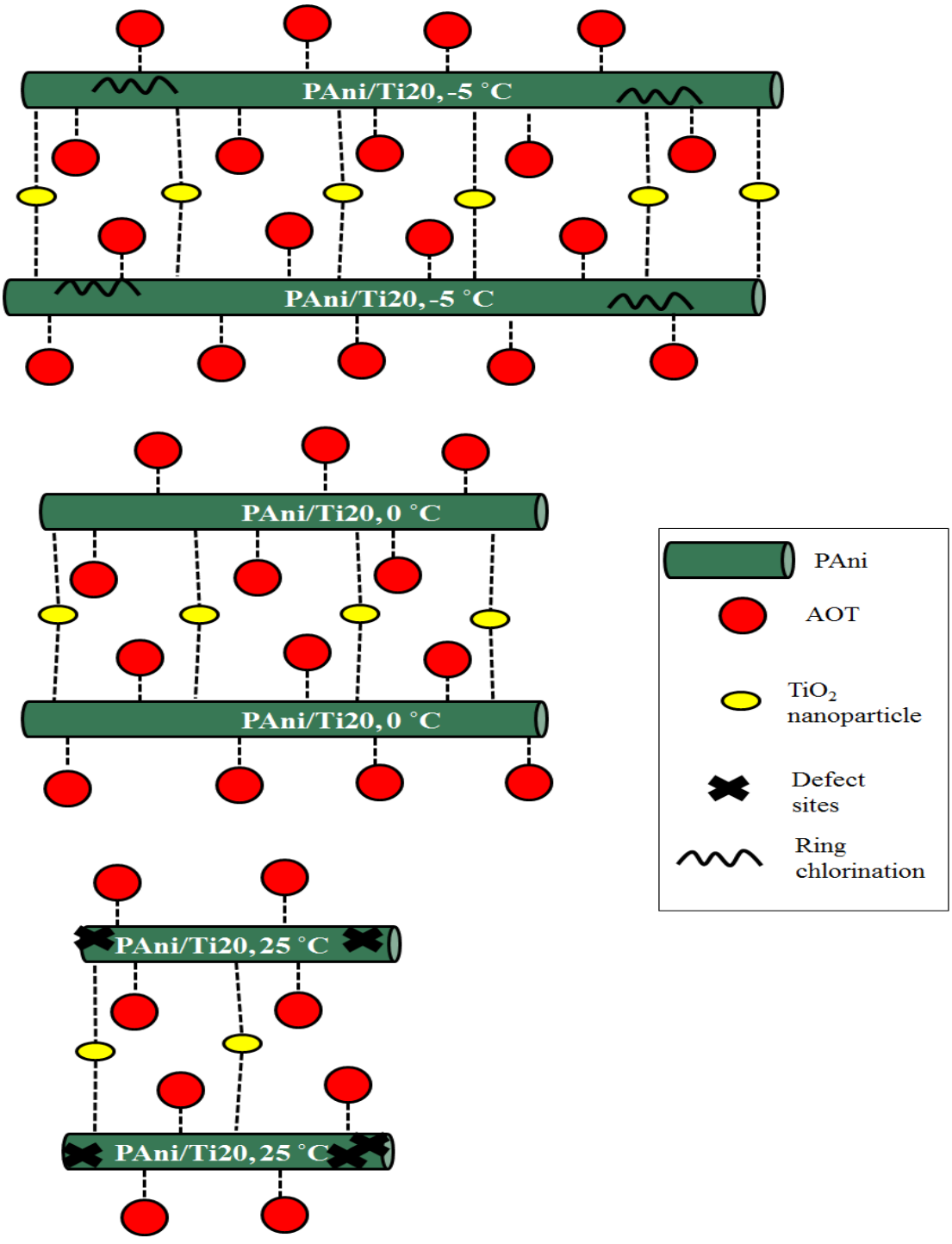

Figure 4.45 Schematic diagram of PAni/Ti20 synthsized at different polymerization temperatures.

4.5 Sensor performance of PAni/Ti20, -5 ˚C in hydrazine detection

In this study, two series of PAni were synthesized by manipulating their synthesis parameters. The first series was PAni/AOT with different dopant ratio (Section 4.1) and different polymerization temperatures (Section 4.2). The second series was PAni/TiO_2 nanocomposites with different TiO_2 ratio (Section 4.3) and different polymerization temperatures (Section 4.4). All these sections were discussed on the sensor responses of PAni in hydrazine detection from 1 – 100 ppm of hydrazine.

Among all PAni obtained in this study, PAni/Ti20, -5 ˚C clearly exhibits the best performance in hydrazine detection with significant results in both UV-Vis and conductivity responses upon immersion in hydrazine. Hence, the sensor performance of PAni/Ti20, -5 ˚C was studied in detail for hydrazine detection such as effect of film thickness, reusability, selectivity and long term stability (UV-Vis analysis).

4.5.1 Effect of film thickness

Figure 4.46 shows the effect of film thickness of PAni/Ti20, -5 ˚C nanocomposite in UV-Vis response during hydrazine detection (1 ppm). Equation 3.5 was utilized to obtain the UV-Vis response of PAni/Ti20, -5 ˚C with different film thicknesses.

In general, UV-Vis response of PAni/Ti20, -5 ˚C decreased with the increase film thicknesses during hydrazine detection. Among all different film thicknesses of PAni/Ti20, -5 ˚C, film thickness of 1 µm showed the most significant response of 1.27. Meanwhile, PAni/Ti20, -5 ˚C with thicker films of 3, 5.5, 7 and 9 µm showed poor

responses of 1.09, 1.08, 1.06 and 1.04, respectively. PAni/Ti20, -5 ˚C nanocomposites with the thinnest film (1 µm) showed the best result due to the presence optimum amount of reactive sites at the surface of the film (Xie et al., 2002). On other hand, the sensitivity of thicker films (3, 5.5, 7 and 9 µm) were reduced due to the overlapping of films which might restrict the active sites for the interaction with hydrazine (Gill et al., 2010).

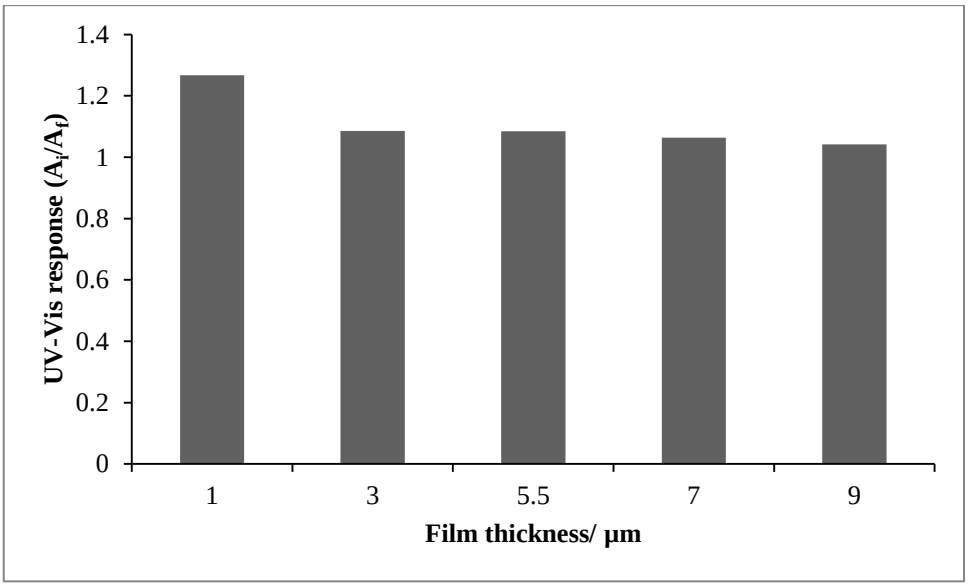

Figure 4.46 UV-Vis response of PAni/Ti20, -5 ˚C with different film thickness in hydrazine detection (1 ppm) at 0.12 min.

4.5.2 Reusability study

During hydrazine detection, PAni/Ti20, -5 ˚C nanocomposite will change from ES to LE due to dedoping process. In order to reuse the PAni/Ti20, -5 ˚C nanocomposite, HCl (1 M) is used to redope the PAni/Ti20, -5 ˚C nanocomposite to transfer the LE to ES state. Therefore, in this study, 1 M of HCl (for redoping) and 1 ppm of hydrazine (for dedoping) is used to study the reusability in Figure 4.47.

PAni/Ti20, -5 ˚C nanocomposite possess the highest normalized UV-Vis absorbance at polaron peak (~777 nm) before immersion in hydrazine. The normalized UV-Vis absorbance decreased after immersion in hydrazine within 0.12 min (7 s). Then, in order to reuse the PAni/Ti20, -5 ˚C nanocomposite, 1 M of HCl was used to redope and the normalized UV-Vis absorbance of PAni/Ti20, -5 ˚C nanocomposite increased within 0.08 min (5 s) but never attained the initial absorbance value of ES. Presumably the heavy reaction products (hydrazine) hardly leave the interface of polyaniline backbone after hydrazine detection. Similar phenomenon was observed by Raut et al., (2012) and Tai et al., (2008).

Before immersion in hydrazine, PAni/Ti20, -5 ˚C in the ES state will possess numerous polarons (mobile charge carriers) that will give rise to the peak at ~777 nm in the UV-Vis spectrum (Figure 4.36). However, ES of PAni/Ti20, -5 ˚C will be dedoped by hydrazine to produce LE with lesser polarons which will cause the decrease in the polaron peak. During the reusability process, LE will gain the polarons upon interaction with HCl and reproduce the ES (Malinauskas and Holze, 1999). Thus, the conversion between ES and LE is a reversible mechanism as demonstrated in Figure 4.48 (Salvatierra et al., 2010). In summary, PAni/Ti20, -5 ˚C shows good reusability up to 10 cycles with shortest respond and recovery time of 0.12 min and 0.08 min, respectively.

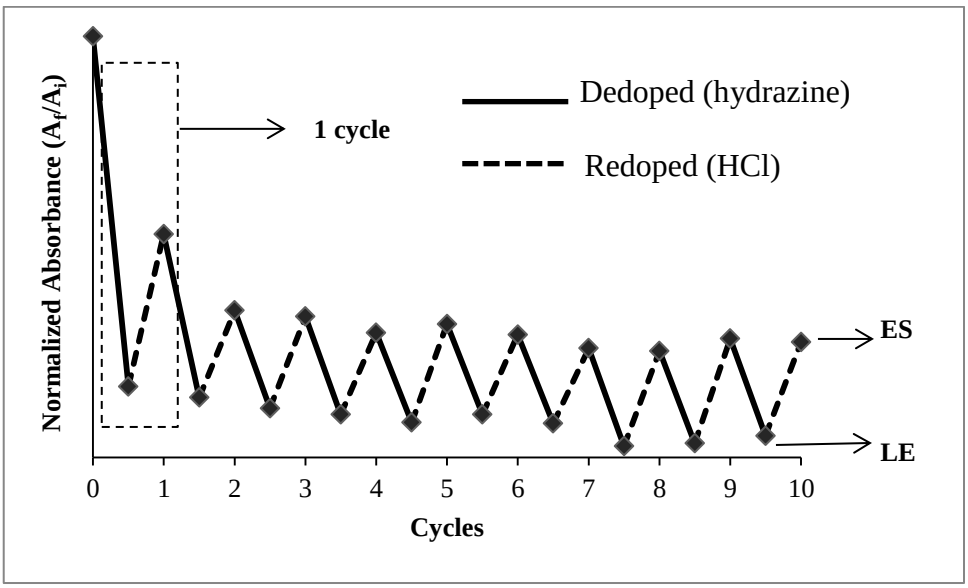

Figure 4.47 Reusability of PAni/Ti20, -5 ˚C during hydrazine detection (Dedoped by hydrazine and redoped by HCl).

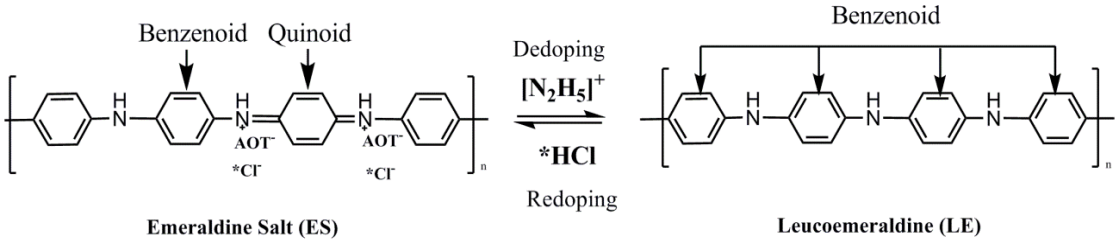

Figure 4.48 Reversible mechanism of ES state (before immersion in hydrazine) and LE state (after immersion in hydrazine) of PAni/Ti20, -5 ˚C upon dedoping (hydrazine) and redoping (HCl) processes.

4.5.3 Selectivity of PAni/Ti20, -5 ˚C nanocomposite in hydrazine detection

Selectivity can be defined as the ability of a chemical sensor to differentiate the target species in the presence of other species (Raut et al., 2012). In this study, selectivity of PAni/Ti20, -5 ˚C nanocomposite in hydrazine detection was performed by using UV-Vis measurement since PAni can exhibit different absorbance peaks at

different states according to the nature of reacting species such as acid, base, reducing agent and oxidizing agent (Wei et al., 1994).

In essence, hydrazine that detected by PAni/Ti20, -5 ˚C nanocomposites in this study is a weak base and strong reducing agent. Thus, other interfering species such as formic acid (reducing agent), 2-propanol (reducing agent), sodium hydroxide (base) and ammonia (base) have been selected in the UV-Vis measurement for selectivity study.

Figure 4.49 shows UV-Vis spectra of (a) PAni/Ti20, -5 ˚C before immersion and its spectra after immersion in (b) hydrazine, (c) formic acid, (d) 2-propanol, (e) sodium hydroxide, (f) ammonia and (g) combination of hydrazine and other interfering species in the wavelength range of 450 – 900 nm for selectivity study. In general, the polaron peak of PAni/Ti20, -5 ˚C (~780 nm) shifted to different wavelengths when immersed in basic species or decrease in intensities when immersed in reducing agent.

Before hydrazine detection, PAni/Ti20, -5 ˚C exist in the ES state that possess strong polaron peak at ~780 nm (Figure 4.49 (a)). Significant decrease in the polaron peak was observed upon immersion of PAni/Ti20, -5 ˚C in hydrazine (reducing agent) due to the reduction of ES to LE state. However, PAni/Ti20, -5 ˚C did not show significant decrease at polaron peak for other reducing agents such as formic acid and 2-propanol (Wei et al., 1994).

On the other hand, polaron peak of PAni/Ti20, -5 ˚C (ES) that centered at ~780 nm is shifted to shorter wavelength of 580 and 563 nm for basic species such as sodium hydroxide and ammonia, respectively. This phenomenon is due to the interaction of ES

with a strong base to produce emeraldine base (EB) that will shift the absorption peak to shorter wavelength of ~580 nm (Wei et al., 1994).

PAni/Ti20, -5 ˚C exhibits 77% of decrease in the polaron peak after immersion in hydrazine (Figure 4.49 (b)). Meanwhile, immersion of PAni/Ti20, -5 ˚C in combination of all analytes in the sensing environment (Figure 4.49 (g)) exhibits 74% of decrease in the polaron peak that is close to hydrazine detection peak. Therefore, PAni/Ti20, -5 ˚C shows good selectivity in hydrazine detection in the presence of other interfering species.

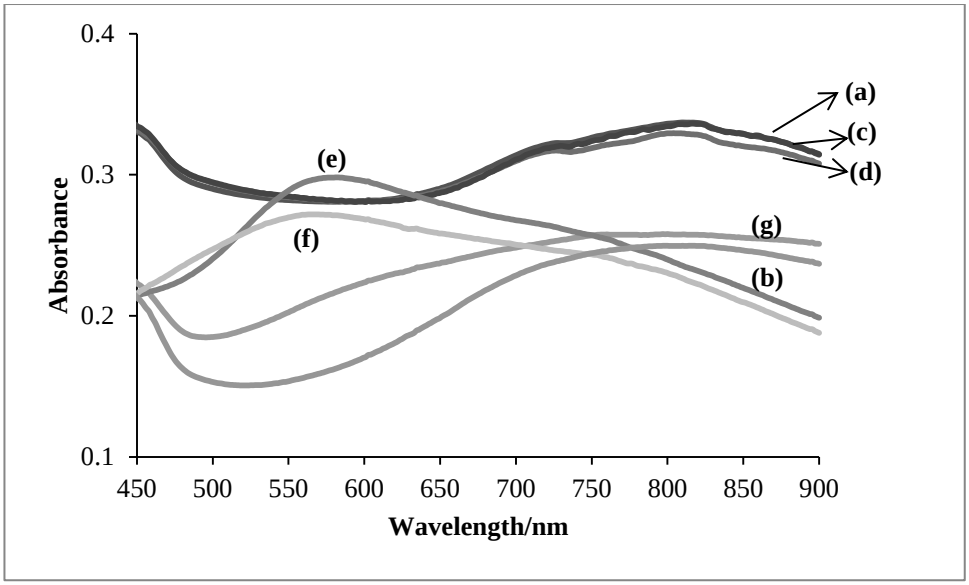

Figure 4.49 UV-Vis spectra of (a) PAni/Ti20, -5 ˚C before immersion and after immersion in (b) hydrazine (c) formic acid, (d) 2-propanol, (e) sodium hydroxide, (f) ammonia and (g) combination of hydrazine and other interfering species for selectivity study.

4.5.4 Long term stability of PAni/Ti20, -5 ˚C nanocomposites in hydrazine detection

In this study, long term stability of PAni/Ti20, -5 ˚C in hydrazine detection (1 ppm) was evaluated up to 60 days as shown in Figure 4.50. The sensor response of PAni/Ti20, -5 ˚C shows gradual decrease in normalized absorbance with 13% changes (compare to initial response) in the first 12 days due to the aging process of PAni/Ti20, -5 ˚C. Zheng and co-workers (2008) have found similar phenomenon during the detection of trimethylamine by using PAni films. After that, the sensor response showed slight decrease in normalized UV-Vis absorbance range of 13 – 20% and maintained the normalized UV-Vis absorbance at ~0.70 – 0.60 up to 60 days. From the data obtained, it can be significantly concluded that the PAni/Ti20, -5 ˚C nanocomposite shows good long term stability up to 60 days in hydrazine detection compare to previous research (Wang et al., 2014; Zhu et al., 2015).

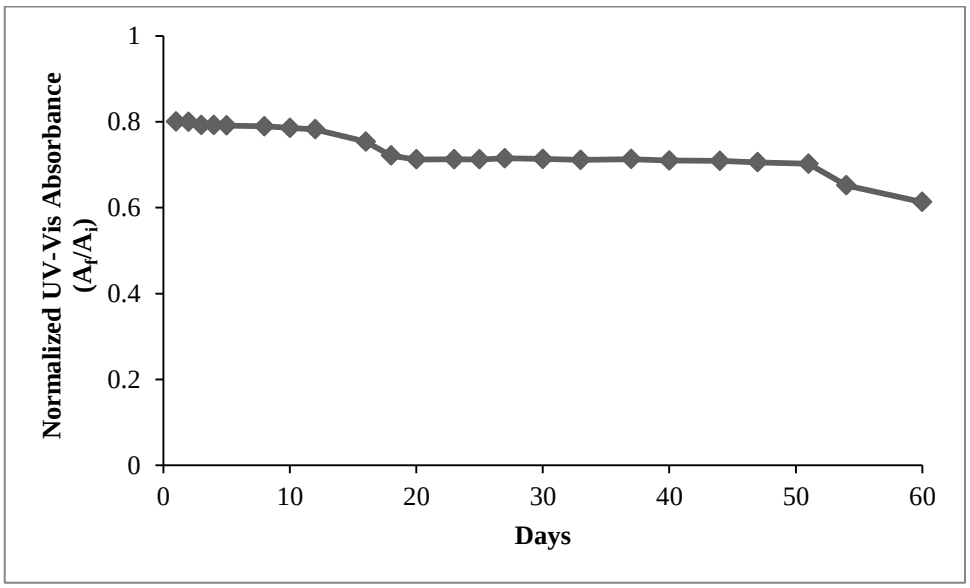

Figure 4.50 Long term stability of PAni/Ti20, -5 ˚C up to 60 days.

4.6 Method Validation

In this part, the best PAni under different synthesis parameters such as PAni **3**, PAni, -5 ˚C, PAni/Ti20 and PAni/Ti20, -5 ˚C are selected and tested in different calibration curves to understand their reliabilities in sensing mechanism. Lower concentration range of hydrazine (0.05 – 5.00 ppm) was used to construct the calibration curve for all PAni in hydrazine detection since the limit of detection (LOD) recommended by Occupational Safety and Health Administration (OSHA) is 1 ppm (Liu et al., 2014).

In general, all PAni obtained in this study showed good linearity in their calibration curves with R^2 of 0.9900 – 0.9928 and possessed LOD that is lower than that set by OSHA. Among all PAni, PAni/Ti20, -5 ˚C exhibited the best sensor performance with the highest linearity (0.9928), sensitivity (0.0473 L/mg) and lowest LOD (0.05 ppm) in its calibration curve (Figure 4.51).

Table 4.13 shows the analytical performance of PAni synthesized with different synthesis parameters such as sensitivity, linearity (R^2), LOD and limit of quantitation (LOQ) during hydrazine detection. Besides, LOD and LOQ of all resulted PAni were calculated based on equations 3.7 and 3.8, respectively.

Since hydrazine is a toxic substance that can cause cancer, OSHA and Chinese National Standard GB 18061-2000 have set LOD for hydrazine to be 1.00 ppm and 0.20 ppm, respectively (Gao et al., 2013; B. Liu et al., 2014). Among all PAni, PAni/Ti20, 0 ˚C and PAni/Ti20, -5 ˚C have shown an excellent LOD of 0.10 and 0.05 ppm, respectively, which is lower than the standard set by both OSHA and Chinese National

Standard GB 18061-2000. Calibration curves for other PAni such as PAni **3**, PAni, -5 ˚C and PAni/Ti20 were shown in Appendix C1 – C3.

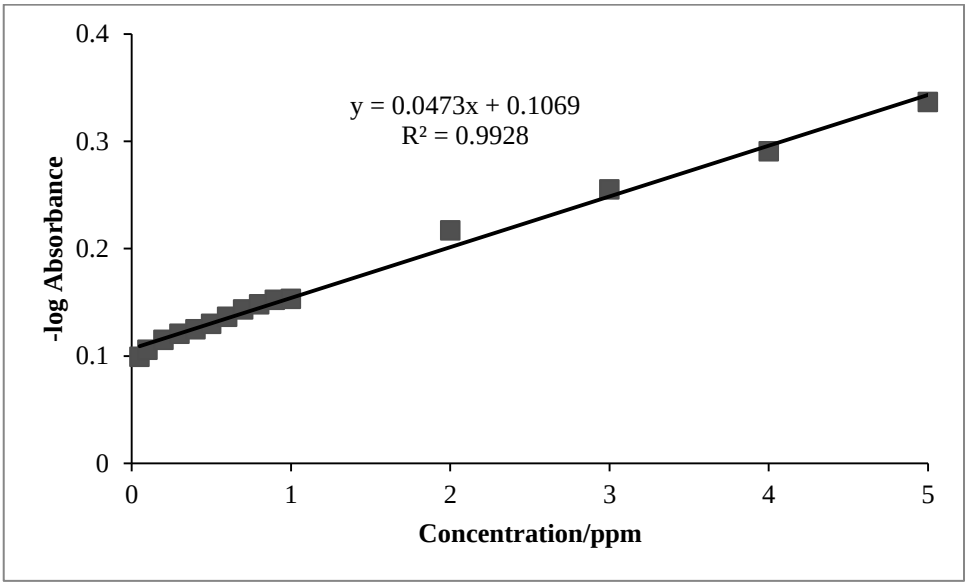

Figure 4.51 Calibration curve of PAni/Ti20, -5 ˚C in hydrazine detection with concentration range of 0.05 – 5.00 ppm.

Table 4.13 Analytical performance of PAni sensors (different synthesis parameters) in hydrazine detection that obtained from calibration curves.

Polymer	**Linear range (ppm)**	**Sensitivity (L/mg)**	**R^2**	**LOD (ppm)**	**LOQ (ppm)**
PAni **3**	0.05 – 5.00	0.0053	0.9900	0.49	1.62
PAni, -5 ˚C	0.05 – 5.00	0.0106	0.9915	0.24	0.81
PAni/Ti20	0.05 – 5.00	0.0268	0.9927	0.10	0.32
PAni/Ti20, -5 ˚C	0.05 – 5.00	0.0473	0.9928	0.05	0.18

4.7 Real sample analysis

The applicability of the proposed PAni/Ti20, -5 ˚C nanocomposite was validated using the real environmental sample by UV-Vis measurement. The real water samples were collected from two destinations. The first real sample was the tap water that collected from a Polymer Research Lab (FD-L4-24) at Department of Chemistry, University of Malaya. The second real sample was collected from Sungai Batu nearby Selayang, Selangor that surrounded by a rubber factory, heavy construction area and some residential areas (Figure 4.52). Both real water samples were filtered by Buchner filtration method to get rid of any large debris before experiment.

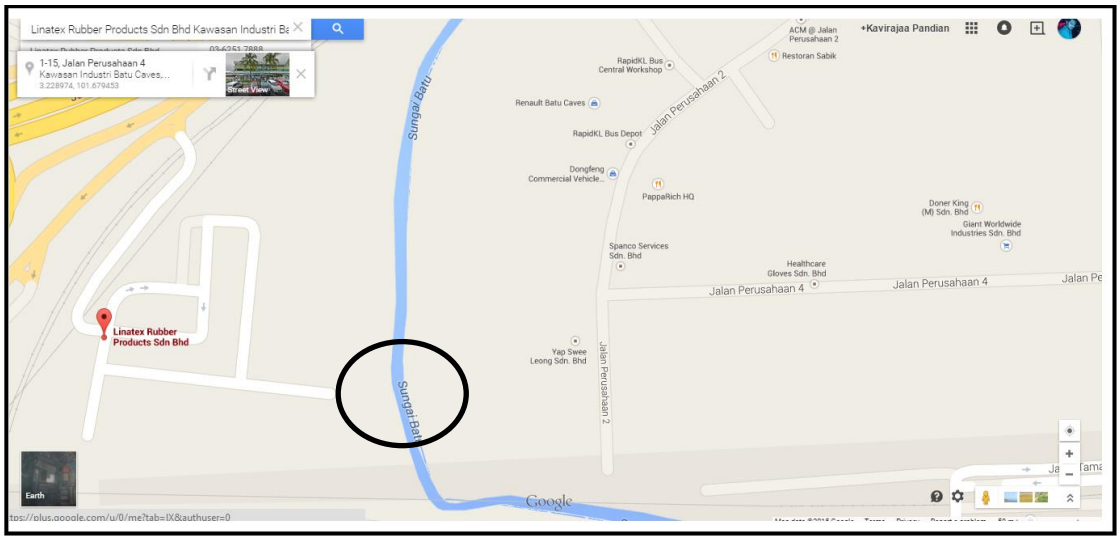

Figure 4.52 The water used for real sample analysis was collected from Sungai Batu, Selayang.

PAni/Ti20, -5 ˚C nanocomposite is analysed by UV-Vis spectrometer for the determination of known concentration of hydrazine in the spiked real water sample as mentioned earlier (tap and river water). UV-Vis responses of PAni/Ti20, -5 ˚C nanocomposite on both real water samples are repeated four times (B1 – B4) in different concentrations of hydrazine (0.50, 1.00 and 4.00 ppm). Typically, the

absorbances obtained from PAni/Ti20, -5 ˚C nanocomposite at ~777 nm upon immersion in different concentrations of hydrazine in tap and river are substituted in the linear equation of calibration curve (y = 0.0473× + 0.1068) to get the concentration as shown by Table 4.14 and Table 4.15 (B1 – B4). Hereafter, recovery and relative standard deviation (RSD%) PAni/Ti20, -5 ˚C in both tap and river water were calculated based on Equations 3.9 and 3.10, respectively.

Table 4.14 and Table 4.15 show the spiked concentration of hydrazine (0.50 – 4.00 ppm), found (detected amount of hydrazine by using UV-Vis) with its respective mean, recovery and relative standard deviation (RSD%) for both tap water and river water during hydrazine detection. In this study, PAni/Ti20, -5 ˚C nanocomposites possess the good recovery and RSD of ~90 – 110 % and 0.31 – 4.21 %, respectively which are satisfactory according to the previously reported articles (Raoov et al., 2014).

Table 4.14 Spiked, found, recovery and RSD values of PAni/Ti20, -5 ˚C in tap water during hydrazine detection.

Spiked (ppm)	Found (ppm)				Mean	Recovery	RSD%
	B1	B2	B3	B4			
0.50	0.49	0.45	0.45	0.46	0.46	94%	3.51
1.00	0.91	0.94	0.93	0.95	0.93	93%	1.51
4.00	3.86	3.88	3.88	3.89	3.88	97%	0.31

Table 4.15 Spiked, found, recovery and RSD values of PAni/Ti20, -5 ˚C in river water during hydrazine detection.

Spiked (ppm)	Found (ppm)				Mean	Recovery	RSD%
	B1	B2	B3	B4			
0.50	0.51	0.51	0.53	0.52	0.52	104%	1.46
1.00	1.09	1.08	1.01	1.01	1.05	105%	3.94
4.00	4.11	4.45	4.11	4.48	4.29	105%	4.21

4.8 Summary of PAni sensors in hydrazine detection

PAni is one of the conducting polymers that have been studied extensively by many researchers (Gao et al., 2008; Koul et al., 2001; Nicolas-Debarnot et al., 2003). It is because the unique properties of PAni can be fine-tuned by its synthesis parameters according to the desired applications. Therefore, this section is focusing on the summary of the research findings in this study such as the overall sensor performance and the chemical interaction between PAni and hydrazine during hydrazine detection.

Table 4.16 describes the summary of PAni synthesized with different dopant ratio in hydrazine detection. Among all PAni, PAni **3** with optimum Ani:AOT ratio of 5:7 that possess the highest conductivity will give the best sensor response (UV-Vis) in hydrazine detection. It is because, PAni **3** contains numerous reactive sites along the PAni backbone for hydrazine detection.

Table 4.16 Effect of conductivity on PAni (different dopant ratio) in sensor performance during hydrazine detection.

PAni	Conductivity (S/cm)	Sensor response (UV-Vis)*	Sensor Performance	Explanation
PAni **1**	0.42	0.998	Poor	Little reactive sites
PAni **2**	0.58	0.941	Moderate	Moderate reactive sites
PAni **3**	0.79	0.918	Best	Numerous reactive sites

*The lower the normalized UV-Vis absorbance, the higher the performance of PAni sensor.

Since PAni **3** exhibited the best performance in hydrazine detection, the similar Ani:AOT (5:7) ratio was selected for the manipulation on different polymerization temperatures form -10 ˚C to 25 ˚C. Table 4.17 describes the summary of PAni synthesized with different polymerization temperature in hydrazine detection. Among all PAni, PAni, -5 ˚C with longer chains that possess the highest conductivity will give the best sensor response (UV-Vis) in hydrazine detection. It is because, PAni, -5 ˚C contains numerous reactive sites along the extended PAni backbone for hydrazine detection.

Table 4.17 Effect of conductivity on PAni (different polymerization temperatures) in sensor performance during hydrazine detection.

PAni	Conductivity (S/cm)	Sensor response (UV-Vis)*	Sensor Performance	Explanation
PAni, -10 ˚C	0.23	0.928	Moderate	Longer chain length with ring chlorination
PAni, -5 ˚C	1.81	0.874	Best	Longer chain length with numerous reactive sites
PAni, 0 ˚C	0.82	0.918	Moderate	Moderate chain length with numerous reactive sites
PAni, 25 ˚C	0.01	0.932	Poor	Defects in PAni chains

In the third part of this research work, in-situ incorporation of TiO_2 nanoparticles in PAni with Ani:AOT ratio of 5:7 that synthesized at 0 ˚C with different TiO_2 ratio were investigated. Table 4.18 describes the summary of PAni synthesized with different TiO_2 ratio in hydrazine detection. Among all PAni/TiO_2 nanocomposites, PAni/Ti20 with optimum amount TiO_2 nanoparticles (20%) in PAni chains, that possess the highest conductivity have given the best sensor response (UV-Vis) in hydrazine detection. It is because, PAni/Ti20 with optimum amount TiO_2 nanoparticles would create effective bridiging between PAni chains that enhances the electron delocalization during hydrazine detection.

Table 4.18 Effect of conductivity on PAni/TiO_2 nanocomposites (different TiO_2 ratio) in sensor performance during hydrazine detection.

PAni	Conductivity (S/cm)	Sensor response (UV-Vis)*	Sensor Performance	Explanation
PAni/Ti10	0.90	0.851	Moderate	Doesn't have optimum amount of TiO_2
PAni/Ti20	1.60	0.829	Best	Possess optimum amount of TiO_2
PAni/Ti40	0.60	0.967	Poor	Excess TiO_2 blocked conductive pathway of PAni

The last part of this research work is focused on the manipulation of polymerization temperature (-5 ˚C to 25 ˚C) in PAni/Ti20 nanocomposites that synthesized with Ani:AOT ratio of 5:7 with 20% of TiO_2 nanoparticles for hydrazine detection. Table 4.19 describes the summary of PAni/Ti20 nanocomposites synthesized with different polymerization temperatures for hydrazine detection. Among all PAni/Ti20 nanocomposites, PAni/Ti20, -5 ˚C, that possess the longest chain with defect free sites exhibists highest conductivity and given the best sensor response (UV-Vis) in hydrazine detection.

Table 4.19 Effect of conductivity on PAni/Ti20 nanocomposites (different polymerization temperature) in sensor performance during hydrazine detection.

PAni	Conductivity (S/cm)	Sensor response (UV-Vis)*	Sensor Performance	Explanation
PAni/Ti20, -5 ˚C	1.99	0.809	Best	Highest dopant ratio, longer PAni chain and optimum amount of TiO_2 nanoparticles
PAni/Ti20, 0 ˚C	1.60	0.829	Moderate	Moderate PAni length
PAni/Ti20, 25 ˚C	0.0028	0.942	Poor	Numerous defect sites in PAni chain

CHAPTER 5 CONCLUSION AND RECOMMENDATIONS

5.1 Conclusion

In this research work, two series of PAni were synthesized for hydrazine detection. The first series was synthesis of PAni/AOT with different dopant ratio and different polymerization temperatures. The second series was the synthesis of PAni/TiO_2 nanocomposites with different TiO_2 ratio and different polymerization temperatures. FTIR, UV-Vis and XRD spectra obtained confirmed the chemical structures of resulted PAni. FESEM and EDX were done simultaneously to investigate the morphology and the composition (elements present) in PAni matrix.

PAni with optimum Ani:AOT ratio of 5:7 produce the numerous reactive sites and polarons that significantly increase the conductivity of PAni. PAni/AOT that synthesized with different polymerization temperatures provided a good knowledge on the PAni chain length where PAni synthesized at -5 ˚C possessed longer PAni chain length that improved the conductivity due more reactive sites for the interaction with hydrazine. In addition, well known complementary behavior of p-type, PAni and n-type, TiO_2 nanoparticles which was not investigated in hydrazine detection, elsewhere was investigated in this research work. PAni with optimum amount of TiO_2 nanoparticles (20 %) show significant response in hydrazine detection in comparison with PAni/Ti10 and PAni/Ti40. Hence, the knowledge in manipulation of polymerization temperature in extending the conjugation length of PAni/Ti20 was also investigated at different polymerization temperatures. Similarly, PAni/Ti20, -5 ˚C with high conductivity due to the subzero temperature posses numerous reactive sites has shown remarkable response in hydrazine detection.

Since PAni/Ti20, -5 ˚C showed the significant response in both UV-Vis and conductivity responses, it was selected in the optimization of sensor properties such as effect of film thickness, reusability, selectivity, long term stability, method validation and real sample analysis. PAni/Ti20, -5 ˚C with optimum film thickness of 1 µm, showed the best sensor performance in hydrazine detectcion. PAni/Ti20, -5 ˚C shows good reusability up to 10 cycles with shortest respond and recovery time of 0.12 min and 0.08 min, respectively. Besides, PAni/Ti20, -5 ˚C exhibited excellent selectivity in the presence of other interfering species that composed of both strong base and reducing agents such as ammonia, sodium hydroxide, formic acid and 2-propanol. Another important criteria of sensor is the long term stability or in another words shelf-life of sensor. PAni/Ti20, -5 ˚C showed good long term stability up to 60 days in hydrazine detection (1 ppm).

The final part of this research work is to apply PAni/Ti20, -5 ˚C in real water samples during hydrazine detection. The water samples were collected from laboratory tap water and river water. Among all best PAni from each sections, PAni/Ti20, -5 ˚C exhibited good linear regression (0.9928) and highest sensitivity (0.0473 L/mg) and lowest LOD (0.05 ppm). The, known concentrations of hydrazine were spiked in the real water samples (tap and river water) and tested by using PAni/Ti20, -5 ˚C. It showed satisfactory results for all the known concentration of hydrazine that were spiked in the real water samples.

In conclusion, all the objectives set in this research work were accomplished. Therefore, PAni/Ti20, -5 ˚C is highly recommended as an effective, sensitive, selective and inexpensive sensor for hydrazine detection with good reusability (10 cycles), selectivity and long term stability (60 days). Besides, PAni/Ti20, -5 ˚C also exhibits good analytical performances such as linearity (0.9928), sensitivity (0.0473 L/mg) and the lowest LOD (0.05 ppm).

5.2 Suggestions for future works

As discussed in Section 4.1, very few reports are found in the use of AOT as dopants for PAni. Thus, similar methodology can be carried out to develop a sensitive sensor for other analytes.

The dopant used in this study (AOT) played an important key role in producing soluble PAni in organic solvent. Solubility is a very important characteristic of PAni to prepare a uniform coating that will possess the good qualities of sensors. Therefore, as a recommendation, PAni can be synthesized with substituted aniline such as alkyl substituted aniline monomers which will also improve the solubility of resulting PAni (Falcou et al., 2005). However, typical characterizations and appropriate sensor measurements are needed to validate the PAni.

In this study, UV-Vis measurements were carried out to make the sensor to be applied in a cost-effective manner and UV-Vis spectrometer is an instrument that can be found even in simple laboratories. In spite of that, electrochemical measurements possessed lesser instrumental error and high accuracy and sensitivity in an open discussion of sensors. Therefore, the PAni synthesized in this study can be evaluated by using electrochemical measurements to achieve even low LOD that set by WHO.

The synergetic behavior between PAni (p-type) and inorganic nanoparticles (n-type) such as tin oxide (SnO_2), ferric oxide (Fe_3O_4), gold (Au) and silver (Ag) nanoparticles can be investigated to obtain a PAni with synergetic effects that might improve the performance of PAni as a sensor in hydrazine detection.

REFERENCES

Abaci, S., Nessark, B., Boukherroub, R., & Lmimouni, K. (2011). Electrosynthesis and analysis of the electrochemical properties of a composite material: Polyaniline+titanium oxide. *Thin Solid Films*, *519*(11), 3596–3602. doi:10.1016/j.tsf.2011.01.277

Adhikari, B., & Majumdar, S. (2004). Polymers in sensor applications. *Progress in Polymer Science*, *29*(7), 699–766. doi:10.1016/j.progpolymsci.2004.03.002

Advani, G. N., Komem, Y., Hasenkopf, J., & Jordan, A. G. (1981). Improved performance of SnO2 thin-film gas sensors due to gold diffusion. *Sensors and Actuators*, *2*, 139–147. doi:10.1016/0250-6874(81)80033-9

Ameen, S., Akhtar, M. S., & Shin, H. S. (2012). Hydrazine chemical sensing by modified electrode based on in situ electrochemically synthesized polyaniline/graphene composite thin film. *Sensors and Actuators B: Chemical*, *173*, 177–183. doi:10.1016/j.snb.2012.06.065

Amlathe, S., & Gupta, V. K. (1988). Spectrophotometric determination of trace amounts of hydrazine in polluted water. *The Analyst*, *113*(9), 1481. doi:10.1039/an9881301481

Amrithesh, M., Aravind, S., Jayalekshmi, S., & Jayasree, R. S. (2008). Enhanced luminescence observed in polyaniline–polymethylmethacrylate composites. *Journal of Alloys and Compounds*, *449*(1-2), 176–179. doi:10.1016/j.jallcom.2006.02.096

Ando, M., Swart, C., Pringsheim, E., Mirsky, V. M., & Wolfbeis, O. S. (2005). Optical ozone-sensing properties of poly(2-chloroaniline), poly(N-methylaniline) and polyaniline films. *Sensors and Actuators B: Chemical*, *108*(1-2), 528–534. doi:10.1016/j.snb.2004.12.083

Andreu, Y., de Marcos, S., Castillo, J. R., & Galbán, J. (2005). Sensor film for Vitamin C determination based on absorption properties of polyaniline. *Talanta*, *65*(4), 1045–51. doi:10.1016/j.talanta.2004.08.036

Anitha, G., & Subramanian, E. (2003). Dopant induced specificity in sensor behaviour of conducting polyaniline materials with organic solvents. *Sensors and Actuators B: Chemical*, *92*(1-2), 49–59. doi:10.1016/S0925-4005(03)00007-8

Ansari, M. O., & Mohammad, F. (2011). Thermal stability, electrical conductivity and ammonia sensing studies on p-toluenesulfonic acid doped polyaniline:titanium dioxide (pTSA/Pani:TiO2) nanocomposites. *Sensors and Actuators B: Chemical*, *157*(1), 122–129. doi:10.1016/j.snb.2011.03.036

Asazawa, K., Sakamoto, T., Yamaguchi, S., Yamada, K., Fujikawa, H., Tanaka, H., & Oguro, K. (2009). Study of Anode Catalysts and Fuel Concentration on Direct Hydrazine Alkaline Anion-Exchange Membrane Fuel Cells. *Journal of The Electrochemical Society*, *156*(4), B509. doi:10.1149/1.3082129

Ateh, D. D., Navsaria, H. A., & Vadgama, P. (2006). Polypyrrole-based conducting polymers and interactions with biological tissues. *Journal of the Royal Society, Interface / the Royal Society*, *3*(11), 741–52. doi:10.1098/rsif.2006.0141

Bagheri, H., Daliri, R., & Roostaie, A. (2013). A novel magnetic poly(aniline-naphthylamine)-based nanocomposite for micro solid phase extraction of rhodamine B. *Analytica Chimica Acta*, *794*, 38–46. doi:10.1016/j.aca.2013.07.066

Bahceci, S., & Esat, B. (2013). A polyacetylene derivative with pendant TEMPO group as cathode material for rechargeable batteries. *Journal of Power Sources*, *242*, 33–40. doi:10.1016/j.jpowsour.2013.05.051

Bai, H., Chen, Q., Li, C., Lu, C., & Shi, G. (2007). Electrosynthesis of polypyrrole/sulfonated polyaniline composite films and their applications for ammonia gas sensing. *Polymer*, *48*(14), 4015–4020. doi:10.1016/j.polymer.2007.05.033

Berthet, G., Blanc, J. P., Germain, J. P., Larbi, A., Maleysson, C., & Robert, H. (1987). Electroactive polymers in thin layers: A potential application as a gas sensor. *Synthetic Metals*, *18*(1-3), 715–720. doi:10.1016/0379-6779(87)90967-2

Bhadra, S., Singha, N. K., & Khastgir, D. (2007). Electrochemical synthesis of polyaniline and its comparison with chemically synthesized polyaniline. *Journal of Applied Polymer Science*, *104*(3), 1900–1904. doi:10.1002/app.25867

Bian, L., Xiao, J., Zeng, J., Xing, S., Yin, C., & Jia, A. (2014). Effects of thermal treatment on the mechanical properties of poly(p-phenylene benzobisoxazole) fiber reinforced phenolic resin composite materials. *Materials & Design*, *54*, 230–235. doi:10.1016/j.matdes.2013.08.058

Bidan, G., & Ehui, B. (1989). One-step electrosynthesis and characterization of poly(aniline)?Nafion and poly(3-methylthiophene)?Nafion composite films. *Journal of the Chemical Society, Chemical Communications*, (20), 1568. doi:10.1039/c39890001568

Bláha, M., Varga, M., Prokeš, J., Zhigunov, A., & Vohlídal, J. (2013). Effects of the polymerization temperature on the structure, morphology and conductivity of polyaniline prepared with ammonium peroxodisulfate. *European Polymer Journal*, *49*(12), 3904–3911. doi:10.1016/j.eurpolymj.2013.08.018

Bloch, R., Shatkay, A., & Saroff, H. A. (1967). Fabrication and evaluation of membranes as specific electrodes for calcium ions. *Biophysical Journal*, *7*(6), 865–77. doi:10.1016/S0006-3495(67)86626-8

Bott, B., & Jones, T. A. (1986). The use of multisensor systems in monitoring hazardous atmospheres. *Sensors and Actuators*, *9*(1), 19–25. doi:10.1016/0250-6874(86)80003-8

Bowman, D., & Mattes, B. R. (2005). Conductive Fibre Prepared From Ultra-High Molecular Weight Polyaniline for Smart Fabric and Interactive Textile Applications. *Synthetic Metals*, *154*(1-3), 29–32. doi:10.1016/j.synthmet.2005.07.017

Brunink, J. A. J., Haak, J. R., Bomer, J. G., Reinhoudt, D. N., McKervey, M. A., & Harris, S. J. (1991). Chemically modified field-effect transistors; a sodium ion selective sensor based on calix[4]arene receptor molecules. *Analytica Chimica Acta*, *254*(1-2), 75–80. doi:10.1016/0003-2670(91)90011-S

Campo, B. J., Bevk, D., Kesters, J., Gilot, J., Bolink, H. J., Zhao, J., … Vanderzande, D. (2013). Ester-functionalized poly(3-alkylthiophene) copolymers: Synthesis, physicochemical characterization and performance in bulk heterojunction organic solar cells. *Organic Electronics*, *14*(2), 523–534. doi:10.1016/j.orgel.2012.11.021

Cao, Y., & Smith, P. (1993). Liquid-crystalline solutions of electrically conducting polyaniline. *Polymer*, *34*(15), 3139–3143. doi:10.1016/0032-3861(93)90381-J

Cao, Y., Smith, P., & Heeger, A. J. (1992). Counter-ion induced processibility of conducting polyaniline and of conducting polyblends of polyaniline in bulk polymers. *Synthetic Metals*, *48*(1), 91–97. doi:10.1016/0379-6779(92)90053-L

Cao, Y., Treacy, G. M., Smith, P., & Heeger, A. J. (1992). Solution-cast films of polyaniline: Optical-quality transparent electrodes. *Applied Physics Letters*, *60*(22), 2711. doi:10.1063/1.106852

Cataldo, F., & Maltese, P. (2002). Synthesis of alkyl and N-alkyl-substituted polyanilines. *European Polymer Journal*, *38*(9), 1791–1803. doi:10.1016/S0014-3057(02)00070-8

Chakraborty, S., & Raj, C. R. (2010). Carbon nanotube supported platinum nanoparticles for the voltammetric sensing of hydrazine. *Sensors and Actuators B: Chemical*, *147*(1), 222–227. doi:10.1016/j.snb.2010.03.036

Chatterjee, A., & Islam, M. S. (2008). Fabrication and characterization of TiO2–epoxy nanocomposite. *Materials Science and Engineering: A*, *487*(1-2), 574–585. doi:10.1016/j.msea.2007.11.052

Chaudhari, H. K., & Kelkar, D. S. (1997). Investigation of Structure and Electrical Conductivity in Doped Polyaniline. *Polymer International*, *42*(4), 380–384. doi:10.1002/(SICI)1097-0126(199704)42:4<380::AID-PI727>3.0.CO;2-F

Chen, S.-A., Chuang, K.-R., Chao, C.-I., & Lee, H.-T. (1996). White-light emission from electroluminescence diode with polyaniline as the emitting layer. *Synthetic Metals*, *82*(3), 207–210. doi:10.1016/S0379-6779(96)03790-3

Chiang, C., Fincher, C., Park, Y., Heeger, A., Shirakawa, H., Louis, E., … MacDiarmid, A. (1977). Electrical Conductivity in Doped Polyacetylene. *Physical Review Letters*, *39*(17), 1098–1101. doi:10.1103/PhysRevLett.39.1098

Choi, B. G., Park, H., Im, H. S., Kim, Y. J., & Hong, W. H. (2008). Influence of oxidation state of polyaniline on physicochemical and transport properties of Nafion/polyaniline composite membrane for DMFC. *Journal of Membrane Science*, *324*(1-2), 102–110. doi:10.1016/j.memsci.2008.06.061

Choudhary, G., & Hansen, H. (1998). Human health perspective of environmental exposure to hydrazines: A review. *Chemosphere*, *37*(5), 801–843. doi:10.1016/S0045-6535(98)00088-5

Choudhury, A. (2009). Polyaniline/silver nanocomposites: Dielectric properties and ethanol vapour sensitivity. *Sensors and Actuators B: Chemical*, *138*(1), 318–325. doi:10.1016/j.snb.2009.01.019

Cochet, M., Maser, W. K., Benito, A. M., Callejas, M. A., Martínez, M. T., Benoit, J.-M., … Chauvet, O. (2001). Synthesis of a new polyaniline/nanotube composite: "in-situ" polymerisation and charge transfer through site-selective interaction. *Chemical Communications*, (16), 1450–1451. doi:10.1039/b104009j

Deivanayaki, S., Ponnuswamy, V., Ashokan, S., Jayamurugan, P., & Mariappan, R. (2013). Synthesis and characterization of TiO2-doped Polyaniline nanocomposites by chemical oxidation method. *Materials Science in Semiconductor Processing*, *16*(2), 554–559. doi:10.1016/j.mssp.2012.07.004

Deivanayaki, S., Ponnuswamy, V., Mariappan, R., & Jayamurugan, P. (2013). Synthesis and characterization of polypyrrole/TiO2 composites by chemical oxidative method. *Optik - International Journal for Light and Electron Optics*, *124*(12), 1089–1091. doi:10.1016/j.ijleo.2012.02.029

Dhaoui, W., Bouzitoun, M., Zarrouk, H., Ouada, H. Ben, & Pron, A. (2008). Electrochemical sensor for nitrite determination based on thin films of sulfamic acid doped polyaniline deposited on Si/SiO2 structures in electrolyte/insulator/semiconductor (E.I.S.) configuration. *Synthetic Metals*, *158*(17-18), 722–726. doi:10.1016/j.synthmet.2008.04.020

Dhawale, D. S., Salunkhe, R. R., Patil, U. M., Gurav, K. V., More, A. M., & Lokhande, C. D. (2008). Room temperature liquefied petroleum gas (LPG) sensor based on p-polyaniline/n-TiO2 heterojunction. *Sensors and Actuators B: Chemical*, *134*(2), 988–992. doi:10.1016/j.snb.2008.07.003

Ding, M., Tang, Y., Gou, P., Reber, M. J., & Star, A. (2011). Chemical sensing with polyaniline coated single-walled carbon nanotubes. *Advanced Materials (Deerfield Beach, Fla.)*, *23*(4), 536–40. doi:10.1002/adma.201003304

Du, X., Skachko, I., Barker, A., & Andrei, E. Y. (2008). Approaching ballistic transport in suspended graphene. *Nature Nanotechnology*, *3*(8), 491–5. doi:10.1038/nnano.2008.199

Dubbe, A., Wiemho¨fer, H.-D., Sadaoka, Y., & Go¨pel, W. (1995). Microstructure and response behaviour of electrodes for CO2 gas sensors based on solid electrolytes. *Sensors and Actuators B: Chemical*, *25*(1-3), 600–602. doi:10.1016/0925-4005(95)85131-3

Epstein, A. ., Ginder, J. ., Zuo, F., Bigelow, R. ., Woo, H.-S., Tanner, D. ., … MacDiarmid, A. . (1987). Insulator-to-metal transition in polyaniline. *Synthetic Metals*, *18*(1-3), 303–309. doi:10.1016/0379-6779(87)90896-4

Falcou, A., Duchêne, A., Hourquebie, P., Marsacq, D., & Balland-Longeau, A. (2005). A new chemical polymerization process for substituted anilines. *Synthetic Metals*, *149*(2-3), 115–122. doi:10.1016/j.synthmet.2004.12.001

Fu, Y., & Elsenbaumer, R. L. (1994). Thermochemistry and Kinetics of Chemical Polymerization of Aniline Determined by Solution Calorimetry. *Chemistry of Materials*, *6*(5), 671–677. doi:10.1021/cm00041a018

Furukawa, Y., Ueda, F., Hyodo, Y., Harada, I., Nakajima, T., & Kawagoe, T. (1988). Vibrational spectra and structure of polyaniline. *Macromolecules*, *21*(5), 1297–1305. doi:10.1021/ma00183a020

Gabor, H. (2006). Tutorial Polymer films in sensor applications : a review of present uses and future possibilities Ga. *Sensors Review*, *20*(2), 98–105.

Gao, W., Xi, J., Chen, Y., Xiao, S., Wang, X., Li, J., … Chen, Y. (2013). Hydrogen-Bonding Recognition-Induced Colorimetric Determination of Hydrazine Based on the Tryptophan Capped Gold Nanoparticles. *Journal of Spectroscopy*, *2013*, 1–7. doi:10.1155/2013/517613

Gao, Y., Guo, F., Gokavi, S., Chow, A., Sheng, Q., & Guo, M. (2008). Quantification of water-soluble vitamins in milk-based infant formulae using biosensor-based assays. *Food Chemistry*, *110*(3), 769–776. doi:10.1016/j.foodchem.2008.03.007

Gao, Y., Li, X., Gong, J., Fan, B., Su, Z., & Qu, L. (2008). Polyaniline Nanotubes Prepared Using Fiber Mats Membrane as the Template and their Gas-response Behavior. *The Journal of Physical Chemistry C*, *112*(22), 8215–8222. doi:10.1021/jp711601f

Gaponik, N. P., Talapin, D. V., & Rogach, A. L. (1999). A light-emitting device based on a CdTe nanocrystal/polyaniline composite. *Physical Chemistry Chemical Physics*, *1*(8), 1787–1789. doi:10.1039/a808619b

Ghavami, M., Kassaee, M. Z., Mohammadi, R., Koohi, M., & Haerizadeh, B. N. (2014). Polyaniline nanotubes coated with TiO2&γ-Fe2O3@graphene oxide as a novel and effective visible light photocatalyst for removal of rhodamine B from water. *Solid State Sciences*, *38*, 143–149. doi:10.1016/j.solidstatesciences.2014.09.010

Gill, E., Arshak, a., Arshak, K., & Korostynska, O. (2010). Response mechanism of novel polyaniline composite conductimetric pH sensors and the effects of polymer binder, surfactant and film thickness on sensor sensitivity. *European Polymer Journal*, *46*(10), 2042–2050. doi:10.1016/j.eurpolymj.2010.07.012

Gill, W., Bludau, W., Geiss, R., Grant, P., Greene, R., Mayerle, J., & Street, G. (1977). Structure and Electronic Properties of Polymeric Sulfur Nitride (SN)x Modified by Bromine. *Physical Review Letters*, *38*(22), 1305–1308. doi:10.1103/PhysRevLett.38.1305

Golabi, S. M., & Zare, H. R. (1999). Electrocatalytic oxidation of hydrazine at a chlorogenic acid (CGA) modified glassy carbon electrode. *Journal of Electroanalytical Chemistry*, *465*(2), 168–176. doi:10.1016/S0022-0728(99)00082-0

Gonçalves, R. H., Schreiner, W. H., & Leite, E. R. (2010). Synthesis of TiO2 nanocrystals with a high affinity for amine organic compounds. *Langmuir : The ACS Journal of Surfaces and Colloids*, *26*(14), 11657–62. doi:10.1021/la1007473

Greene, R., Street, G., & Suter, L. (1975). Superconductivity in Polysulfur Nitride (SN)x. *Physical Review Letters*, *34*(10), 577–579. doi:10.1103/PhysRevLett.34.577

Grodzka, E., Winkler, K., Esteban, B. M., & Kvarnstrom, C. (2010). Capacitance properties of electrochemically deposited polyazulene films. *Electrochimica Acta*, *55*(3), 970–978. doi:10.1016/j.electacta.2009.09.054

Gu, H., Wang, Z., & Hu, Y. (2012). Hydrogen gas sensors based on semiconductor oxide nanostructures. *Sensors (Basel, Switzerland)*, *12*(5), 5517–50. doi:10.3390/s120505517

Gupta, K., Chakraborty, G., Jana, P. C., & Meikap, A. K. (2011). Temperature dependent dc and ac electrical transport properties of the composite of a polyaniline nanorod with copper chloride. *Solid State Communications*, *151*(7), 573–578. doi:10.1016/j.ssc.2011.01.001

Hatano, M., Kambara, S., & Okamoto, S. (1961). Paramagnetic and electric properties of polyacetylene. *Journal of Polymer Science*, *51*(156), S26–S29. doi:10.1002/pol.1961.1205115623

Heiland, G., & Kohl, D. (1985). Problems and possibilities of oxidic and organic semiconductor gas sensors. *Sensors and Actuators*, *8*(3), 227–233. doi:10.1016/0250-6874(85)85005-8

Hermans, E. C. M. (1984). CO, CO2, CH4 and H2O sensing by polymer covered interdigitated electrode structures. *Sensors and Actuators*, *5*(3), 181–186. doi:10.1016/0250-6874(84)80008-6

Hino, T., Taniguchi, S., & Kuramoto, N. (2006). Syntheses of conductive adhesives based on epoxy resin and polyanilines by usingN-tert-butyl-5-methylisoxazolium perchlorate as a thermally latent curing reagent. *Journal of Polymer Science Part A: Polymer Chemistry*, *44*(2), 718–726. doi:10.1002/pola.21085

Hosoda, M., Hino, T., & Kuramoto, N. (2007). Facile preparation of conductive paint made with polyaniline/dodecylbenzenesulfonic acid dispersion and poly(methyl methacrylate). *Polymer International*, *56*(11), 1448–1455. doi:10.1002/pi.2304

Hosseini, M., & Momeni, M. M. (2010). Silver nanoparticles dispersed in polyaniline matrixes coated on titanium substrate as a novel electrode for electro-oxidation of hydrazine. *Journal of Materials Science*, *45*(12), 3304–3310. doi:10.1007/s10853-010-4347-1

Hosseini, S. H., & Entezami, A. A. (2001). Preparation and characterization of polyaniline blends with polyvinyl acetate, polystyrene and polyvinyl chloride for toxic gas sensors. *Polymers for Advanced Technologies*, *12*(8), 482–493. doi:10.1002/pat.107

Howe, A. T., & Shilton, M. G. (1979). Studies of layered uranium(VI) compounds. I. High proton conductivity in polycrystalline hydrogen uranyl phosphate tetrahydrate. *Journal of Solid State Chemistry*, *28*(3), 345–361. doi:10.1016/0022-4596(79)90085-9

Huang, L.-M., Wen, T.-C., & Gopalan, A. (2003). Synthesis and characterization of soluble conducting poly(aniline-co-2, 5-dimethoxyaniline). *Materials Letters*, *57*(12), 1765–1774. doi:10.1016/S0167-577X(02)01066-2

Hübert, T., Boon-Brett, L., Black, G., & Banach, U. (2011). Hydrogen sensors – A review. *Sensors and Actuators B: Chemical*, *157*(2), 329–352. doi:10.1016/j.snb.2011.04.070

Ibrahim, A. A., Dar, G. N., Zaidi, S. A., Umar, A., Abaker, M., Bouzid, H., & Baskoutas, S. (2012). Growth and properties of Ag-doped ZnO nanoflowers for highly sensitive phenyl hydrazine chemical sensor application. *Talanta*, *93*, 257–63. doi:10.1016/j.talanta.2012.02.030

Ihdene, Z., Mekki, A., Mettai, B., Mahmoud, R., Hamada, B., & Chehimi, M. M. (2014). Quartz crystal microbalance VOCs sensor based on dip coated polyaniline emeraldine salt thin films. *Sensors and Actuators B: Chemical*, *203*, 647–654. doi:10.1016/j.snb.2014.07.030

Ikeda, S. (1995). Carbon dioxide sensor using solid electrolytes with zirconium phosphate framework (2). Properties of the CO2 gas sensor using Mg1.15Zr4P5.7Si0.3O24 as electrolyte. *Solid State Ionics*, *79*, 354–357. doi:10.1016/0167-2738(95)00087-M

Imanaka, N., Murata, T., Kawasato, T., & Adachi, G. (1993). CO2 detection with lithium solid electrolyte sensors. *Sensors and Actuators B: Chemical*, *13*(1-3), 476–479. doi:10.1016/0925-4005(93)85431-9

Irimia-Vladu, M., & Fergus, J. W. (2006). Suitability of emeraldine base polyaniline-PVA composite film for carbon dioxide sensing. *Synthetic Metals*, *156*(21-24), 1401–1407. doi:10.1016/j.synthmet.2006.11.005

Ito, T., Shirakawa, H., & Ikeda, S. (1974). Simultaneous polymerization and formation of polyacetylene film on the surface of concentrated soluble Ziegler-type catalyst solution. *Journal of Polymer Science: Polymer Chemistry Edition*, *12*(1), 11–20. doi:10.1002/pol.1974.170120102

Ito, T., Shirakawa, H., & Ikeda, S. (1975). Thermal cis–trans isomerization and decomposition of polyacetylene. *Journal of Polymer Science: Polymer Chemistry Edition*, *13*(8), 1943–1950. doi:10.1002/pol.1975.170130818

Ivanov, S., Lange, U., Tsakova, V., & Mirsky, V. M. (2010a). Electrocatalytically active nanocomposite from palladium nanoparticles and polyaniline: Oxidation of hydrazine. *Sensors and Actuators B: Chemical*, *150*(1), 271–278. doi:10.1016/j.snb.2010.07.004

Ivanov, S., Lange, U., Tsakova, V., & Mirsky, V. M. (2010b). Electrocatalytically active nanocomposite from palladium nanoparticles and polyaniline: Oxidation of hydrazine. *Sensors and Actuators B: Chemical*, *150*(1), 271–278. doi:10.1016/j.snb.2010.07.004

Jain, S., Samui, A. B., Patri, M., Hande, V. R., & Bhoraskar, S. V. (2005). FEP/polyaniline based multilayered chlorine sensor. *Sensors and Actuators B: Chemical*, *106*(2), 609–613. doi:10.1016/j.snb.2004.07.025

Jayasri, D., & Narayanan, S. S. (2007). Amperometric determination of hydrazine at manganese hexacyanoferrate modified graphite-wax composite electrode. *Journal of Hazardous Materials*, *144*(1-2), 348–54. doi:10.1016/j.jhazmat.2006.10.038

Jiang, H., Geng, Y., Li, J., Jing, X., & Wang, F. (1997). Organic acid doped polyaniline derivatives. *Synthetic Metals*, *84*(1-3), 125–126. doi:10.1016/S0379-6779(97)80677-7

Joshi, S. S., Lokhande, C. D., & Han, S.-H. (2007). A room temperature liquefied petroleum gas sensor based on all-electrodeposited n-CdSe/p-polyaniline junction. *Sensors and Actuators B: Chemical*, *123*(1), 240–245. doi:10.1016/j.snb.2006.08.023

Jurga, J., Woźniak-Braszak, A., Fojud, Z., & Jurga, K. (2004). Proton longitudinal NMR relaxation of poly(p-phenylene sulfide) in the laboratory and the rotating frames reference. *Solid State Nuclear Magnetic Resonance*, *25*(1-3), 47–52. doi:10.1016/j.ssnmr.2003.03.014

Kamyabi, M. A., Shahabi, S., & Hosseini-Monfared, H. (2008). Electrocatalytic Oxidation of Hydrazine at a Cobalt(II) Schiff-Base-Modified Carbon Paste Electrode. *Journal of The Electrochemical Society*, *155*(1), F8. doi:10.1149/1.2800166

Kang, E. T., Ting, Y. P., Neoh, K. G., & Tan, K. L. (1995). Electroless recovery of precious metals from acid solutions by N-containing electroactive polymers. *Synthetic Metals*, *69*(1-3), 477–478. doi:10.1016/0379-6779(94)02533-5

Kar, P., & Choudhury, A. (2013). Carboxylic acid functionalized multi-walled carbon nanotube doped polyaniline for chloroform sensors. *Sensors and Actuators B: Chemical*, *183*, 25–33. doi:10.1016/j.snb.2013.03.093

Karabulut, S. (2009). Electro-Induced Early Transition Metal Metathesis Catalyst Systems for the Production of Polyacetylene. *Polymer Journal*, *41*(8), 629–633. doi:10.1295/polymj.PJ2009011

Katoch, A., Burkhart, M., Hwang, T., & Kim, S. S. (2012). Synthesis of polyaniline/TiO2 hybrid nanoplates via a sol–gel chemical method. *Chemical Engineering Journal*, *192*, 262–268. doi:10.1016/j.cej.2012.04.004

Kilmartin, P. A., Gizdavic-Nikolaidis, M., Zujovic, Z., Travas-Sejdic, J., Bowmaker, G. A., & Cooney, R. P. (2005). Free radical scavenging and antioxidant properties of conducting polymers examined using EPR and NMR spectroscopies. *Synthetic Metals*, *153*(1-3), 153–156. doi:10.1016/j.synthmet.2005.07.170

Kim, B.-J., Oh, S.-G., Han, M.-G., & Im, S.-S. (2001). Synthesis and characterization of polyaniline nanoparticles in SDS micellar solutions. *Synthetic Metals*, *122*(2), 297–304. doi:10.1016/S0379-6779(00)00304-0

Kim, J., Yeo, J.-S., Jeong, H.-G., Yun, J.-M., Kim, Y.-A., & Kim, D.-Y. (2014). A thienylenevinylene-phthalimide copolymer based polymer solar cell with high open circuit voltage: Effect of additive concentration on the open circuit voltage. *Solar Energy Materials and Solar Cells*, *125*, 253–260. doi:10.1016/j.solmat.2014.02.038

Kim, J.-S., Sohn, S.-O., & Huh, J.-S. (2005). Fabrication and sensing behavior of PVF2 coated-polyaniline sensor for volatile organic compounds. *Sensors and Actuators B: Chemical*, *108*(1-2), 409–413. doi:10.1016/j.snb.2004.11.072

Konyushenko, E. N., Stejskal, J., Trchová, M., Blinova, N. V., & Holler, P. (2008). Polymerization of aniline in ice. *Synthetic Metals*, *158*(21-24), 927–933. doi:10.1016/j.synthmet.2008.06.015

Kordić, S., & Van der Jagt, P. C. M. (1985). Theory and practice of electronic implementation of the sensitivity-variation offset-reduction method. *Sensors and Actuators*, *8*(3), 197–217. doi:10.1016/0250-6874(85)85003-4

Koul, S., Chandra, R., & Dhawan, S. . (2001). Conducting polyaniline composite: a reusable sensor material for aqueous ammonia. *Sensors and Actuators B: Chemical*, *75*(3), 151–159. doi:10.1016/S0925-4005(00)00685-7

LeBlanc, O. H., & Grubb, W. T. (1976). Long-lived potassium ion selective polymer membrane electrode. *Analytical Chemistry*, *48*(12), 1658–1660. doi:10.1021/ac50006a008

Lee, I. S., Cho, M. S., & Choi, H. J. (2005). Preparation of polyaniline coated poly(methyl methacrylate) microsphere by graft polymerization and its electrorheology. *Polymer*, *46*(4), 1317–1321. doi:10.1016/j.polymer.2004.11.068

Letheby, H. (1862). On the production of a blue substance by the electrolysis of sulphate of aniline. *Journal of the Chemical Society*, *15*, 161. doi:10.1039/js8621500161

Li, J., Xie, H., & Chen, L. (2011). A sensitive hydrazine electrochemical sensor based on electrodeposition of gold nanoparticles on choline film modified glassy carbon electrode. *Sensors and Actuators B: Chemical*, *153*(1), 239–245. doi:10.1016/j.snb.2010.10.040

Li, Q., Cruz, L., & Phillips, P. (1993). Granular-rod model for electronic conduction in polyaniline. *Physical Review B*, *47*(4), 1840–1845. doi:10.1103/PhysRevB.47.1840

Li, X., Wang, G., Li, X., & Lu, D. (2004). Surface properties of polyaniline/nano-TiO2 composites. *Applied Surface Science*, *229*(1-4), 395–401. doi:10.1016/j.apsusc.2004.02.022

Li, Y., Yu, Y., Wu, L., & Zhi, J. (2013). Processable polyaniline/titania nanocomposites with good photocatalytic and conductivity properties prepared via peroxo-titanium complex catalyzed emulsion polymerization approach. *Applied Surface Science*, *273*, 135–143. doi:10.1016/j.apsusc.2013.01.213

Lin, H., Yang, J., Liu, J., Huang, Y., Xiao, J., & Zhang, X. (2013). Properties of Pd nanoparticles-embedded polyaniline multilayer film and its electrocatalytic activity for hydrazine oxidation. *Electrochimica Acta*, *90*, 382–392. doi:10.1016/j.electacta.2012.11.122

Liu, B., Liu, Q., Shah, M., Wang, J., Zhang, G., & Pang, Y. (2014). Fluorescence monitor of hydrazine in vivo by selective deprotection of flavonoid. *Sensors and Actuators B: Chemical*, *202*, 194–200. doi:10.1016/j.snb.2014.05.010

Liu, Y.-C., & Hwang, B.-J. (2000). Enhancement of conductivity stability of polypyrrole films modified by valence copper and polyethylene oxide in an oxygen atmosphere. *Thin Solid Films*, *360*(1-2), 1–9. doi:10.1016/S0040-6090(99)00964-5

Liu, Y.-Y., Schmeltz, I., & Hoffmann, D. (1974). Chemical studies on tobacco smoke. Quantitative analysis of hydrazine in tobacco and cigarette smoke. *Analytical Chemistry*, *46*(7), 885–889. doi:10.1021/ac60343a046

Lloyd, J. P., Petty, M. C., Roberts, G. G., Lecomber, P. G., & Spear, W. E. (1983). Amorphous silicon/Langmuir-Blodgett film field effect transistor. *Thin Solid Films*, *99*(1-3), 297–304. doi:10.1016/0040-6090(83)90396-6

Lu, J., Moon, K.-S., Kim, B.-K., & Wong, C. P. (2007). High dielectric constant polyaniline/epoxy composites via in situ polymerization for embedded capacitor applications. *Polymer*, *48*(6), 1510–1516. doi:10.1016/j.polymer.2007.01.057

Lu, W.-K., Elsenbaumer, R. L., & Wessling, B. (1995). Corrosion protection of mild steel by coatings containing polyaniline. *Synthetic Metals*, *71*(1-3), 2163–2166. doi:10.1016/0379-6779(94)03204-J

Lyutov, V., & Tsakova, V. (2011). Palladium-modified polysulfonic acid-doped polyaniline layers for hydrazine oxidation in neutral solutions. *Journal of Electroanalytical Chemistry*, *661*(1), 186–191. doi:10.1016/j.jelechem.2011.07.043

MacDiarmid, A. C., & Huang, F. (1999). Role of ionic species in determining characteristics of polymer LEDs. *Synthetic Metals*, *102*(1-3), 1026–1029. doi:10.1016/S0379-6779(98)90203-X

MacDiarmid, A. G. (1997). Polyaniline and polypyrrole: Where are we headed? *Synthetic Metals*, *84*(1-3), 27–34. doi:10.1016/S0379-6779(97)80658-3

Macdiarmid, A. G., Chiang, J.-C., Halpern, M., Huang, W.-S., Mu, S.-L., Nanaxakkara, L. D., … Yaniger, S. I. (1985). "Polyaniline": Interconversion of Metallic and Insulating Forms. *Molecular Crystals and Liquid Crystals*, *121*(1-4), 173–180. doi:10.1080/00268948508074857

MacDiarmid, A. G., & Epstein, A. J. (1994). The concept of secondary doping as applied to polyaniline. *Synthetic Metals*, *65*(2-3), 103–116. doi:10.1016/0379-6779(94)90171-6

Madru, M., Guillaud, G., Sadoun, M. A., Maitrot, M., Clarisse, C., Contellec, M. L., … Simon, J. (1987). The first field effect transistor based on an intrinsic molecular semiconductor. *Chemical Physics Letters*, *142*(1-2), 103–105. doi:10.1016/0009-2614(87)87259-7

Mahmoudian, M. R., Alias, Y., Basirun, W. J., Moradi Golsheikh, a., & Jamali-Sheini, F. (2013). Synthesis of polypyrrole coated manganese nanowires and their application in hydrogen peroxide detection. *Materials Chemistry and Physics*, *141*(1), 298–303. doi:10.1016/j.matchemphys.2013.05.014

Maleki, N., Safavi, A., Farjami, E., & Tajabadi, F. (2008). Palladium nanoparticle decorated carbon ionic liquid electrode for highly efficient electrocatalytic oxidation and determination of hydrazine. *Analytica Chimica Acta*, *611*(2), 151–5. doi:10.1016/j.aca.2008.01.075

Malinauskas, A., & Holze, R. (1999). A UV-vis spectroelectrochemical study of redox reactions of solution species at a polyaniline electrode in the conducting and the reduced state. *Journal of Electroanalytical Chemistry*, *461*(1-2), 184–193. doi:10.1016/S0022-0728(98)00319-2

Mazerolles, L., Folch, S., & Colomban, P. (1999). Study of Polyanilines by High-Resolution Electron Microscopy. *Macromolecules*, *32*(25), 8504–8508. doi:10.1021/ma991290a

McCall, R. ., Ginder, J. ., Leng, J. ., Coplin, K. ., Ye, H. ., Epstein, A. ., … Macdiarmid, A. . (1991). Photoinduced absorption and erasable optical information storage in polyanilines. *Synthetic Metals*, *41*(3), 1329–1332. doi:10.1016/0379-6779(91)91618-K

Menefee, E., & Pao, Y.-H. (1962). Electron Conduction in Charge-Transfer Molecular Crystals. *The Journal of Chemical Physics*, *36*(12), 3472. doi:10.1063/1.1732482

Meng, C., Liu, C., & Fan, S. (2009). Flexible carbon nanotube/polyaniline paper-like films and their enhanced electrochemical properties. *Electrochemistry Communications*, *11*(1), 186–189. doi:10.1016/j.elecom.2008.11.005

Mi, H., Zhou, J., Cui, Q., Zhao, Z., Yu, C., Wang, X., & Qiu, J. (2014). Chemically patterned polyaniline arrays located on pyrolytic graphene for supercapacitors. *Carbon*, *80*, 799–807. doi:10.1016/j.carbon.2014.09.036

Mirmohseni, A., & Oladegaragoze, A. (2004). Determination of chlorinated aliphatic hydrocarbons in air using a polymer coated quartz crystal microbalance sensor. *Sensors and Actuators B: Chemical*, *102*(2), 261–270. doi:10.1016/j.snb.2004.04.027

Miura, N., Kato, H., Ozawa, Y., Yamazoe, N., & Seiyama, T. (1984). Amperometric gas sensor using solid state proton conductor sensitive to hydrogen in air at room temperature. *Chemistry Letters*, *11*, 1905–1908. doi:10.1246/cl.1984.1905

Mokwa, W., Kohl, D., & Heiland, G. (1985). An SnO2 thin film for sensing arsine. *Sensors and Actuators*, *8*(2), 101–108. doi:10.1016/0250-6874(85)87008-6

Mori, M., Tanaka, K., Xu, Q., Ikedo, M., Taoda, H., & Hu, W. (2004). Highly sensitive determination of hydrazine ion by ion-exclusion chromatography with ion-exchange enhancement of conductivity detection. *Journal of Chromatography A*, *1039*(1-2), 135–139. doi:10.1016/j.chroma.2004.03.075

Moulton, S. ., Innis, P. ., Kane-Maguire, L. A. ., Ngamna, O., & Wallace, G. . (2004a). Polymerisation and characterisation of conducting polyaniline nanoparticle dispersions. *Current Applied Physics*, *4*(2-4), 402–406. doi:10.1016/j.cap.2003.11.059

Moulton, S. ., Innis, P. ., Kane-Maguire, L. a. ., Ngamna, O., & Wallace, G. . (2004b). Polymerisation and characterisation of conducting polyaniline nanoparticle dispersions. *Current Applied Physics*, *4*(2-4), 402–406. doi:10.1016/j.cap.2003.11.059

Müller, R., & Lange, E. (1986). Multidimensional sensor for gas analysis. *Sensors and Actuators*, *9*(1), 39–48. doi:10.1016/0250-6874(86)80005-1

Nasirian, S., & Milani Moghaddam, H. (2014). Hydrogen gas sensing based on polyaniline/anatase titania nanocomposite. *International Journal of Hydrogen Energy*, *39*(1), 630–642. doi:10.1016/j.ijhydene.2013.09.152

Nassef, H. M., Radi, A.-E., & O'Sullivan, C. K. (2006). Electrocatalytic oxidation of hydrazine at o-aminophenol grafted modified glassy carbon electrode: Reusable hydrazine amperometric sensor. *Journal of Electroanalytical Chemistry*, *592*(2), 139–146. doi:10.1016/j.jelechem.2006.05.007

Navale, S. T., Mane, A. T., Khuspe, G. D., Chougule, M. A., & Patil, V. B. (2014). Room temperature NO2 sensing properties of polythiophene films. *Synthetic Metals*, *195*, 228–233. doi:10.1016/j.synthmet.2014.06.017

Nicolas-Debarnot, D., & Poncin-Epaillard, F. (2003). Polyaniline as a new sensitive layer for gas sensors. *Analytica Chimica Acta*, *475*(1-2), 1–15. doi:10.1016/S0003-2670(02)01229-1

Nitta, M., & Haradome, M. (1979). Co gas detection by ThO2-Doped SnO2. *Journal of Electronic Materials*, *8*(5), 571–580. doi:10.1007/BF02657079

Nohria, R., Khillan, R. K., Su, Y., Dikshit, R., Lvov, Y., & Varahramyan, K. (2006). Humidity sensor based on ultrathin polyaniline film deposited using layer-by-layer nano-assembly. *Sensors and Actuators B: Chemical*, *114*(1), 218–222. doi:10.1016/j.snb.2005.04.034

Olad, A., Behboudi, S., & Entezami, A. A. (2013). Effect of polyaniline as a surface modifier of TiO2 nanoparticles on the properties of polyvinyl chloride/TiO2 nanocomposites. *Chinese Journal of Polymer Science*, *31*(3), 481–494. doi:10.1007/s10118-013-1236-5

Park, O., Jeevananda, T., Kim, N., Kim, S., & Lee, J. (2009). Effects of surface modification on the dispersion and electrical conductivity of carbon nanotube/polyaniline composites. *Scripta Materialia*, *60*(7), 551–554. doi:10.1016/j.scriptamat.2008.12.005

Paulraj, P., Janaki, N., Sandhya, S., & Pandian, K. (2011). Single pot synthesis of polyaniline protected silver nanoparticles by interfacial polymerization and study its application on electrochemical oxidation of hydrazine. *Colloids and Surfaces A: Physicochemical and Engineering Aspects*, *377*(1-3), 28–34. doi:10.1016/j.colsurfa.2010.12.001

PELLOUX, A., QUESSADA, J., FOULETIER, J., FABRY, P., & KLEITZ, M. (1980). Utilization of a dilute solid electrolyte in an oxygen gauge. *Solid State Ionics*, *1*(5-6), 343–354. doi:10.1016/0167-2738(80)90033-8

Peng, H., Alemany, L. B., Margrave, J. L., & Khabashesku, V. N. (2003). Sidewall carboxylic acid functionalization of single-walled carbon nanotubes. *Journal of the American Chemical Society*, *125*(49), 15174–82. doi:10.1021/ja037746s

Petrov, D. V., Gomes, A. S. L., de Araújo, C. B., de Souza, J. M., de Azevedo, W. M., de Melo, J. V., & Diniz, F. B. (1995). Nonlinear-optical properties of a poly(vinyl alcohol)-polyaniline interpenetrating polymer network. *Optics Letters*, *20*(6), 554. doi:10.1364/OL.20.000554

Ping, Z. (1996). In situ FTIR?attenuated total reflection spectroscopic investigations on the base?acid transitions of polyaniline. Base?acid transition in the emeraldine form of polyaniline. *Journal of the Chemical Society, Faraday Transactions*, *92*(17), 3063–3067. doi:10.1039/ft9969203063

Piya-areetham, P., Rempel, G. L., & Prasassarakich, P. (2014). Hydrogenated nanosized polyisoprene as a thermal and ozone stabilizer for natural rubber blends. *Polymer Degradation and Stability*, *102*, 112–121. doi:10.1016/j.polymdegradstab.2014.01.032

Qi, J., Xinxin, X., & Lau, K. T. (2014). Fabrication of textile based conductometric polyaniline Gas sensor. *Sensors and Actuators B: Chemical*. doi:10.1016/j.snb.2014.05.138

Qiang, Z., Liang, G., Gu, A., & Yuan, L. (2014). Hyperbranched polyaniline: A new conductive polyaniline with simultaneously good solubility and super high thermal stability. *Materials Letters*, *115*, 159–161. doi:10.1016/j.matlet.2013.10.043

Qu, R., Sun, X., Sun, C., Zhang, Y., Wang, C., Ji, C., … Yin, P. (2012). Chemical modification of waste poly(p-phenylene terephthalamide) fibers and its binding behaviors to metal ions. *Chemical Engineering Journal*, *181-182*, 458–466. doi:10.1016/j.cej.2011.12.001

Raoov, M., Mohamad, S., bin Abas, M. R., & Surikumaran, H. (2014). New macroporous β-cyclodextrin functionalized ionic liquid polymer as an adsorbent for solid phase extraction with phenols. *Talanta*, *130*, 155–163. doi:10.1016/j.talanta.2014.06.067

Raut, B. T., Chougule, M. A., Nalage, S. R., Dalavi, D. S., Mali, S., Patil, P. S., & Patil, V. B. (2012). CSA doped polyaniline/CdS organic-inorganic nanohybrid: Physical and gas sensing properties. *Ceramics International*, *38*(7), 5501–5506.

Ravichandran, K., & Baldwin, R. P. (1983). Liquid chromatographic determination of hydrazines with electrochemically pretreated glassy carbon electrodes. *Analytical Chemistry*, *55*(11), 1782–1786. doi:10.1021/ac00261a031

Ren, F., Zhu, G., Ren, P., Wang, Y., & Cui, X. (2014). In situ polymerization of graphene oxide and cyanate ester–epoxy with enhanced mechanical and thermal properties. *Applied Surface Science*, *316*, 549–557. doi:10.1016/j.apsusc.2014.07.159

Ren, J., He, F., Zhang, L., Su, C., & Liu, Z. (2007). A new B-PAn-P system for the detection of bacteria population. *Sensors and Actuators B: Chemical*, *125*(2), 510–516. doi:10.1016/j.snb.2007.02.053

Ren, L., & Zhang, X. F. (2010). Preparation and characterization of polyaniline micro/nanotubes with dopant acid mordant dark yellow GG. *Synthetic Metals*, *160*(7-8), 783–787. doi:10.1016/j.synthmet.2010.01.022

Rose, J. D., & Statham, F. S. (1950). Acetylene reactions. Part VI. Trimerisation of ethynyl compounds. *Journal of the Chemical Society (Resumed)*, 69. doi:10.1039/jr9500000069

Roth, S., & Graupner, W. (1993). Conductive polymers: Evaluation of industrial applications. *Synthetic Metals*, *57*(1), 3623–3631. doi:10.1016/0379-6779(93)90487-H

Ruschau, G. R., Newnham, R. E., Runt, J., & Smith, B. E. (1989). 0–3 ceramic/polymer composite chemical sensors. *Sensors and Actuators*, *20*(3), 269–275. doi:10.1016/0250-6874(89)80125-8

Safavi, A. (2002). Flow injection chemiluminescence determination of hydrazine by oxidation with chlorinated isocyanurates. *Talanta*, *58*(4), 785–792. doi:10.1016/S0039-9140(02)00362-4

Safavi, A., & Tohidi, M. (2012). Silver paste nanocomposite electrode as a new metallic electrode for amperometric determination of hydrazine. *Analytical Methods*, *4*(8), 2233. doi:10.1039/c2ay05851k

Saïdi, S., Aymen, M., Bouzitoun, M., & Mohamed, A. B. (2014). Effect of α- to β-transformation on the dc and ac conductivity mechanism in polyaniline: Polyvinylidene fluoride composites films. *Materials Science in Semiconductor Processing*, *26*, 336–342. doi:10.1016/j.mssp.2014.04.012

Sakaguchi, T., Sato, M., & Hashimoto, T. (2013). Synthesis of silyl-disubstituted poly(p-phenylenevinylene) membranes and their gas permeability. *Polymer*, *54*(9), 2272–2277. doi:10.1016/j.polymer.2013.03.007

Sakamoto, T., Asazawa, K., Sanabria-Chinchilla, J., Martinez, U., Halevi, B., Atanassov, P., … Tanaka, H. (2014). Combinatorial discovery of Ni-based binary and ternary catalysts for hydrazine electrooxidation for use in anion exchange membrane fuel cells. *Journal of Power Sources*, *247*, 605–611. doi:10.1016/j.jpowsour.2013.08.107

Salvatierra, R. V., Oliveira, M. M., & Zarbin, A. J. G. (2010). One-Pot Synthesis and Processing of Transparent, Conducting, and Freestanding Carbon Nanotubes/Polyaniline Composite Films. *Chemistry of Materials*, *22*(18), 5222–5234. doi:10.1021/cm1012153

Sambasevam, K. P., Mohamad, S., & Phang, S.-W. (2015). Enhancement of polyaniline properties by different polymerization temperatures in hydrazine detection. *Journal of Applied Polymer Science*, *132*(13), 41746 (1–8). doi:10.1002/app.41746

Sánchez, C. O., Bernede, J. C., Cattin, L., & Díaz, F. R. (2011). Oligo(benzo[c]thiophene-2-oxide) a poly(isothianaphthene) derivative with good photovoltaic properties. *Synthetic Metals*, *161*(21-22), 2335–2338. doi:10.1016/j.synthmet.2011.08.044

Sayyed, M. M., & Maldar, N. N. (2010). Novel poly (arylene-ether-ether-ketone)s containing preformed imide unit and pendant long chain alkyl group. *Materials Science and Engineering: B*, *168*(1-3), 164–170. doi:10.1016/j.mseb.2009.11.015

Schindler, K., Schmeisser, D., Vohrer, U., Wiemhöfer, H. D., & Göpel, W. (1989). Spectroscopic and electrical studies of yttria-stabilized zirconia for oxygen sensors. *Sensors and Actuators*, *17*(3-4), 555–568. doi:10.1016/0250-6874(89)80045-9

Schulthess, P., Ammann, D., Kraeutler, B., Caderas, C., Stepanek, R., & Simon, W. (1985). Nitrite-selective liquid membrane electrode. *Analytical Chemistry*, *57*(7), 1397–1401. doi:10.1021/ac00284a048

Seifart, H. I., Gent, W. L., Parkin, D. P., van Jaarsveld, P. P., & Donald, P. R. (1995). High-performance liquid chromatographic determination of isoniazid, acetylisoniazid and hydrazine in biological fluids. *Journal of Chromatography B: Biomedical Sciences and Applications*, *674*(2), 269–275. doi:10.1016/0378-4347(96)82886-6

Sengupta, P. P., & Adhikari, B. (2007). Influence of polymerization condition on the electrical conductivity and gas sensing properties of polyaniline. *Materials Science and Engineering: A*, *459*(1-2), 278–285. doi:10.1016/j.msea.2007.02.021

Shirakawa, H., & Ikeda, S. (1971). Infrared Spectra of Poly(acetylene). *Polymer Journal*, *2*(2), 231–244. doi:10.1295/polymj.2.231

Shirakawa, H., Louis, E. J., MacDiarmid, A. G., Chiang, C. K., & Heeger, A. J. (1977). Synthesis of electrically conducting organic polymer: halogen derivatives of polyacetylene, (CH)x. *Chemical Communications*, 578–580.

Smela, E., Lu, W., & Mattes, B. R. (2005). Polyaniline actuators. *Synthetic Metals*, *151*(1), 25–42. doi:10.1016/j.synthmet.2005.03.009

Song, D., Li, M., Wang, T., Fu, P., Li, Y., Jiang, B., … Zhao, X. (2014). Dye-sensitized solar cells using nanomaterial/PEDOT–PSS composite counter electrodes: Effect of the electronic and structural properties of nanomaterials. *Journal of Photochemistry and Photobiology A: Chemistry*, *293*, 26–31. doi:10.1016/j.jphotochem.2014.07.014

Sovey, J. S., Curran, F. M., Haag, T. W., Patterson, M. J., Pencil, E. J., Rawlin, V. K., & Sankovic, J. M. (1993). Development of arcjet and ion propulsion for spacecraft stationkeeping. *Acta Astronautica*, *30*, 151–164. doi:10.1016/0094-5765(93)90107-8

Stejskal, J., Riede, A., Hlavat, D., Proke, J., Helmstedt, M., & Holler, P. (1998). SYflTH | TIIC I-Ifl | TRLS The effect of polymerization temperature on molecular weight , crystallinity , and electrical conductivity of polyaniline, *96*, 55–61.

Stejskal, J., Riede, A., Hlavatá, D., Prokeš, J., Helmstedt, M., & Holler, P. (1998). The effect of polymerization temperature on molecular weight, crystallinity, and electrical conductivity of polyaniline. *Synthetic Metals*, *96*(1), 55–61. doi:10.1016/S0379-6779(98)00064-2

Stejskal, J., Sapurina, I., & Trchová, M. (2010). Polyaniline nanostructures and the role of aniline oligomers in their formation. *Progress in Polymer Science*, *35*(12), 1420–1481. doi:10.1016/j.progpolymsci.2010.07.006

Stepánek, R., Kräutler, B., Schulthess, P., Lindemann, B., Ammann, D., & Simon, W. (1986). Aquocyanocobalt(III)-hepta(2-phenylethyl)-cobyrinate as a cationic carrier for nitrite-selective liquid-membrane electrodes. *Analytica Chimica Acta*, *182*, 83–90. doi:10.1016/S0003-2670(00)82439-3

Stoller, M. D., Park, S., Zhu, Y., An, J., & Ruoff, R. S. (2008). Graphene-based ultracapacitors. *Nano Letters*, *8*(10), 3498–502. doi:10.1021/nl802558y

Su, L., & Gan, Y. X. (2012). Experimental study on synthesizing TiO2 nanotube/polyaniline (PANI) nanocomposites and their thermoelectric and photosensitive property characterization. *Composites Part B: Engineering*, *43*(2), 170–182. doi:10.1016/j.compositesb.2011.07.015

Syed, A. A., & Dinesan, M. K. (1990). Polyaniline: Reaction stoichiometry and use as an ion-exchange polymer and acid/base indicator. *Synthetic Metals*, *36*(2), 209–215. doi:10.1016/0379-6779(90)90053-N

Tadeusz Hepel. (2012). *Functional Nanoparticles for Bioanalysis, Nanomedicine, and Bioelectronic Devices Volume 2*. (M. Hepel & C.-J. Zhong, Eds.) (Vol. 1113). Washington, DC: American Chemical Society. doi:10.1021/bk-2012-1113

Tai, H., Jiang, Y., Xie, G., Yu, J., Chen, X., & Ying, Z. (2008). Influence of polymerization temperature on NH3 response of PANI/TiO2 thin film gas sensor. *Sensors and Actuators B: Chemical*, *129*(1), 319–326. doi:10.1016/j.snb.2007.08.013

Talaie, A., Lee, J. Y., Lee, Y. K., Jang, J., Romagnoli, J. A., Taguchi, T., & Maeder, E. (2000). Dynamic sensing using intelligent composite: an investigation to development of new pH sensors and electrochromic devices. *Thin Solid Films*, *363*(1-2), 163–166. doi:10.1016/S0040-6090(99)00987-6

Trchová, M., Seděnková, I., Konyushenko, E. N., Stejskal, J., Holler, P., & Cirić-Marjanović, G. (2006). Evolution of polyaniline nanotubes: the oxidation of aniline in water. *The Journal of Physical Chemistry. B*, *110*(19), 9461–9468. doi:10.1021/jp057528g

Tseng, R. J., Huang, J., Ouyang, J., Kaner, R. B., & Yang, Y. (2005). Polyaniline nanofiber/gold nanoparticle nonvolatile memory. *Nano Letters*, *5*(6), 1077–80. doi:10.1021/nl050587l

Tung, N. T., Lee, H., Song, Y., Nghia, N. D., & Sohn, D. (2010). Structure and properties of selenious acid doped polyaniline with varied dopant content. *Synthetic Metals*, *160*(11-12), 1303–1306. doi:10.1016/j.synthmet.2010.04.004

Turyan, I., & Mandler, D. (1997). Selective Determination of Cr(VI) by a Self-Assembled Monolayer-Based Electrode. *Analytical Chemistry*, *69*(5), 894–7. doi:10.1021/ac9607525

Umar, A., Abaker, M., Faisal, M., Hwang, S. W., Baskoutas, S., & Al-Sayari, S. A. (2011). High-Yield Synthesis of Well-Crystalline α-Fe2O3 Nanoparticles: Structural, 3474–3480. Retrieved from http://www.ingentaconnect.com/content/asp/jnn/2011/00000011/00000004/art00097?token=00401834c9bae300275c277b42572b67667d772573706e766c592f3f3b2ced5b

Umasankar, Y., Huang, T.-Y., & Chen, S.-M. (2011). Vitamin B(12) incorporated with multiwalled carbon nanotube composite film for the determination of hydrazine. *Analytical Biochemistry*, *408*(2), 297–303. doi:10.1016/j.ab.2010.09.037

Virji, S., Huang, J., Kaner, R. B., & Weiller, B. H. (2004). Polyaniline Nanofiber Gas Sensors: Examination of Response Mechanisms. *Nano Letters*, *4*(3), 491–496. doi:10.1021/nl035122e

Virji, S., Kaner, R. B., Weiller, B. H., & Angeles, L. (2005). Hydrazine Detection by Polyaniline Using Fluorinated Alcohol Additives. *Chemistry of Materials*, *17*(May 2003), 1256–1260.

Vishnu Vardhanan, R., Zhou, L., & Gao, Z. (1999). Schottky and heterojunction diodes based on poly(3-octylthiophene) and poly(3-methylthiophene) films of high tensile strength. *Thin Solid Films*, *350*(1-2), 283–288. doi:10.1016/S0040-6090(99)00275-8

Walatka, V., Labes, M., & Perlstein, J. (1973). Polysulfur Nitride—a One-Dimensional Chain with a Metallic Ground State. *Physical Review Letters*, *31*(18), 1139–1142. doi:10.1103/PhysRevLett.31.1139

Wang, C., Shen, Y., Wang, X., Zhang, H., & Xie, A. (2013). Synthesis of novel NiZn-ferrite/Polyaniline nanocomposites and their microwave absorption properties. *Materials Science in Semiconductor Processing*, *16*(1), 77–82. doi:10.1016/j.mssp.2012.06.015

Wang, G., Gu, A., Wang, W., Wei, Y., Wu, J., Wang, G., … Fang, B. (2009). Copper oxide nanoarray based on the substrate of Cu applied for the chemical sensor of hydrazine detection. *Electrochemistry Communications*, *11*(3), 631–634. doi:10.1016/j.elecom.2008.12.061

Wang, G., Zhang, C., He, X., Li, Z., Zhang, X., Wang, L., & Fang, B. (2010). Detection of hydrazine based on Nano-Au deposited on Porous-TiO2 film. *Electrochimica Acta*, *55*(24), 7204–7210. doi:10.1016/j.electacta.2010.07.053

Wang, G., Zhang, J., Kuang, S., Liu, S., & Zhuo, S. (2014). The production of cobalt sulfide/graphene composite for use as a low-cost counter-electrode material in dye-sensitized solar cells. *Journal of Power Sources*, *269*, 473–478. doi:10.1016/j.jpowsour.2014.07.018

Wang, J., & Tuzhi, P. (1986). Selectivity and sensitivity improvements at perfluorinated ionomer/cellulose acetate bilayer electrodes. *Analytical Chemistry*, *58*(14), 3257–3261. doi:10.1021/ac00127a076

Wang, L., Hua, E., Liang, M., Ma, C., Liu, Z., Sheng, S., … Feng, W. (2014). Graphene sheets, polyaniline and AuNPs based DNA sensor for electrochemical determination of BCR/ABL fusion gene with functional hairpin probe. *Biosensors & Bioelectronics*, *51*, 201–207. doi:10.1016/j.bios.2013.07.049

Wang, X., Shao, M., Shao, G., Wu, Z., & Wang, S. (2009). A facile route to ultra-long polyaniline nanowires and the fabrication of photoswitch. *Journal of Colloid and Interface Science*, *332*(1), 74–7. doi:10.1016/j.jcis.2008.12.033

Watson, J. (1984). The tin oxide gas sensor and its applications. *Sensors and Actuators*, *5*(1), 29–42. doi:10.1016/0250-6874(84)87004-3

Wei, Y., Hsueh, K. F., & Jang, G. W. (1994). A study of leucoemeraldine and effect of redox reactions on molecular weight of chemically prepared polyaniline. *Macromolecules*, *27*(2), 518–525. doi:10.1021/ma00080a028

Wu, T.-M., Lin, Y.-W., & Liao, C.-S. (2005). Preparation and characterization of polyaniline/multi-walled carbon nanotube composites. *Carbon*, *43*(4), 734–740. doi:10.1016/j.carbon.2004.10.043

Xia, H., & Wang, Q. (2001). Synthesis and Characterization of Conductive Polyaniline Nanoparticles Through Ultrasonic Assisted Inverse Microemulsion Polymerization. *Journal of Nanoparticle Research*, *3*(5-6), 399–409. doi:10.1023/A:1012564814745

Xie, D., Jiang, Y., Pan, W., Li, D., Wu, Z., & Li, Y. (2002). Fabrication and characterization of polyaniline-based gas sensor by ultra-thin film technology. *Sensors and Actuators B: Chemical*, *81*, 158–164.

Xie, F., Huang, L., Liu, Y., & Leng, J. (2014). Synthesis and characterization of high temperature cyanate-based shape memory polymers with functional polybutadiene/acrylonitrile. *Polymer*, *55*(23), 5873–5879. doi:10.1016/j.polymer.2014.07.035

Xin, M., Lin, H., Yang, J., Chen, M., Ma., X., & Liu, J. (2014). Preparation of Polyaniline/Au 0 Nanocomposites Modified Electrode and Application for Hydrazine Detection. *Electroanalysis*, *26*(10), 2216–2223. doi:10.1002/elan.201400299

Xu, J.-C., Liu, W.-M., & Li, H.-L. (2005). Titanium dioxide doped polyaniline. *Materials Science and Engineering: C*, *25*(4), 444–447. doi:10.1016/j.msec.2004.11.003

Yamada, K., Yasuda, K., Fujiwara, N., Siroma, Z., Tanaka, H., Miyazaki, Y., & Kobayashi, T. (2003). Potential application of anion-exchange membrane for hydrazine fuel cell electrolyte. *Electrochemistry Communications*, *5*(10), 892–896. doi:10.1016/j.elecom.2003.08.015

Yamazoe, N., Hisamoto, J., Miura, N., & Kuwata, S. (1987). Potentiometric solid-state oxygen sensor using lanthanum fluoride operative at room temperature. *Sensors and Actuators*, *12*(4), 415–423. doi:10.1016/0250-6874(87)80060-4

Yamazoe, N., Kurokawa, Y., & Seiyama, T. (1983). Effects of additives on semiconductor gas sensors. *Sensors and Actuators*, *4*, 283–289. doi:10.1016/0250-6874(83)85034-3

Yan, H., & Liu, C.-C. (1994). A solid polymer electrolyte-bases electrochemical carbon monoxide sensor. *Sensors and Actuators B: Chemical*, *17*(2), 165–168. doi:10.1016/0925-4005(94)87045-4

Yang, D., Fadeev, A. G., Adams, P. N., & Mattes, B. R. (2007). GPC characterization of emeraldine base in NMP containing ionic liquids. *Synthetic Metals*, *157*(22-23), 988–996. doi:10.1016/j.synthmet.2007.10.002

Yang, D., Lu, W., Goering, R., & Mattes, B. R. (2009). Investigation of polyaniline processibility using GPC/UV–vis analysis. *Synthetic Metals*, *159*(7-8), 666–674. doi:10.1016/j.synthmet.2008.12.013

Yang, H., Lu, B., Guo, L., & Qi, B. (2011). Cerium hexacyanoferrate/ordered mesoporous carbon electrode and its application in electrochemical determination of hydrous hydrazine. *Journal of Electroanalytical Chemistry*, *650*(2), 171–175. doi:10.1016/j.jelechem.2010.10.018

Yang, Y., & Heeger, A. J. (1994). Polyaniline as a transparent electrode for polymer light-emitting diodes: Lower operating voltage and higher efficiency. *Applied Physics Letters*, *64*(10), 1245. doi:10.1063/1.110853

Yano, J., Terayama, K., Yamasaki, S., & Aoki, K. (1998). Logarithmic time dependence of the oxidative coloration of polyaniline film. *Electrochimica Acta*, *44*(2-3), 337–343. doi:10.1016/S0013-4686(98)00081-4

Yavuz, A. G., & Gök, A. (2007). Preparation of TiO2/PANI composites in the presence of surfactants and investigation of electrical properties. *Synthetic Metals*, *157*(4-5), 235–242. doi:10.1016/j.synthmet.2007.03.001

Yoon, S.-B., Yoon, E.-H., & Kim, K.-B. (2011). Electrochemical properties of leucoemeraldine, emeraldine, and pernigraniline forms of polyaniline/multi-wall carbon nanotube nanocomposites for supercapacitor applications. *Journal of Power Sources*, *196*(24), 10791–10797. doi:10.1016/j.jpowsour.2011.08.107

Yoshioka, Y., & Jabbour, G. E. (2006). Desktop inkjet printer as a tool to print conducting polymers. *Synthetic Metals*, *156*(11-13), 779–783. doi:10.1016/j.synthmet.2006.03.013

Yue, F., Tan, S. N., & Ge, H. (1996). A novel paper pH sensor based on polypyrrole. *Sensors and Actuators B: Chemical*, *32*, 33–39.

Zare, H. R., & Nasirizadeh, N. (2007). Hematoxylin multi-wall carbon nanotubes modified glassy carbon electrode for electrocatalytic oxidation of hydrazine. *Electrochimica Acta*, *52*(12), 4153–4160. doi:10.1016/j.electacta.2006.11.037

Zhang, L., Liu, P., & Su, Z. (2006). Preparation of PANI–TiO2 nanocomposites and their solid-phase photocatalytic degradation. *Polymer Degradation and Stability*, *91*(9), 2213–2219. doi:10.1016/j.polymdegradstab.2006.01.002

Zhang, L., Wan, M., & Wei, Y. (2005). Polyaniline/TiO2 microspheres prepared by a template-free method. *Synthetic Metals*, *151*(1), 1–5. doi:10.1016/j.synthmet.2004.12.021

Zhen, S., Xu, J., Lu, B., Zhang, S., Zhao, L., & Li, J. (2014). Tuning the optoelectronic properties of polyfuran by design of furan-EDOT monomers and free-standing films with enhanced redox stability and electrochromic performances. *Electrochimica Acta*, *146*, 666–678. doi:10.1016/j.electacta.2014.09.034

Zheng, J., Li, G., Ma, X., Wang, Y., Wu, G., & Cheng, Y. (2008). Polyaniline–TiO2 nano-composite-based trimethylamine QCM sensor and its thermal behavior studies. *Sensors and Actuators B: Chemical*, *133*(2), 374–380. doi:10.1016/j.snb.2008.02.037

Zheng, L., & Song, J. (2009). Curcumin multi-wall carbon nanotubes modified glassy carbon electrode and its electrocatalytic activity towards oxidation of hydrazine. *Sensors and Actuators B: Chemical*, *135*(2), 650–655. doi:10.1016/j.snb.2008.09.035

Zhu, Q., Gao, F., Yang, Y., Zhang, B., Wang, W., Hu, Z., & Wang, Q. (2015). Electrochemical preparation of polyaniline capped Bi2S3 nanocomposite and its application in impedimetric DNA biosensor. *Sensors and Actuators B: Chemical*, *207*, 819–826. doi:10.1016/j.snb.2014.10.120

Zou, F., Xue, L., Yu, X., Li, Y., Zhao, Y., Lu, L., … Qu, Y. (2013). One step biosynthesis of chiral, conducting and water soluble polyaniline in AOT micellar solution. *Colloids and Surfaces A: Physicochemical and Engineering Aspects*, *429*, 38–43. doi:10.1016/j.colsurfa.2013.03.054

Zou, Y., Sang, G., Wu, W., Liu, Y., & Li, Y. (2009). A polythiophene derivative with octyloxyl triphenylamine-vinylene conjugated side chain: Synthesis and its applications in field-effect transistor and polymer solar cell. *Synthetic Metals*, *159*(3-4), 182–187. doi:10.1016/j.synthmet.2008.08.010

Zou, Y., Sun, L., & Xu, F. (2007). Prussian Blue electrodeposited on MWNTs-PANI hybrid composites for H(2)O(2) detection. *Talanta*, *72*(2), 437–42. doi:10.1016/j.talanta.2006.11.001

APPENDICES

Section A: FTIR Analysis

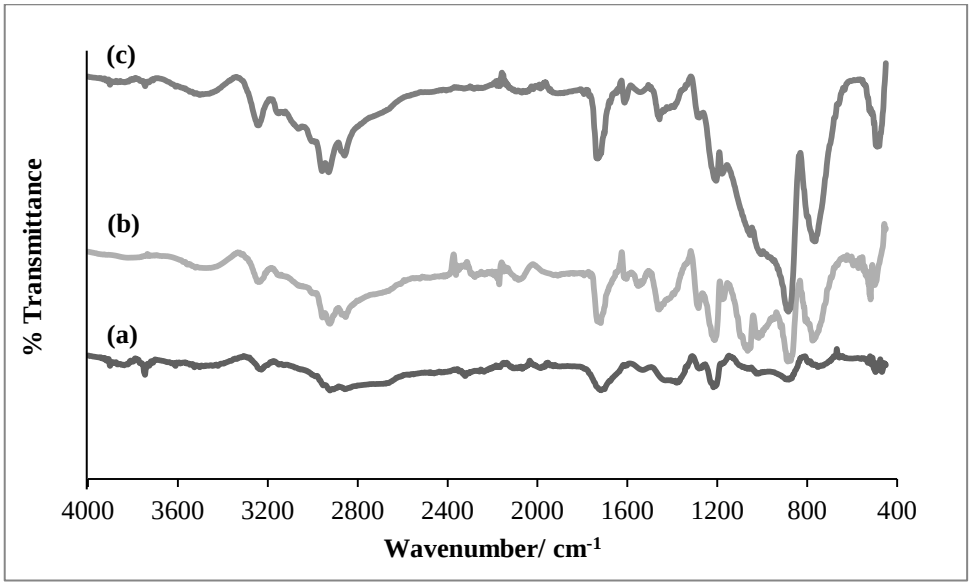

Appendix A1: FTIR spectra of a) PAni 1, b) PAni 2 and c) PAni 3 in the wavenumber range of 400 – 4000 cm^{-1}.

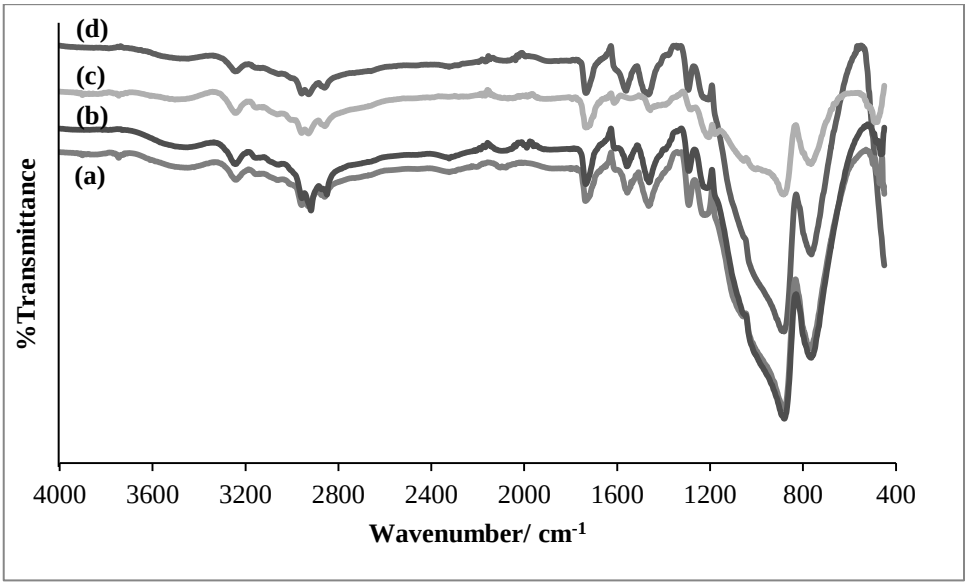

Appendix A2: FTIR spectra of (a) PAni, -10 ˚C, (b) PAni, -5 ˚C, (c) PAni, 0 ˚C and (d) PAni, 25 ˚C.

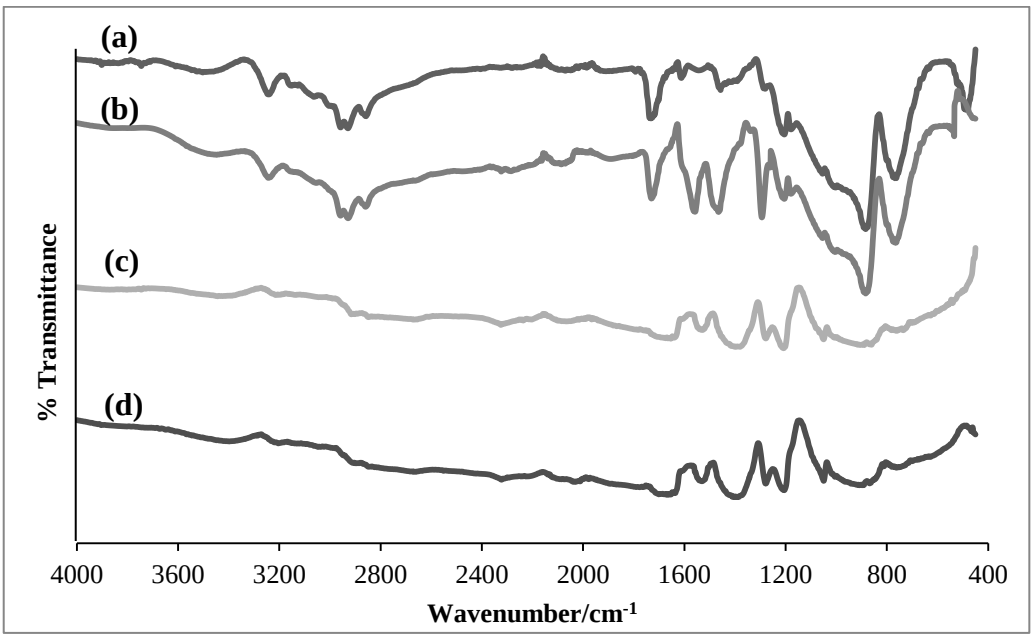

Appendix A3: FTIR spectra of pristine a) PAni, b) PAni/Ti20, c) PAni/T10 and d) PAni/Ti40 nanocomposites.

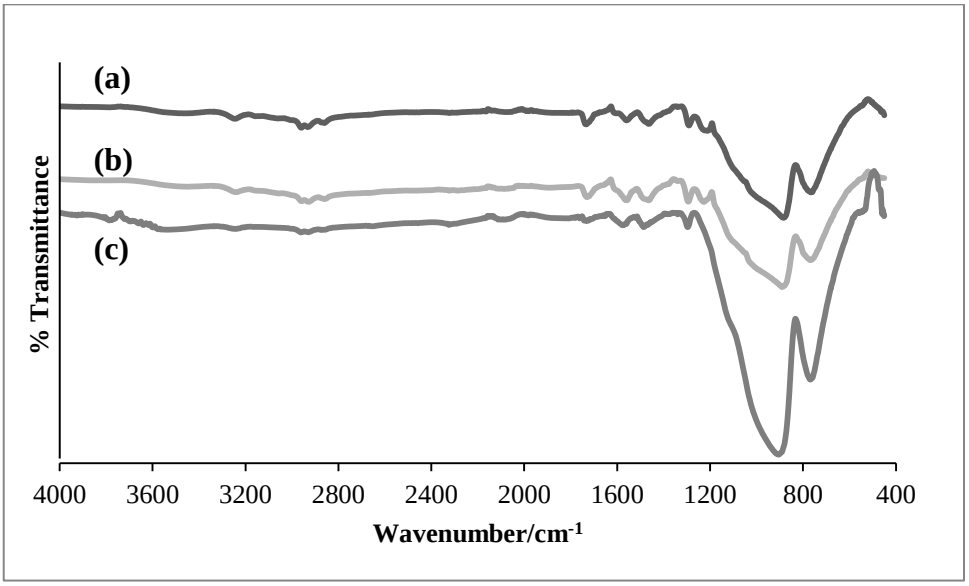

Appendix A4: FTIR spectra of a) PAni/Ti20, -5 ˚C, b) PAni/Ti20, 0 ˚C and c) PAni/Ti20, 25 ˚C

Section B: Conductivity Measurement

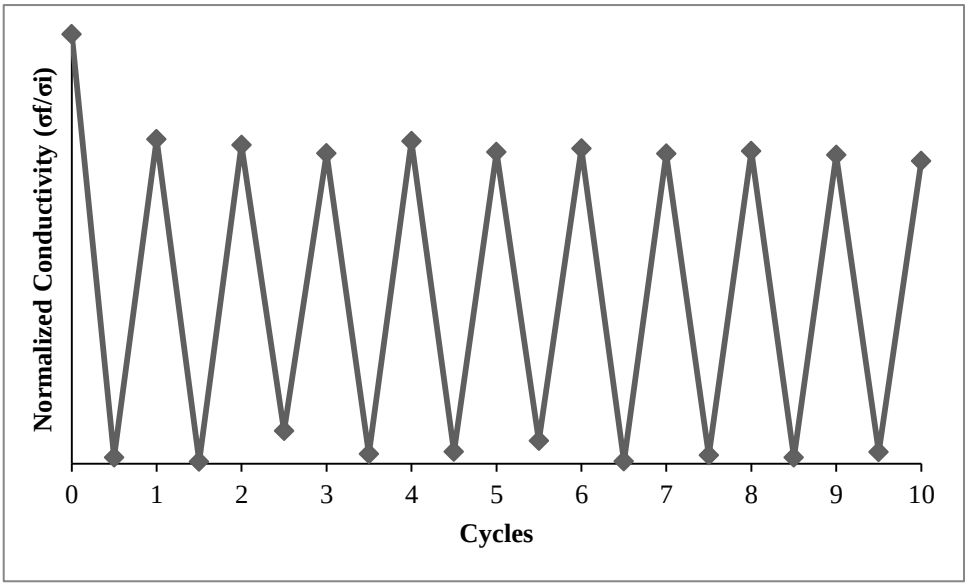

Appendix B1: Normalized conductivity response for the reusability study of PAni/Ti20, -5 ˚C.

Section C: Calibration Curves of PAni

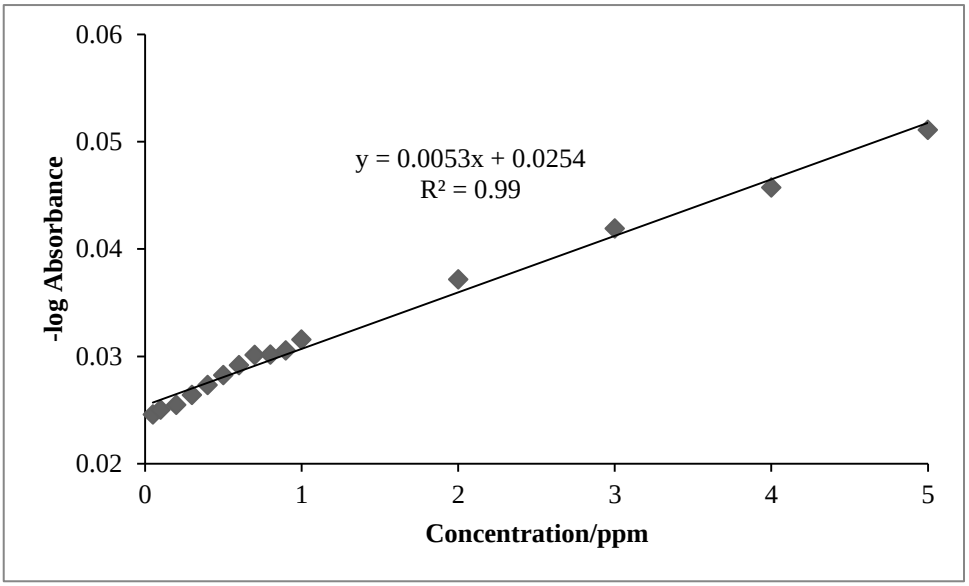

Appendix C1: Calibration of PAni**3** in a hydrazine concentration range of 0.05 – 5.00 ppm.

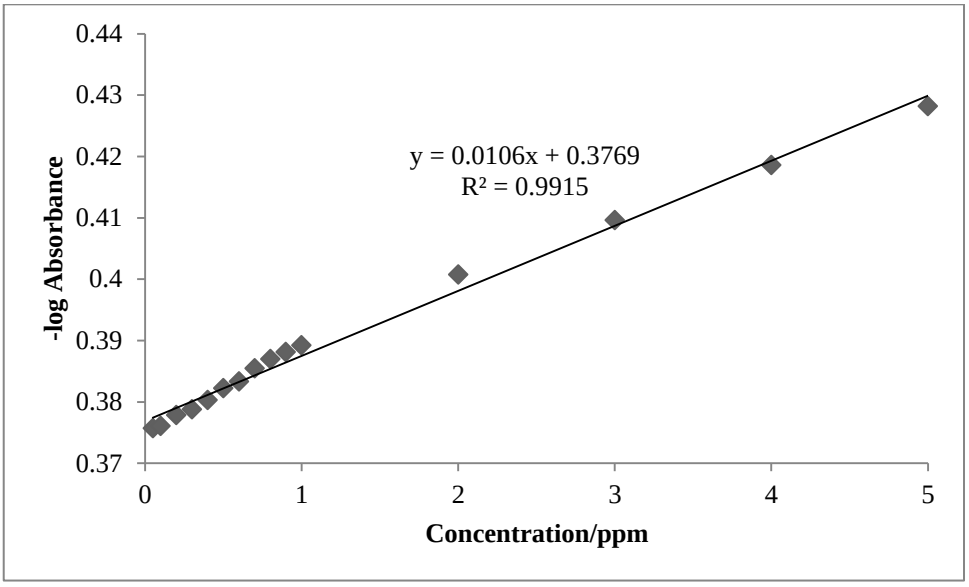

Appendix C2: Calibration of PAni, -5 ˚C in a hydrazine concentration range of 0.05 – 5.00 ppm.

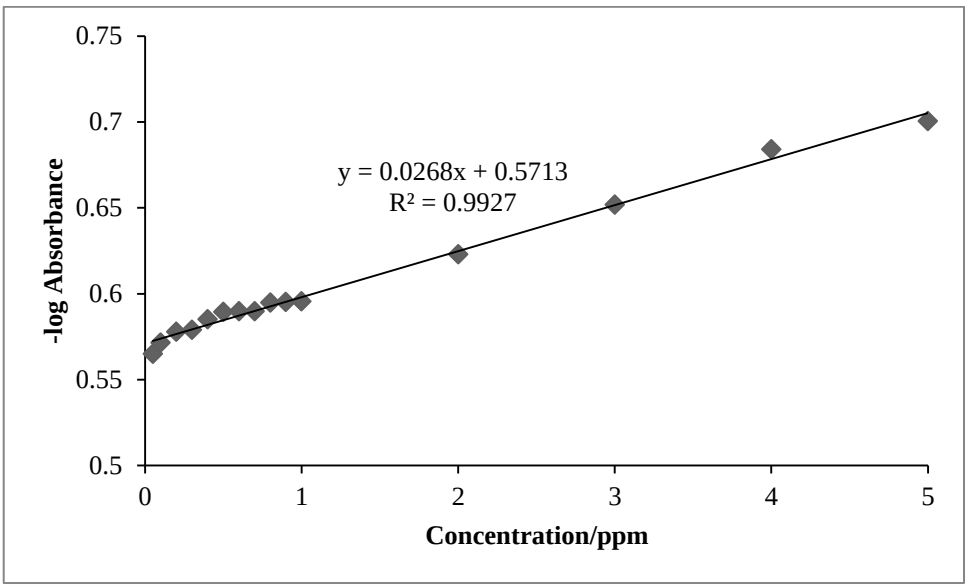

Appendix C3: Calibration of PAni/Ti20, 0˚C in a hydrazine concentration range of 0.05 – 5.00 ppm.

Section D: List of Publications

Appendix D1: PAni sensors in hydrazine detection

1. **Sambasevam, K. P.**, Mohamad, S., and Phang, S.-W. (2015). Enhancement of polyaniline properties by different polymerization temperatures in hydrazine detection. *Journal of Applied Polymer Science*, *132*(13), 41746. doi:10.1002/app.41746.
2. **Sambasevam, K.P.**, Mohamad, S., and Phang, S.-W. (2015). Effect of dopant concentration on polyaniline for hydrazine detetcion. 33, 24-31 *Materials Science in Semiconductor Processing*.doi:10.1016/j.mssp.2015.01.008.
3. **Sambasevam, K.P.**, Mohamad, S., and Phang, S.-W. (2015). PAni/TiO_2 nanocomposites in hydrazine detection. *RSC Adavances*. **SUBMITTED**.
4. **Sambasevam, K.P.**, Mohamad, S., and Phang, S.-W. (2015). Effect of polymerization temperature on PAni/TiO_2 nanocomposites in hydrazine detection. *Sensors and Actuartors B:Chemical*. **SUBMITTED**.

Appendix D2: PAni related applications

5. Kawata, K., Gan, S.-N., Ang, D. T.-C., **Sambasevam, K. P.**, Phang, S.-W., and Kuramoto, N. (2013). Preparation of polyaniline/TiO_2 nanocomposite film with good adhesion behavior for dye-sensitized solar cell application. *Polymer Composites*, 34(11), 1884–1891. doi:10.1002/pc.22595
6. Koh, Y., **Sambasevam, K. P.**, Yahya, R., and Phang, S. (2013). Improvement of Microwave Absorption for PAni/HA/TiO_2/Fe_3O_4 Nanocomposite After Chemical Treatment. *Polymer Composites*, 34(7), 1186–1194. doi:10.1002/pc22595.

Appendix D3: Other publications

7. **Sambasevam, K. P.,** Mohamad, S., Sarih, N. M., and Ismail, N. A. (2013). Synthesis and Characterization of the Inclusion Complex of β-cyclodextrin and Azomethine. *International Journal of Molecular Sciences*, 14(2), 3671–82. doi:10.3390/ijms14023671.
8. Mohamad, S., Nor Kartini, A. B., Ahmad Razali, I., Surikumaran, H., **Sambasevam, K. P.,** Mohamad Zain, N. N., and Chandrasekaram, K. (2014). Removal of Phosphate by Paper Mill Sludge: Adsorption Isotherm and Kinetic Study. *Asian Journal of Chemistry*, 26(12), 3545–3552.

Appendix E: List of Proceedings

1. **Kavirajaa Pandian Sambasevam**, Sharifah Mohamad. 2010. Synthesis and characterization of β-cyclodextrin and azomethine inclusion complex. 16th Malaysian Chemical Congress (16th MCC) 2010. 12-14 October 2010, Kuala Lumpur.
2. **Kavirajaa Pandian Sambasevam**, Phang Sook Wai. 2011. Synthesis, Characterization and Conductivity Studies of Novel Polyaniline Nanocomposite. Malaysia Polymer International Conference (MPIC 2011). 19-20 October 2011, Bangi-Putrajaya.
3. **Kavirajaa Pandian Sambasevam**, Sharifah Mohamad, Phang Sook Wai. 2012. Application of Conducting Polymer as a Chemical Sensor for Hydrazine Detection. 17th Malaysian Chemical Congress (17th MCC). 15-17 October 2012, Kuala Lumpur
4. **Kavirajaa Pandian Sambasevam**, Sharifah Mohamad, Phang Sook Wai. 2012. Detection of Hydrazine by using Conducting Polymer as a Chemical Sensor. 5th International Conference on Postgraduate Education (5th ICPE 2012) 18-19 December 2012, Universiti Teknologi Malaysia, Skudai, Johor.
5. **Kavirajaa Pandian Sambasevam**, Sharifah Mohamad, Phang Sook Wai. 2013. Effect of synthesis parameter on conducting polymer chemical sensor for hydrazine detection. 2013 International Symposium on Fundamental and Applied Sciences (ISFAS 2013). 27-29 June 2013, Seoul, South Korea.
6. **Kavirajaa Pandian Sambasevam**, Sharifah Mohamad, Phang Sook Wai. 2013. Effect of polymerization temperature on conducting polymer chemical sensor for hydrazine detection. 7th International Conference on Materials for Advanced Technologies (7th ICMAT 2013). 1-5 July 2013, Suntec City, Singapore.

7. Nirosa Raman, **Kavirajaa Pandian Sambasevam**, Phang Sook Wai. 2013. Comparison studies of polyaniline nanocomposite with and without TiO_2 for hydrazine detection. Malaysia Polymer International Conference (MPIC 2013). 25-26 September 2013, Bangi-Putrajaya.
8. **Kavirajaa Pandian Sambasevam**, Sharifah Mohamad, Phang Sook Wai. 2014. Synthesis, characterization and application of polyaniline/TiO_2 nanocomposites in hydrazine detection. 6^{th} International Conference on Postgraduate Education (ICPE-6 2014). 17-18 December 2014, UTem Main Hall, Melaka.

Appendix F: Awards

1. **Best poster award in MPIC, 2011:**

   Kavirajaa Pandian Sambasevam, Phang Sook Wai. 2011. Synthesis, Characterization and Conductivity Studies of Novel Polyaniline Nanocomposite. Malaysia Polymer International Conference (MPIC 2011). 19-20 October 2011, Bangi-Putrajaya.

2. **Best poster award in 17th MCC, 2012:**

   Kavirajaa Pandian Sambasevam, Sharifah Mohamad, Phang Sook Wai. 2012. Application of Conducting Polymer as a Chemical Sensor for Hydrazine Detection. 17th Malaysian Chemical Congress (17th MCC). 15-17 October 2012, Kuala Lumpur.